Université d'Ottawa · University of Ottawa

Université d'Ottawa · University of Ottawa

FACULTÉ DES ÉTUDES SUPÉRIEURES ET POSTDOCTORALES

FACULTY OF GRADUATE AND POSTDOCTORAL STUDIES

Doan Anh TRAN

AUTEUR DE LA THÈSE - AUTHOR OF THESIS

M. A. Sc. (Chemical Engineering)

GRADE - DEGREE

Department of Chemical Engineering

FACULTÉ, ÉCOLE, DÉPARTEMENT - FACULTY, SCHOOL, DEPARTMENT

TITRE DE LA THÈSE - TITLE OF THE THESIS

Development of and Gas Permeation Study of Homo from the Family of Polyphenylene Oxides

B. Kruczek

DIRECTEUR DE LA THÈSE - THESIS SUPERVISOR

CO-DIRECTEUR DE LA THÈSE - THESIS CO-SUPERVISOR

EXAMINATEURS DE LA THÈSE - THESIS EXAMINERS

C. Lan

D. Taylor

J.-M. De Koninck, Ph.D.

LE DOYEN DE LA FACULTÉ DES ÉTUDES SUPÉRIEURES ET POSTDOCTORALES

DEAN OF THE FACULTY OF GRADUATE AND POSTDOCTORAL STUDIES

DEVELOPMENT OF AND GAS PERMEATION STUDY OF HOMO AND COPOLYMERS FROM THE FAMILY OF POLYPHENYLENE OXIDES

by

Anh Tran

A thesis submitted to the school of Graduate Studies and Research in partial fulfillment
of the requirements for the degree of
MASTER OF APPLIED SCIENCE
In the Department of Chemical Engineering
University of Ottawa

Your file Votre référence
ISBN: 0-494-01620-5
Our file Notre référence
ISBN: 0-494-01620-5

Abstract

Membrane gas separation emerged as a commercial process on a large scale during the 1980s. When compared to other gas separation processes such as cryogenics, adsorption and absorption, membrane separation competes primarily on the basis of overall economics and convenience, but not on the basis of product purity. For example, membranes have been used for offshore natural gas processing because they reduce the size and the weight of the processing units, require less maintenance and less operator supervision. In order to improve product purity, development of new membrane materials, and modification of existing membrane material for better gas separation properties, is required.

This research focused on preparation and characterization of new copolymers from the family of polyphenylene oxides. This family of polymers was chosen because of the properties of its best-known representative, poly(2,6-dimethyl-1,4-phenylene oxide), which shows one of the highest rates of permeability for gases among glassy polymers, exhibits excellent film-forming properties, and is resistant to a number of chemical agents.

The study was divided into two parts: (1) homopolymers and both block and random copolymers of different composition were synthesized by oxidative coupling of 2,6-diphenylphenol and 2,6- dimethylphenol; (2) the physical and gas transport properties of the polymers were determined.

The number average molecular weight of synthesized polymers was in the range of 10,000-70,000. The actual compositions of copolymers were close to the targeted values. The differential thermal analysis confirmed that both random and block structures were formed. The former showed a single decomposition temperature while the latter showed two distinct decomposition temperatures of 467°C and 583°C, corresponding to the decomposition temperatures of poly(2,6-dimethyl-1,4-phenylene oxide), DMPO, and poly(2,6-diphenyl-1,4-phenylene oxide), DPPO, respectively. The decomposition temperature of random copolymers increased with the content of DPPO.

The study of transport properties showed that the CO_2 and O_2 permeability coefficients generally decreased with increasing content of DPPO. This decrease in the

CO_2 and O_2 permeability coefficients was associated with an increase in the CO_2/CH_4 and O_2/N_2 permeability ratios, respectively. The observed CO_2/CH_4 permeability ratios were in the range of 30 to 50, and the O_2/N_2 permeability ratios were in the range of 4 to 8.5.

Gas transport properties of block copolymers of DMPO and DPPO have never been reported in the literature. While the properties of some random copolymers of DMPO and DPPO have been reported previously, the properties of the compositions considered in this project are reported for the first time. Generally, for a given DPPO content, random copolymers exhibit more favorable gas transport properties than their block counterparts.

The plots of the O_2/N_2 permeability ratio versus the O_2 permeability coefficient, and the CO_2/CH_4 permeability ratio versus the CO_2 permeability coefficient, suggest that most of the polymers synthesized in this study were above the so-called upper-bound line. These remarkable results have led to a re-examination of the permeation rates measured, using a soap bubble flow meter. A steady-state model was developed to account for the effects of diffusion of air into the bubble flow meter tube, and back permeation of this air through the membrane during the measurements of the flow rate of gases. It was found that if the measured flow rates were less than 0.05 mL/min, the calculated permeability coefficients could be under or overestimated due to back diffusion and back permeation of air. For low permeation rates close to the minimum detectable flow rate of the utilized bubble flow meter of 0.01 mL/min, the error in the permeability coefficient could be as high as 30%. Quantification of the error in the permeability coefficient due to back diffusion and back permeation of air in a constant pressure testing system has never been reported in the literature.

Résumé

La séparation membranaire des gaz est apparue comme procédé commercial sur une grande échelle durant les années 1980. Elle rivalise avec les autres techniques de séparation des gaz comme la cryogénie, l'adsorption et l'absorption en raison de son côté pratique et économique, mais non pas pour la pureté du produit. Par exemple, les membranes ont été utilisées pour le traitement du gaz naturel marin, parce qu'elles diminuent la taille et le poids des unités de traitement et qu'elles nécessitent moins d'entretien et de supervision. Afin d'améliorer la pureté du produit, le développement de nouvelles matières de membranes ou l'amélioration de la séparation des gaz des matières déjà existantes est nécessaire.

Cette recherche porte sur la préparation et la caractérisation de nouveaux copolymères de la famille des polyphénylènes oxydés. La famille des polymères a été choisie pour les propriétés de son représentant le plus connu, poly (2,6-dimethyl-1,4-phenyle oxyde), qui facilite la formation de couche, résiste à bon nombre d'agents chimiques, et possède l'une des plus grandes perméabilités des gaz parmi les polymères vitreux.

L'étude a été divisée en deux parties: (1) homo et les copolymères à blocs et les copolymères aléatoires de composition différente ont été synthétisés par couplage oxydatif de 2,6-diphenylphenol et 2,6-dimethylphenol; (2) les propriétés physiques et de transport des gaz des polymères ont été déterminés.

Les poids moléculaires moyens des polymères synthétisés ont varié entre 10 000 et 17 000. Les compositions des copolymères synthétisés étaient très près des valeurs prévues. L'analyse thermique différentielle a confirmé qu'à la fois des structures de copolymères aléatoires et de copolymères à blocs ont été formés. Les premiers ont présenté une seule température de dégradation alors que les seconds ont montré deux températures de dégradation distinctes de 467°C et 583°C, qui correspondent aux températures respectives du poly (2,6-dimethyl-1,4-phenylene oxide), DMPO, et poly (2,6-diphenyl-1,4-phenylene oxide), DDPO. La température de dégradation des copolymères aléatoires augmente avec une plus grande quantité de DDPO.

L'étude des propriétés de transport des gaz a montré que les coefficients de perméabilité du CO_2 et de l'O_2 diminuent avec une plus grande quantité de DDPO. Cette diminution est associée avec une augmentation des taux respectifs de perméabilité de CO_2/CH_4 et de O_2/N_2. Le taux de CO_2/CH_4 se situait autour de 4 – 8,5.

Alors que les propriétés des copolymères de DMPO et de DPPO ont déjà été étudiées, les propriétés de transport de gaz des copolymères aléatoires de DMPO et de DPPO ne l'ont jamais été. Les propriétés des compositions étudiées dans le cadre de cette recherche sont donc signalées pour la première fois.

Les graphiques du taux de perméabilité de O_2/N_2 par opposition au coefficient de perméabilité de l'O_2, et le taux de perméabilité de CO_2/CH_4 par opposition au coefficient de perméabilité du CO_2 suggèrent que la plupart des polymères synthétisés dans le cadre de la recherche se situaient au-dessus de la soi-disant ligne de borne supérieure. Ces résultats remarquables ont mené à la réexamination des taux d'infiltration, mesurés en utilisant un débitmère à film de savon. Un modèle à régime permanent a été établi pour rendre compte des effets de la diffusion de l'air dans le tube du débitmère et de la rétrodiffusion de cet air à travers la membrane durant la mesure du débit des gaz. Il a été constaté que si le débit mesuré est de moins de 0,05 ml/min, la perméabilité pourrait être sous-estimée ou surestimée en raison de la rétrodiffusion et de la rétro-infiltration de l'air. Pour de faibles taux d'infiltration situés près du débit minimum détectable du débitmère de 0,01 ml/min, le taux d'erreur dans le coefficient de perméabilité pouvait s'élever jusqu'à 30 %. Le calcul du taux d'erreur dans le coefficient de perméabilité, causé par la rétrodiffusion et la rétro-infiltration de l'air dans un système expérimental à pression constante, n'a jamais été rapporté dans la littérature scientifique.

Acknowledgements

I wish to express my gratitude to Professor B. Kruczek and Professor T. Matsuura for their encouragement, guidance and advice. I also wish to thank my family and friends for their constant support. The financial support of Air Products is also greatly appreciated.

I also would like to thank Dr. G. Chowdhury for her help and assistance at the beginning of this work; Ms. Delgado from the Natural Research Council for IR and TG analysis; Dr. G. Facey from the University of Ottawa for the ^{1}H NMR analysis; Dr. M. Day and Mr. Gilles from NRC for letting me use their laboratory and the equipment for the DSC analysis; and Dr. M. Dubé and his student Ms. R. Jovanovic for the molecular weight analysis.

The technical assistance and help of Mr. L. Tremblay, Mr. F. Ziroldo, and Mr. G. Nina during the course of this work is greatly appreciated. I also acknowledge colleagues from the Industrial Membrane Research Institute for their help and valuable discussions.

TABLE OF CONTENTS

List of Tables

List of Figures

Nomenclature

Abbreviations

ADP	Degree of polymerization
BrDMPO	Brominated poly-2, 6-dimethyl-1, 4-phenylene oxide
CP	Constant pressure system
DMP	2,6-dimethyl phenol
DMPO	Poly-2, 6-dimethyl-1, 4-phenylene oxide
DPP	2,6-diphenyl phenol
DPPO	Poly-2, 6-diphenyl-1, 4-phenylene oxide
PPO	Polyphenylene Oxide
SDMPO	Sulfonated poly-2, 6-dimethyl-1, 4-phenylene oxide
VDMPO	Vinyl poly-2, 6-dimethyl-1, 4-phenylene oxide

Symbols

A	Membrane area, cm^2
C	Concentration, cm^3 (STP)/cm^3
c	Solution concentration, g/100mL
C_D	Henry's solubility constant, cm^3 (STP)/(cm^3 polymer cmHg)
CED	Cohesive energy density, J/cm^3
D	Diffusivity coefficient, cm^2/s
D_k	Kinetic diameter, Å
D_o	Pre-exponential diffusion coefficient, dimensionless
d	Inner diameter of the tube, cm
E	Diffusion activating energy, J/mol
E_{coh}	Structural component of the overall solubility parameter, J/mol
ΔE	Molar energy of vaporization, J/mol
ΔE_d	London dispersion force, J/mol
ΔE_p	Dipole force, J/mol
f	Gas-phase fugacity
ΔG_m	Gibbs free energy of mixing, J/mol

ΔH	Heat of solution, J/mol
ΔH_m	Enthalpy of mixing, J/mol
I	Intensity of peak, cm^{-1}
l	Membrane thickness, cm
M	Molecular weight, g/mol
n	Number of moles, dimensionless
N	Number of molecules, dimensionless
P	Permeability, Barrer = 10^{-10} cm^3 (STP) cm/(cm^2 s cmHg)
p	Pressure, cmHg
Δp	Pressure gradient across the membrane, cmHg.
Q	Steady state permeation rate, cm^3 (STP)/sec
R	Universal Gas constant, =8.314 J/mol K
S	Solubility coefficient, cm^3 (STP)/(cm^3 cmHg)
ΔS_m	Entropy change of mixing, J/mol K
S_o	Pre-exponential solubility coefficient, dimensionless
T	Temperature, K
T_d	Decomposition Temperature, K
T_g	Glass transition temperature, K
T_c	Critical temperature, K
t	Film thickness, cm
V	Molar volume, m^3/mol
V_m	Molar volume of mixture, m^3/mol
w	Weight fraction, dimensionless
x_A	Mole fraction of A
v_m	Velocity of the bulk phase, cm/s
v_A	The net velocity of A, cm/s
z	The distance from the permeate side of membrane, cm

Greek Symbols

δ_{sp}	Solubility parameter, $MPa^{1/2}$
δ_d	Dispersion force component of the solubility parameter, $MPa^{1/2}$
δ_h	Hydrogen bond component of the solubility parameter, $MPa^{1/2}$
δ_p	Dipole component of the solubility parameter, $MPa^{1/2}$
α_o	Ideal selectivity, dimensionless
α_S	Solubility selectivity, dimensionless
α_D	Diffusivity selectivity, dimensionless
Φ_g	Volume fraction of gas in the polymer, dimensionless
β_g	Thermal expansion coefficient, K^{-1}
χ	Polymer solvent interaction parameter, dimensionless
η	Intrinsic viscosity, dL/g

CHAPTER 1 Introduction

1.1 Membranes and the membrane industry

The demand for a cleaner environment has increased in the last decade. This has led to an increase in the development of new processes and improvements of existing processes and materials. Membrane gas separation is an emerging technology with a multidisciplinary character that can be used in a large number of separation processes. The basic concept of this technology is the selective permeation of gases through membranes. A membrane can be generally defined as a selective barrier between two phases. It can be made from various materials as long as it exhibits the following characteristics (Mulder, 1996):

- A high permeability and selectivity toward a specific component (or components) to be separated from a gas mixture in order to minimize the capital investment and the power cost
- Chemical inertness and physical stability
- Continuity, that is, absence of pinholes or other mechanical defects

There are over 100 membrane separation plants operating in the United States, Europe and Japan. Today, gas separation membranes are used for the separation of H_2 from various industrial gas streams, such as NH_3 in CH_3OH synthesis, in petroleum refining, and in petrochemical operations. There are also membrane applications in separations of CO_2 from the natural and landfill gases, and in enhanced oil recovery. Membranes are also important in air separation for the production of 96% N_2 for "inerting" fuel tanks. In addition to gas separation, membrane technology is well established in water desalination by reverse osmosis, and ultra- and microfiltration applications (Stern, 1984). The driving forces utilized in membrane separation include the difference in pressure, temperature, concentration and the electrical potential across the membrane.

The interest in membrane gas separation is mainly due to the following benefits (Spillman, 1989):

- Separation can be carried out continuously

- Energy consumption is generally low compared to other processes such as cryogenic distillation, absorption and pressure swing adsorption
- Membrane processes can easily be combined with other separation processes (hybrid processes)
- Separation can be carried out under mild conditions
- Up-scaling is easy
- Membrane properties are adjustable

As is the case with other processes, membrane technology also has some drawbacks (Robeson, 1991) that include:

- Low membrane lifetime
- Inverse relationship between productivity and selectivity

The future developments in membrane gas separation as an alternative gas separation technology strongly depends on the development of new, high-performance membrane materials. Hence, the major motivation for this research was the improvement of gas transport properties of polymeric membranes via the synthesis of homopolymers and new copolymers from the family of polyphenylene oxides (PPO). The properties of most polymers synthesized in this study have not been reported previously in the literature.

1.2 Scope of the research and the major objectives

This research project was divided into two parts, reflecting the two main objectives of this project, that is, (1) the synthesis of and (2) the characterization of new polymers for gas separation membranes. The first part focused on the synthesis of polymers from the family of polyphenylene oxide (PPO). Poly-2,6-dimethyl-1,4-phenylene oxide (DMPO) is a best-known representative of the PPO family. The DMPO is a commercially available material known for its high permeability and relatively low selectivity for gases. The synthesis of polymers included homopolymers such as DMPO and 2,6-diphenyl-1,4-phenylene oxide (DPPO), as well as various block and random copolymers containing DMPO and DPPO units.

The second part of this study focused on the characterization of physical and gas transport properties of synthesized polymers, in order to identify suitable candidates for the preparation of air separation membranes.

While executing the second part of this project, it became apparent that some polymers synthesized in this project showed remarkable and rather unexpected gas transport properties. This led to the investigation of the technique used in measuring gas permeation rates through the membrane. As a result, a steady-state model that accounts for effects of back permeation of air components through the membrane was developed. The model was used to correct experimentally-obtained permeation data.

1.3 Objectives

To accomplish the two main objectives of this work, the following specific objectives were set:

1. To synthesize DMPO, DPPO and their block and random copolymers with three different molar percentages of DPPO.
2. To characterize the synthesized polymers by means of their actual chemical structure, the molecular weight and the molecular weight distribution, and to determine their thermal properties, such as the glass transition and the decomposition temperatures
3. To identify a single solvent that could dissolve all synthesized polymers, and to evaluate the interactions, both theoretically and experimentally (intrinsic viscosity measurements), between the selected solvent and the polymers
4. To prepare solution-cast homogeneous membranes using the solvent identified in No.3
5. To determine the gas transport properties of membranes prepared from the synthesized polymers by carrying out single gas permeation tests in a constant pressure testing system
6. To evaluate the effects (if any) of the polymer chemistry (i.e., the percent of DPPO and the structure (block versus random), on gas transport properties of the synthesized polymers)

The additional objective that arose during the analysis of the experimental gas transport properties was to develop a steady-state model to account for the effects of back permeation of air components through the membrane, and to apply this model to the experimental gas permeation data.

PART I Literature Review

CHAPTER 2 Gas Transport in Polymeric Membranes

2.1 Membrane classification

The membranes can be divided into two groups: porous and nonporous. They can be made from polymers, ceramics, and metals materials. Porous membranes have fixed pores of size, ranging from 4-5 Å to several μm. The pore size and pore size distribution mainly determine which particles or molecules are retained and which pass through the membrane. The membrane material is generally of little importance in determining the separation performance in porous membranes.

Nonporous or dense membranes have no fixed pores, and the material is mainly determining the performance. The schematic drawing of a porous and a nonporous membrane is shown below (Mulder, 1996):

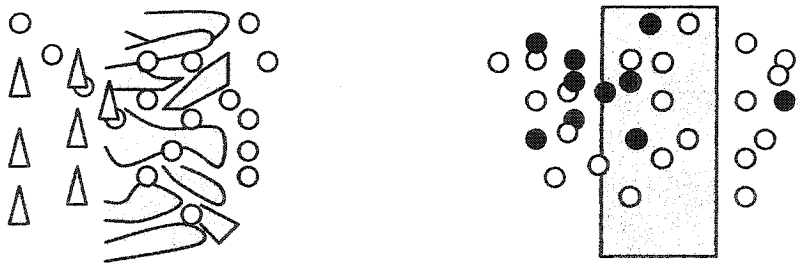

Porous membrane
Microfiltration/ Ultrafiltration

Nonporous or dense membrane
Gas separation/ pervaporation

Figure 2.1: Schematic diagram of a porous and a nonporous membrane

Membranes come in a wide range of forms and structures. At the macro scale, there are three main forms: flat sheet, hollow fiber, and tubular. Tubular membranes differ from hollow fibers only by means of their diameter and the fact that they have to be supported.

2.2 *Gas permeation in nonporous membranes*

The permeation of small molecules through polymers and the ability of polymers to separate gas mixtures was observed and described analytically over a century ago. In all membrane gas separations, the driving force for the permeation of a gas across the membrane is the difference between its partial pressures at the high-pressure side and the low-pressure side.

In general, gases permeate through polymeric membranes following a three-step solution-diffusion mechanism. First, the gas molecules dissolve at the upstream face of the membrane, then they diffuse from the upstream face to the downstream face of the membrane, and finally desorb (or evaporate) from this face. This solution-diffusion mechanism is driven by the difference in the thermodynamic activities existing between the upstream and downstream faces of a membrane. The activity difference causes a concentration gradient that leads to the diffusion in the direction of decreasing activity. The differences in permeability of different gas species, which results in selective properties of polymer membranes, arise from the differences in diffusivity and the differences in physico-chemical interactions with the membrane material (Kesting & Fritzsche, 1993). Consequently, the permeability coefficient, P, can be expressed as a product of two parameters, the diffusivity coefficient, D, and the solubility coefficient, S:

$$P = D\,S \tag{2.1}$$

The parameters on the right hand side of Eq. (2.1) are defined as:

$$D = D_0 e^{-E/RT} \tag{2.2}$$

and

$$S = S_0\, e^{-\Delta H/RT} \tag{2.3}$$

where D_0 and S_0 are pre-exponential terms, E is the activation energy for diffusion, ΔH is the enthalpy associated with dissolution of gas in a polymer, R is the universal gas constant, and T is the absolute temperature. The parameters, D_0, S_0, E and ΔH, are greatly influenced by the size of the permeating gas, and by the forces holding the polymer chains together. The stronger these forces are, the more difficult it will be for the gas to push aside the chains and diffuse.

The solubility coefficient is a thermodynamic term that expresses the nature and the magnitude of the interaction forces working between the gas molecules and polymer chains. On the other hand, the diffusion coefficient strongly depends on the

microstructure of the polymer, which is influenced by the interaction forces acting between two adjacent polymer chains. The magnitude of these interaction forces is often expressed by the solubility parameter of polymer (δ). The solubility parameter often referred to as the Hildebrand parameter is defined as:

$$\delta_{sp} = \sqrt{CED} = \sqrt{\Delta E / V} \tag{2.4}$$

where CED is the cohesive energy density, which measures the strength of secondary bonds, ΔE is the molar energy of vaporization, and V is the molar volume.

The effect of temperature on gas diffusivity and solubility are normally of opposite signs. For example, diffusivity increases and solubility decreases with increasing temperature (Kesting & Fritzsche, 1993).

The permeability coefficient of a gas can be determined from experimentally measured steady-state permeation rate of the gas through a homogenous membrane

$$P = \frac{Ql}{A\Delta p} \tag{2.5}$$

where Q is the steady-state permeation rate, l is the membrane thickness, A is the permeation area of the membrane, and Δp is the partial pressure gradient across the membrane. Commonly, the permeability coefficient is given in Barrer.

$$1\,\text{Barrer} = 1\text{x}10^{-10}\,\frac{(\text{cm}^3(\text{STP}))\,\text{cm}}{\text{s}\,\text{cm}^2\,\text{cmHg}}$$

Permeability coefficients (or permeances) obtained in single gas permeation tests are used for evaluation of the selective properties of a membrane. The ideal selectivity (α_0) for separation of gases A and B is defined as:

$$\alpha_0 = \frac{P_A}{P_B} \tag{2.6}$$

where P_A and P_B are the permeability coefficients of gases A and B, respectively. Substituting Eq. (2.1) into Eq. (2.6) the ideal selectivity can be expressed as a product of the solubility selectivity (α_S) and the diffusivity selectivity (α_D).

$$\alpha_0 = \frac{S_A D_A}{S_B D_B} = \alpha_S \alpha_D \tag{2.7}$$

2.3 Sorption behavior of gases in polymers

The sorption (solubility) of gases in amorphous polymers depends on whether the polymer is above or below its glass transition temperature (T_g).

2.3.1 Sorption above the glass transition – rubbery polymers

Amorphous polymers above their T_g are considered to be in a rubbery state. At low pressures, gas sorption in rubbery polymers is a linear function of pressure, and can be described using the Henry's law:

$$C = C_D p \tag{2.8}$$

where C is the concentration of a gas in the polymer, C_D is the Henry's law constant, and p is the penetrant gas pressure.

At moderate and high pressures of industrial interest, sorption of gases deviates from Henry's law behavior and the sorption isotherm exhibits a characteristic shape that is convex to the pressure axis. This non-linear behavior is described by the Flory and Huggins theory. In the symmetrically normalized forms, the Flory and Huggins becomes:

$$\ln\left(\frac{f}{f_0}\right) = \ln\Phi_g + \left(1-\Phi_g\right) + \chi\left(1-\Phi_g\right)^2 \tag{2.9}$$

In asymmetrically normalized forms, it becomes:

$$\ln\left(\frac{f}{C_D}\right) = \ln\Phi_g - \Phi_g + \chi\Phi_g\left(\Phi_g - 2\right) \tag{2.10}$$

where f is the gas-phase fugacity, f_0 is the standard state fugacity of the gas, Φ_g is the volume fraction of gas in the polymer, C_D is the Henry's law constant at low pressure, and χ is the Flory-Huggins parameter (Barbari & Conforti, 1994).

2.3.2 Sorption below the glass transition – glassy polymers

Amorphous polymers below T_g are considered to be in a glassy state. The sorption behavior of gases in a glassy polymer is highly nonlinear and, even at low penetrant pressures, cannot be adequately described by the Henry's law. It strongly depends on the thermal and mechanical history of the glassy polymer. There are various models used to

describe gas transport in glassy polymers: the matrix model, the free-volume theory, and the dual mode sorption model. The free-volume theory and the dual mode sorption have been highly successfully applied in the analysis of sorption, unsteady and steady-state permeation in glassy polymers (Kesting & Fritzsche, 1993).

The concept of free volume in a polymer is an extension of the ideas of Cohen and Turnbull, which were first used to describe the phenomenon of self-diffusion in a liquid system. The penetrant gas is assumed to diffuse by a cooperative movement between the polymer segments, from one "hole" to the other. The creation of a "hole" is caused by fluctuations of local density due to thermal motion. According to the free-volume theory, the movement of gas molecules depends on the free volume available, as well on the availability of energy sufficient to overcome polymer-polymer attractive forces. The free volume represents micropores available for the motion of polymer segments and diffusive jumps of gas molecules. For many polymers, the fraction of free volume at the glass transition temperature is approximately 0.025 (Kesting & Fritzsche, 1993).

The dual mode sorption theory postulates the existence of two types of sorption sites in a glassy polymer. The first type of sorption sites represent normally densified regions of the polymer, which accommodate mobile gas molecules following Henry's law. The other sorption sites, Langmuir sites, are unique to glassy polymers, and are correlated with the abrupt change in slope of the specific volume versus temperature curve as the T_g is traversed. The Langmuir sorption sites are associated with micro voids or excess free volume formed from inter-segmental packing defects. The gas molecules sorbed in the Langmuir sites are much less mobile than those in the Henry's sites. However, the two sorbed gas populations are in a rapid equilibrium throughout the membrane (Kesting & Fritzsche, 1993).

Total solubility of gases in glassy polymers is higher than in rubbers, which is consistent with the existence of additional sorption sites in glasses. The enthalpy for sorption in the Langmuir sites is higher than that in Henry's sites. Therefore, the gas sorption in glassy polymers is substantially more exothermic than in rubbers (Kesting & Fritzsche, 1993).

2.4 *Dependence of gas permeability and selectivity on various factors*

The gas permeability and selectivity of polymeric membranes depend on various factors such as condensability, polarity, size, shape, temperature and pressure of penetrants, as well as free volume, chain mobility, crystallinity and crosslinking of polymers.

The solubility coefficient in polymers generally increases with increasing condensibility of gases. The critical temperature (T_c), normal boiling point, or Lennard-Jones force constant are all measures that correlate well with the solubility coefficient. For example, in most polymers CO_2 (T_c = 31°C) is more soluble than CH_4 (T_c = -82.1°C), O_2 (T_c = -118.4°C) or N_2 (T_c = -147°C) (Ghosal & Freeman, 1994).

Gas solubility is also sensitive to specific interactions between the gas molecules and polymer chains. The molecule of CO_2, which has a quadrupole moment, is in general more soluble in polar polymers. Van Amerongen (1950) studied the gas solubility in rubbery poly(butadiene-co-acrylonitrile) as a function of polar acrylonitrile group concentration in the polymer. He found that the solubility of non-polar gases such as N_2, O_2 and H_2 decreases as acrylonitrile concentration increases. On the other hand, solubility of CO_2 increases substantially with increasing acrylonitrile concentration (Amerongen, 1950).

The diffusion coefficient usually decreases with increasing penetrant size. The penetrant size is characterized by Van der Waals volume of the molecule. For example, the Van der Waals volumes of CO_2 and CH_4 are estimated to be 17.5 and 17.2 cm^3/mole. These molecular volumes yield equivalent spherical diameters of 3.33 and 3.31Å, respectively. However, the permeability of CO_2 is typically greater than that of CH_4, because the kinetic diameter of CO_2 (3.30 Å) is smaller than that of CH_4 (3.80 Å). The kinetic diameters of O_2 and N_2 are 3.46 and 3.64 Å, respectively. The kinetic diameter corresponds to the smallest diameter in a zeolite window that allows the gas molecule to enter a zeolite cavity. The diffusion coefficient in polymers is also sensitive to penetrant shape. The diffusivity of linear penetrant molecules such as CO_2 is higher than the diffusivity of spherical molecules of equivalent molecular volume (Chern & Brown, 1990).

The diffusivity coefficient increases appreciably with increasing temperature, unless the polymer undergoes a thermally induced morphological rearrangement such as crystallization over the temperature range of interest. However, the diffusive selectivity decreases as the temperature increases, because increasing temperature elevates the diffusivity of less mobile components more than the diffusivity of the more permeable components (Fritzsche & Kurz, 1990).

The diffusivity, solubility and permeability coefficients vary with the pressure of penetrant in contact with the polymer. For example, the permeability coefficient of CO_2 in polyimides decreases monotonically with increasing pressure (Koros & Hellums, 1989). The decrease in permeability coefficient with pressure is consistent with the dual mode sorption.

Crystalline regions in polymeric membranes reduce the diffusivity and solubility coefficients; hence their presence reduces the permeability coefficient in polymeric membranes. Crosslinking in a polymer also reduces the diffusion coefficient, because it reduces polymer segmental mobility (Stannett, 1968).

2.5 Correlation of separation factor versus permeability for polymeric membranes

On the basis of an exhaustive literature survey, Robeson (1991) developed the "upper bound" concept for different pairs of gases. This concept limits the separation factor (α_{ij}) for a given permeability coefficient (P_i) of the more permeable component. The plot of log α_{ij} versus log P_i yields an upper bound (i.e., a straight line on the log-log plot) above which no data, or very limited data exited at the time Robeson published his work. The closer the data point to the upper-bound line, the better the membrane material for the specific separation. The upper-bound line is given by the following:

$$P_i = k\alpha_{ij}^n \tag{2.11}$$

where k and n are the constants depending on the pair of gases. The numerical values for these constants are listed in Table 2.1.

Table 2.1: The k an n values of several gas pairs for upper-bound line relationship (Robeson, 1991)

Gas pair	k (Barrers)	n
O_2/N_2	389,224	-5.800
CO_2/CH_4	1,073,700	-2.6264
He/N_2	12,500	-1.0242
H_2/N_2	52,918	-1.5275
He/CH_4	5,002	-0.7857
H_2/CH_4	18,500	-1.2112
He/O_2	4,600	-1.295
H_2/O_2	35,760	-2.277
He/H_2	960	-4.9535

Rearrangement of Eq. (2.11) leads to the following expression:

$$\alpha_{ij} = k^{-1/n} P_i^{1/n} \tag{2.12}$$

A trend exits between n and the difference in kinetic diameters of gas molecules in the mixture. According to Robeson (1991),

$$-\frac{1}{n} = d_j - d_i \tag{2.13}$$

where d_j and d_i are the kinetic diameters of the slower and the faster gas, respectively.

CHAPTER 3 Properties of PPO and PPO-Based Polymers

3.1 Introduction

Gas separation membranes can be made from a large number of different organic and inorganic materials. However, only polymeric membranes are currently being used in industrial separations (Stern, 1994). The choice of a given polymer as a membrane material is not arbitrary, but based on very specific properties originating from structural factors that determine the thermal, chemical, and mechanical properties, as well as permeability (Mulder, 1991). For an ideal gas separation, high permeability, high selectivity and durability are desirable. The following sections review the basic definitions and concepts related to polymers and polymer properties. This general review is followed by a more specific discussion on synthesis and properties of polymers from the PPO family, and the properties of the PPO-based membranes.

3.2 Polymers

A polymer is a high molecular weight component built up from a number of basic units, the mers or monomers. The number of structural units linked together to form the "long chain molecule" is defined as the degree of polymerizations. The term macromolecule, or "big molecule," is also used.

A polymer made from only one kind of monomer is called a homopolymer. A polymer containing two or more kinds of monomers is called a copolymer. A copolymer can be combined in various ways and a number of different structures can be distinguished. When the sequence of the structural units is completely irregular, the copolymer is said to be random. The properties of a random polymer can strongly depend on the molar ratios of different monomers. An example of a random copolymer is ABS (acrylonitrile-butadiene-styrene rubber). The other type of copolymer is a block copolymer. In block copolymers, the chain is built up by linking blocks of each of the

monomers. An example of a block copolymer is SIS (styrene-isoprene-styrene) (Mulder, 1991).

A polymer can be either linear or branched. It is generally held together as large molecules by covalent bonds; meanwhile, the separate molecules, or segments of the same molecule, are attracted to each other by intermolecular forces or Van der Waals forces. Covalent bonds are characterized by high energies (35 to 150 kcal/mol), short interatomic distances (0.11 to 0.16 nm), and relatively constant angles between successive bonds. Covalent bonds generally govern the thermal and photochemical stability of the polymer. Bond strength can be used as a clue to degradation mechanisms. For example, sulfur-vulcanized rubber is more likely to degrade through comparatively weak –S–S- bonds rather than strong –C-C- bonds. Secondary forces are more difficult to characterize because they operate between molecules or segments of the same molecule, rather than being localized to a pair of atoms. The secondary forces increase in the presence of polar groups, and decrease with an increase in distance between molecules. These forces determine most physical properties of polymers – for example, melting point and solubility, as well as adsorption, diffusion and deformation properties (Rodriguez, 1996).

It is also possible to connect two or more chains to each other by means of crosslinks. Crosslinking often occurs via chemical reactions. Physical crosslinks can also exist, for example, in semi-crystalline polymers where the crystallites act as crosslinks, or in block copolymers where the domains of the dispersed phases act as physical crosslinks.

3.3 Polymer-solvent interactions

Polymeric membranes are most commonly prepared from polymer solutions. The properties of polymer solutions – in particular, polymer-solvent interactions – may have strong influence on the macrostructure and thus properties of the final membrane. A polymer dissolves in two stages. First, solvent molecules diffuse into the polymer, swelling it to form a gel state. Then the gel gradually disintegrates, and the molecules diffuse into the solvent- rich regions. The concentration of the final solution depends on

the relative proportions of polymer and solvent. The dissolving of polymer material is governed by the free energy of mixing,

$$\Delta G_m = \Delta H_m - T\Delta S_m \tag{3.1}$$

where ΔG_m is the Gibbs free energy of mixing, ΔH_m is the enthalpy of mixing, T is the absolute temperature, and ΔS_m is the entropy change of mixing. A negative ΔG indicates that a process will occur spontaneously. The dissolution of a high-molecular polymer is always associated with a large increase in entropy; therefore, the magnitude of enthalpy term is a deciding factor in determining the sign of the Gibbs free energy. Hildebrand (1950) proposed that,

$$\Delta H_m = V_m \left[\delta_1 - \delta_2\right]^2 \phi_1 \phi_2 \tag{3.2}$$

where V_m is the molar volume of the mixture, ϕ is the volume fraction, δ is the solubility (Hildebrand) parameter defined by Eq. (2.4), and subscripts 1 and 2 indicate the polymer and solvent, respectively. According to Eq. (2.4), δ increases with increase in the heat of vaporization (ΔE). From the physical point of view ΔE indicates the degree of attraction between molecules in a liquid phase. Considering Eq. (3.1) and (3.2), it becomes evident that the polymer becomes more soluble in a solvent when their respective Hildebrand parameters are close to each other.

The difference between the solubility parameters of polymer and solvent is an indication of "strength" of solvent in a given polymer solution. When this difference is small, the solvent is considered to be strong. As the difference increases, the solvent becomes "weak" and eventually "non-solvent" for the polymer. The solvent strength is therefore a measure of the polymer-solvent interactions.

Hansen (1969) and Hoy (1970) proposed that solubility parameter could be divided into dispersive (δ_d), polar (δ_p) and hydrogen bond (δ_h) components using the following expression:

$$\delta = \sqrt{\delta_d^2 + \delta_p^2 + \delta_h^2} \tag{3.3}$$

The solubility parameter and its components can be calculated by applying additive rules to the structural components of the repeat unit of the polymer and to those of the solvent molecule, using the following equations:

$$\delta_d = \sum F_{di} / V \tag{3.4a}$$

$$\delta_p = \sqrt{\sum F_{pi}^2} / V \tag{3.4b}$$

$$\delta_h = \sqrt{\sum E_{hi} / V} \tag{3.4c}$$

where V is the molar volume, and F_{di}, F_{pi}, E_{hi} represent the London dispersion forces, the dipole forces, and the hydrogen bonding forces respectively.

The intrinsic viscosity $[\eta]$ of a given polymer-solvent system, which is often used as an experimental measure of polymer-solvent interaction, is defined as:

$$[\eta] = \lim_{c \to 0} \eta_{rel} = \lim_{c \to 0} \frac{\eta - \eta_s}{c\eta_s} \tag{3.5}$$

where η and η_s are the viscosities of solution and solvent, respectively, and c is the concentration of polymer solution. The intrinsic viscosity increases with an increase in solvent strength. Equilibrium configurations of molecular chains, both in swelling situations and in polymer solutions, depend on the balance between the Gibbs free energy change due to mixing, and that due to elastic deformation. The degree of deformation depends on the relative strengths of intramolecular (segment-segment) and intermolecular (segment-solvent) interactions. In a "strong" solvent, the polymer is unfolded, because of more favorable polymer-solvent interactions. This leads to an increase in viscosity. In a "weak" solvent, the polymer remains folded because of more favorable intramolecular interactions.

The intrinsic viscosity also depends on the properties of isolated polymer molecules, and is related to the viscosity average molecular weight of a polymer (M_v) by the Mark-Houwink expression,

$$[\eta] = K_v M_v^{a_v} \tag{3.6}$$

where K_v and a_v are the constants evaluated by double logarithmic plots of $[\eta]$ against M_v. The constant K_v depends on the characteristics of the polymer and solvent, while the exponent a_v is a function of the shape of the polymer coil in the solution; it also depends on the strength of the polymer-solvent interactions. The exponent a_v ranges from 0.5 in theta weak solvents, through approximately 0.65 in "intermediate" solvents and

approximately 0.8 in "strong" solvents. Eq. (3.6) can also be written in terms of the number average molecular weight (M_n) and the weight average molecular weight (M_w).

$$[\eta] = K_n M_n^{a_n} \tag{3.7}$$

or

$$[\eta] = K_w M_w^{a_w} \tag{3.8}$$

where K_n, K_w and a_n, a_w have similar meaning as K_v and a_v, respectively.

Flory-Huggins (1953) showed that the intrinsic viscosity for a given polymer-solvent system is related to the difference in solubility parameters through the following expression:

$$\log[\eta] = B \log|\delta_1 - \delta_2| + A \tag{3.9}$$

where B and A are constants that depend on the type of polymer and its concentration, but are independent of the nature of the solvent.

3.4 Macromolecular architecture

The macromolecule architecture of a polymer is determined by the molecular weight and the molecular weight distribution, conformation of the polymer chain in space, configuration, and the composition (if applicable) of the copolymer (Kesting & Fritzsche, 1993).

3.4.1 The average molecular weight of polymers

The chain length and molecular weight are important parameters in determining the properties of a polymer. There are three common ways of averaging the molecular weight of a polymer: the number average molecular weight (M_n), the weight average molecular weight (M_w), and the z-average molecular weight (M_z). These terms are defined below in terms of the number of molecules N_i having the molecular weight M_i. The ratio of M_w and M_n is a measure of the broadness of the molecular weight distribution. The ratio M_w/M_n is called the polydispersity index (PDI).

$$M_n = \sum_i N_i M_i$$
$$M_w = \frac{\sum_i N_i M_i^2}{\sum_i N_i M_i} \qquad (3.10)$$
$$M_z = \frac{\sum_i N_i M_i^3}{\sum_i N_i M_i^2}$$

3.4.2 Configuration and conformation

In general, changes in the structure caused by the rotation around single bonds are termed conformations, and isomers that cannot be interchanged without bond-breaking are termed configurations.

In many polymers, the main chain consists entirely of –C-C- bonds. Rotation about each –C-C- bonds is possible, which makes the chain rather flexible. When the chain consists of –C=C- bonds, no rotation is possible and a very rigid chain is obtained. When the chain contains both –C-C- and –C=C- bonds, rotation about –C-C- is still possible and the chain is also flexible. When there are aromatic groups attached to the main chain as side groups, the rotation around the main chain can take place, but the degree of rotation will depend on whether or not steric hindrance occurs. If steric hindrance occurs, the chain flexibility will decrease substantially. The size and shape of bulky groups in both the polymer main chain and the side chains determine fundamental polymer characteristics such as packing density, the rigidity of polymer chain segments, and the accessibility, and hence the participation of functional groups in membrane-penetrant interactions (Kesting & Fritzsche, 1993). If the side group is bulky, it tends to increase interchain displacement and lower the packing density. The absence of bulky groups can lead to an increase in structural regularity, which usually results in the condition of maximum packing density. Also, the more polar the groups, the greater force of attraction between them. Because polarity leads to an increase in net forces of attraction between macromolecules, interchain displacement (d-spacing) and free volume in polar polymers tend to be smaller, assuming everything else to be equal, than they are in non-polar systems (Kesting & Fritzsche, 1993).

The presence of oxygen and nitrogen in the main chain increases chain flexibility, but often aromatic groups are also present at the same time and they tend to dominate the structure, giving the chain a rigid character (Mulder, 1991).

Hence the overall shape and size of the chain, and many of its motions, are determined by its conformation. The configuration properties of a polymer determine if it is crystallizable and, if so, its melting temperature.

3.4.3 Physical states and transitions

The physical state of a polymer is a very important parameter for its mechanical, chemical, thermal and permeation properties. The state of the polymer is defined as the phase in which the polymer appears. There are three basic states in which the polymer can appear: glass, melt or rubber, and crystalline. In glassy state, the rotations around single bonds are impossible. In melt or rubbery state, the polymer chains are in a continuous motion. The energy barrier that a constituent of one chain encounters when it tries to move past a constituent on an adjacent chain is not sufficient to prevent the rotation around single bonds. The higher the temperature, the more intense the molecular motions. In crystalline state, polymer molecules may fit together in such a way that intermolecular attractions stabilize the chains in a regular lattice, even though there are negligible intramolecular barriers to the rotations around single bonds.

The glass transition temperature (T_g) and the melting temperature (T_m) are the two major transition temperatures. The T_g is the temperature below which the free rotations cease because of the intramolecular energy barriers. The T_m is the highest temperature at which a crystal lattice is stable (Rodriguez, 1996).

Segmental mobility, polarity, and chain stiffness affect the T_g of an amorphous polymer. Polymers with high polarity, or high cohesive energy density, have higher T_g than nonpolar materials. Bulky side groups, which hinder rotations around single bonds, also tend to increase T_g. When the single bonds in the polymer chain are replaced by the double bonds, T_g also increases, because double bonds increase the chain stiffness.

For a copolymer in which the monomer units are distributed in a random fashion, polarity and the chain stiffness are roughly the average of those for the individual

homopolymers. Gordon and Taylor proposed the following empirical equation for the calculation of the T_g of copolymer that contains two different monomers.

$$T_g = \frac{w_1(T_g)_1 + kw_2(T_g)_2}{w_1 + kw_2} \tag{3.11}$$

where k is a fitted constant and w is weight fraction of each monomer.

When $k = 1$, a linear relationship results. When $k = (T_g)_1/(T_g)_2$ (using the absolute temperatures), a reciprocal relationship is obtained:

$$\frac{1}{T_g(\text{copolymer})} = \frac{w_1}{(T_g)_1} + \frac{w_2}{(T_g)_2} \tag{3.12}$$

The relationship can be extended into a system with more than two monomers by adding another constant for each additional monomer (Rodriquez, 1996).

3.5 Synthesis and properties of polyphenylene oxides and polyphenylene oxide based polymers

3.5.1 Development of polymers for gas separation membranes

For any membrane-based separation process to be successful, the membrane must possess two key attributes: high permeability and good selectivity, as well as durability. Selectivity depends in part on the difference in penetrants' size, and their solubility in the membrane. While both high permeability and high selectivity are desirable, a general trade-off relationship exists: high permeability is generally associated with low selectivity, and vice versa. There are three possible directions when choosing a membrane material: the utilization of existing polymers, the modification of existing polymers, or the synthesis of new polymers to suit a particular application. Among the many aromatic polymers having high T_g, poly(2,6-dimethyl-1,4-phenylene oxide) (DMPO) has one of the highest permeability to gases.

3.5.2 Properties of polyphenylene oxides

The DMPO is the best-known representative of the family of polyphenylene oxides. It has been commercialized by the General Electric Company under the trade name of PPO. In this thesis, however, the name PPO is used in reference to the family of

polyphenylene oxides, which apart from the DMPO includes homopolymers and copolymers synthesized from any 2,6-disubstituted phenol or phenols. The other polymers belonging to the PPO family include poly(2,6-diphenyl-1,4-phenylene oxide) (DPPO), and copolymers of 2,6-dimethylphenol and 2,6-diphenylphenol. The DMPO is also used as a component of polymer blends. For example, it forms a completely miscible blend with polystyrene, which has been commercialized as a Noryl resin. The Noryl resin is also one of the five major engineering thermoplastics manufactured today (Hay, 1986).

The DMPO has a glass transition temperature T_g ranging from 205 to 210°C (Karasz & O'Reilly, 1965). It is ductile below its T_g and has high impact strength, even down to -200°C. This ductility has been attributed to low temperature transitions assigned to hindered oscillatory motions of the backbone phenylene groups (Laupretre & Monnerie, 1974). The DMPO isolated by the precipitation in methanol has a degree of crystallinity ranging from 5 to 15%. When cooled from its melt, DMPO has practically no crystallinity. The thermal properties of a typical DMPO are given in Table 3.1.

Table 3.1: Thermal properties of typical DMPO

Property	Value
Glass transition temperature T_g, °C	205
Crystal melting temperature T_m, °C	267
Thermal conductivity, W/(m K)	0.192
Coefficient of thermal expansion, K^{-1}	5.2×10^{-5}

The DMPO is soluble in toluene, benzene and halogenated hydrocarbons. Its solubility parameter is between 9.5 and 10.21. The DMPO also dissolves in methylene chloride, but forms an insoluble complex with this solvent at room temperature. This characteristic is used to separate DMPO from the polymer blends.

The DMPO is a linear amorphous thermoplastic with a free phenolic hydroxyl on the head group of each polymer chain. The hydroxyl groups in DMPO undergo the usual reactions, such as ester formation with anhydrides or acid chloride.

The DPPO is synthesized by oxidizing 2,6-diphenylphenol, which is similar to the synthesis of DMPO. It has T_g in the range of 220-235°C. The DPPO can be amorphous or semicrystalline. Above T_g, the DPPO rapidly crystallizes, and then melts at 480°C (Hay, 1969). A summary of the thermal properties of a typical DPPO are given in Table 3.2.

Table 3.2: Thermal properties of typical DPPO (Warsidlo, 1971)

Property	Value
Glass transition temperature T_g, °C	225
Crystal melting temperature T_m, °C	480
Coefficient of thermal expansion below T_g, per °C	45.5×10^{-6}
Coefficient of thermal expansion above T_g, K^{-1}	102×10^{-6}

3.5.3 Synthesis DMPO and DPPO

DMPO (1) is prepared by the oxidative coupling polymerization of 2.6-dimethylphenol. The 2,6-dimethylphenol is preferred as a monomer over phenol, because the latter is multifunctional and a combination of C-C and C-O coupling reactions as well as hydroxylation reactions can take place (Hay, 1998). The 2,6-dimethylphenol is also preferred over other substituted phenols. When the substituents are large and bulky, the polymer cannot form because of steric hindrance and instead, diphenoquinone forms in high yields. No oxidation occurs when both substituents are chloro or nitro. Polymerization of 2,6-dimethylphenol results in high molecular weight, and linear DMPO, along with small amounts of the C-C coupled byproduct, the diphenoquinone (2).

The 2,6-dimethylphenol is polymerized at 25-50°C by passing oxygen through a vigorously stirred solution of monomer containing a catalyst. A typical catalyst is composed of a copper halide salt and one or more aliphatic amines, or pyridine. A desiccant, such as anhydrous magnesium sulfate, can be used along with the catalyst, when the catalyst is susceptible to hydrolysis. Magnesium sulfate also removes water formed in the polymerization reaction.

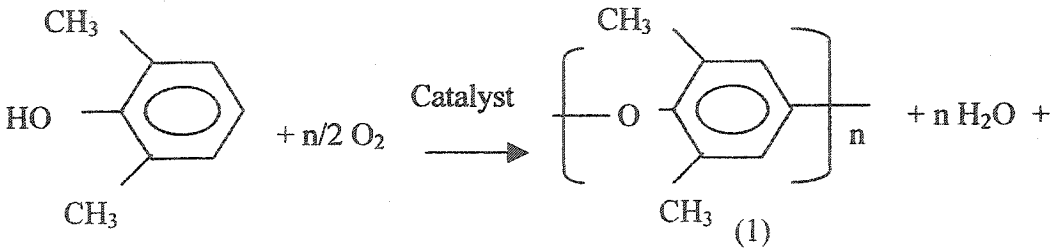

(1)

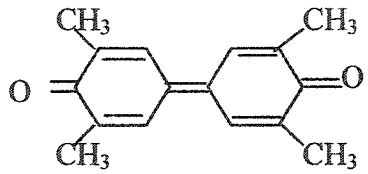

(2)

It has been noted that with monodentate amines, the catalytic activity varied with the ligand to copper ratio (Hay, 1967). With pyridine as ligand, the C-O coupling reaction was optimum at a ligand/Cu ratio of about 100/1 (Finkbeiner et al., 1966). With a bidentate amine such as N,N,N',N'-tetramethylethylene diamine (TMEDA), the C-O coupling reaction has maximized at one diamine per copper. When the polymerization was carried out in a nonpolar solvent such as toluene with an active catalyst like Cu/TMEDA, in the presence of anhydrous $MgSO_4$ to remove the water formed, only a low molecular weight polymer was formed (Hay, 1998). If more polar solvents, such as chlorobenzene or o-dichlorobenzene, were used, higher molecular weight was formed. When larger amounts of TMEDA were added, the molecular weight obtained was further increased. It was shown that as the temperature increases from 25 to 100°C, the reaction changes from the one that predominantly gives C-O coupling to the one that predominantly gives C-C coupling (Hays, 1998).

A variety of mechanisms of the oxidative polymerization reaction have been proposed. These include ionic intermediate, free radical processes, and step growth polymerization mechanisms.

The free radical mechanism (Finkbeiner et al., 1961) includes three stages: an initiation, when the radicals are formed; a propagation, when the products are developed;

and termination, when the radical reaction ends. The free radial mechanism has been most often used to describe the oxidation of 2,6-dimethylphenol. For the oxidation of 2,6-dimethylphenol, in the initiation stage, aryloxy radicals form by oxidation of the monomer using the catalyst; aryloxy radicals react further to form a quinol ether (3), which enolizes to form dimer (4). The oxidation produces the dimer radical, which couples with other radicals present. If it coupled with a 2,6-dimethylphenoxy radical to form quinol ether, enolization would produce the trimer. Oxidation of trimer, followed by coupling with a 2,6-dimethylphenoxy radical, produces tetramer. Higher oligomers convert to the next higher oligomers until high molecular weight is achieved. Coupling could also occur between combinations of oligomers to form ketal. The redistribution reactions of oligomers, ketal formation and sequent dissociation will generate terminal quinol ethers that enolize to the more stable terminal phenol. The enolization drives the reaction to higher molecular weight in two ways. First, it provides both the driving force for the coupling of two oligomeric radicals by forming more stable phenol-terminated oligomers of higher molecular weight than either individual oligomer. Second, it produces a phenolic group that can be oxidized to generate a new aryloxy radical, which enters the redistribution-enolization scheme. The second process occurrs concurrently with the dissociation-redistribution process as an intramolecular rearrangement, in which cyclohexadiene groups appear to move along a polymer chain (Aycock, Abolins & White, 1994).

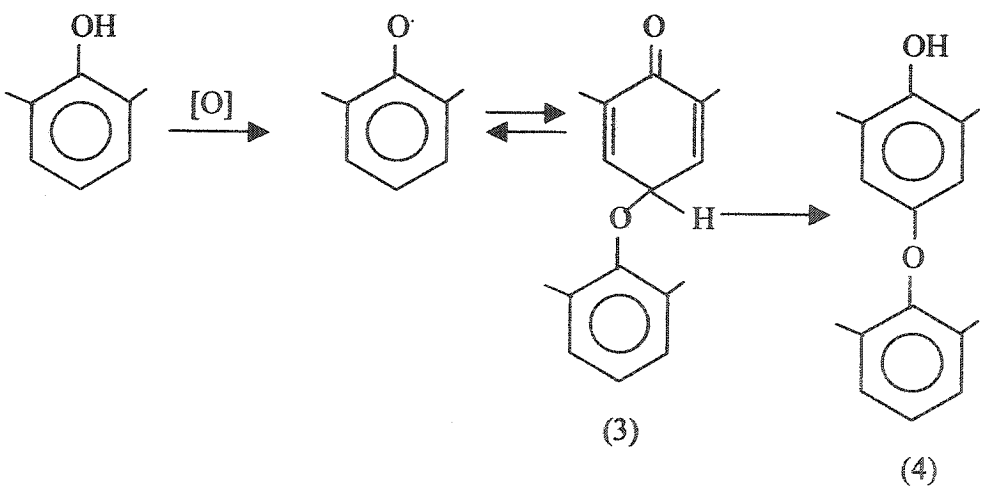

(3) (4)

The kinetic behavior in this polymerization system resembles the Michaelis-Menten model (Mobley, 1984). The rate of oxidative coupling polymerization has been studied by the measurement of the oxygen uptake. The studies showed that the rate of oxygen uptake remained constant, indicating that the reaction was terminated in the very last stage. The assumption was made that initially the catalyst was soluble in the reaction mixture, because of the presence of the polar phenol. In the later stages of the reaction, when the phenol was no longer present, the catalyst became insoluble.

Endres and Kwiatek (1962) showed that oxidation of 2,6-dimethylphenol behaved like a step-growth polymerization. They showed that oxidation of the dimmer, 4 (2,6-dimethoxyl) 2,6-dimethylphenol gave a high molecular weight polymer. Cooper (1965) showed that in the initial stages of the oxidation of the dimmer, an equilibration occurred and monomer, dimer, trimer, and tetramer could be detected by gas phase chromatography.

The DPPO (5) can be prepared by the oxidative coupling polymerization of 2,6-diphenylphenol. The oxidation is carried in oxygen with an equimolar amount of TMEDA and copper (I) bromide as catalyst. Hays (1969) observed that as the temperature of the reaction mixture was raised, a polymer with a higher intrinsic viscosity was obtained and above 60°C, high molecular weight polymers were readily obtained with only a small amount of the diphenoquinones (6) as a by-product.

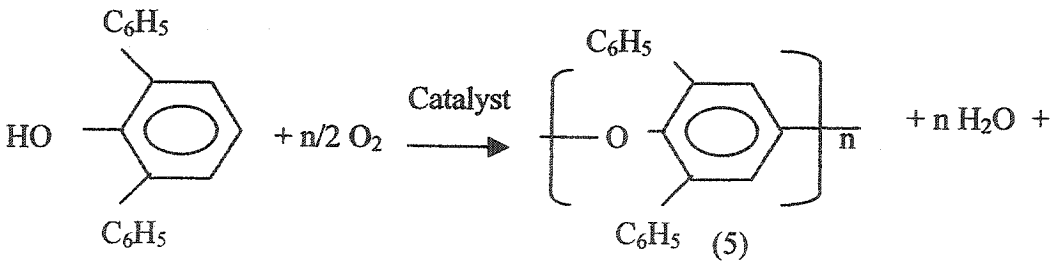

(5)

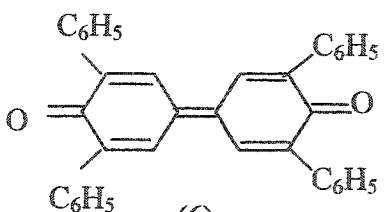

(6)

Copolymers are prepared by oxidation of a mixture of two different phenols simultaneously. The phenylene ether-repeating units are usually arranged randomly in the backbone chain. The formation of block copolymers has also been reported. The formation of block copolymers required a more active polymerization catalyst. Typical examples include polymer from the following phenol pairs: 2,6–dimethylphenol - 2,6-diphenylphenol, 2,6-dimethylphenol - 2-methyl-6-phenylphenol, 2,6-diphenylphenol - 2-methyl-6-phenylphenol, 2,6-dimethylphenol-2-allyl-6-methylphenol.

The block copolymers of DMPO and DPPO require tetramethylbutanediamine-cuprous bromide as a catalyst, because it provides the oxidative coupling of DMPO at 25°C, much faster than its redistribution with polymers to form DPPO (Cooper et al., 1969).

3.5.4 Gas separation membranes from DMPO and modified DMPO

As a material for gas separation membranes, the PPO family – especially DMPO – exhibits one of the highest rates of permeability to gases among glassy polymer. The presence of aromatic groups in the main polymer chain is responsible for high T_g and rigidity of polymers from the PPO family. The high impact strength of these polymers results from rapid conformational transitions by the phenyl rings rotating freely about –C-O bonds. The PPO membranes have excellent chemical and thermal stability (Mulder, 1991).

The high permeability to gases for DMPO is due to the large diffusion coefficient of gases in this polymer as compared to other glassy polymers with a rigid backbone. However, there is a substantial scatter of the permeability data observed by different authors. This could be due to the fact that DMPO can crystallize under some conditions and the variation in the crystallinity can cause the changes in the permeability data. The permeability ratio of CO_2/CH_4 for dense membranes prepared from DMPO has been reported to be in the range of 12-18.5, which is rather low compared to other glassy polymers. The DMPO is also not soluble in conventional membrane formulation solvents.

Percec and Li (1988) chemically modified DMPO by a variety of electrophilic substitution such as bromination, sulfonylation and acylation on the aromatic ring. They

also examined the gas permeation properties, polymer solubility, and thermal behavior of the modified and unmodified DMPO. They found that as the degree of bromination increases, the T_g of the modified polymer increases. The maximum value of 273°C was obtained for 100% brominated DMPO. The CO_2 permeability and the CO_2/CH_4 selectivity increased with an increase of the degree of bromination. For membranes prepared from a 100% substituted polymer (BrDMPO), they reported the CO_2 permeability of 158.08 Barrer and the CO_2/CH_4 permeability ratio of 23.73. These values correspond to 250% of the CO_2 permeability coefficient and 150% of the CO_2/CH_4 permeability ratio, respectively, of the unmodified DMPO. Aryl bromination of DMPO and the properties of BrDMPO were also studied by Chern et al. (1987). They found that the solubility of CO_2, CH_4, and N_2 in BrDMPO increased with increasing extents of bromination, and the change was larger for gases with lower condensability.

For sulfonylated DMPO (SDMPO) membranes, Percec and Li (1998) found that the membranes exhibited generally a lower CO_2 permeability and a higher CO_2/CH_4 selectivity compared to DMPO. The nature of the sulfonyl group had a stronger influence on the permeation properties than the degree of substitution. The best permeation properties were obtained for DMPO containing phenyl sulfone groups. The presence of $-SO_2(OH)$ groups reduced the CO_2 permeability by a factor of three. This was explained by the decrease in local segmental mobility of the polymer chains due to the interactions arising from hydrogen bonding. They also found that the degree of substitution, main chain rigidity, bulkiness, flexibility and polarity of side chains were the major parameters controlling the gas permeation properties of modified DMPO polymers.

Even though DMPO has an excellent CO_2 permeability and an adequate CO_2/CH_4 selectivity, it does not have a sufficient durability to be useful in natural gas separation applications. Morgan and Blinka (1990) developed vinyl substituted derivatives of DMPO (VDMPO), using methods developed by Percec et al. (1990). The modified polymer had similar permeability and selectivity as the base DMPO. The permeability of VDMPO ranged from 44.6 to 79.7 Barrer, while the CO_2/CH_4 selectivity ranged from 17.9 to 21.2. The VDMPO could also be crosslinked by ultraviolet, thermal, or electron beam radiation to improve its durability. Depending on the level of crosslinking, the polymer could be substantially insoluble in solvents – for example, toluene, which would

normally dissolve the uncrosslinked polymer. The solubility of the uncrosslinked VDMPO was improved in comparison to the solubility of DMPO.

Aguilar-Vega and Paul (1993) studied the gas transport properties of DMPO, DPPO and the thioether poly (1,4-phenylene sulfide) (PPS). The average molecular weight of DMPO was 39,000 and the corresponding T_g was 213°C. The intrinsic viscosity of DPPO in chloroform was 0.689 (dL/g), while its T_g was 229°C. The free volume of DPPO was found to be smaller than that of DMPO. Both DMPO and DPPO are amorphous materials. The authors determined that the symmetrical substitution of 1,4 phenylene oxide at the positions 2,6 increased the permeability of the polymer. The permeability increase in cases of smaller methyl substituents (DMPO) was greater than that in cases of larger phenyl substituents (DPPO). The CO_2 permeability and the CO_2/CH_4 permeability ratio at 1.5 atm and 35°C for DPPO membrane were 39.9 Barrer and 14.8, respectively. The O_2 permeability and the O_2/N_2 permeability ratio at the same conditions were 7.7 Barrer and 4.9, respectively. The DPPO was found to be more thermally stable than DMPO.

Alentiev et al. (1998) also studied the gas transport properties of DMPO and DPPO, as well as their random copolymers in the molecular ratios of DPPO and DMPO units of 2.5/97.5 and 25/75. The viscosity average molecular weight of the polymers was in the range of 100,000-120,000, and the purity of all synthesized polymers was greater than 99.9%, with the major impurities being diphenoquinone and traces of the copper catalyst. Using the x-ray diffraction method, the authors found that DMPO and DPPO homopolymers were semicrystalline materials, but all the copolymers were completely amorphous. A distinction between the behavior of an amorphous and a semicrystalline polymer is that in the semicrystalline polymer, the diffusion coefficients of different gases hardly change and all the variation of the permeability values is induced by the changes in the solubility coefficient, whereas the permeability of amorphous polymers changes due to the variation of both the diffusion and solubility coefficients. The substitution of methyl by phenyl side groups resulted in a decrease in permeability. A monotonous decrease in permeability independent of crystallinity was also observed. This was explained assuming that local transport parameters of the crystalline and amorphous regions in PPO do not differ as greatly as in the case of polyethylene or other lower

polyolefins. The crystalline lattice of DMPO is packed relatively loosely in comparison to other polymers. This is indicated by the fact that the heat of melting and entropy of melting of DMPO are lower than those for other semicrystalline polymers (Janeczek et al., 1978). It was also observed that the chemical structure of the side groups in PPO exerts a much stronger influence on the solubility coefficient than on the diffusivity coefficient. The CO_2 permeability coefficient and the CO_2/CH_4 permeability ratio in the DPPO membrane were 32.2 Barrer, and 33.3, respectively. The O_2 permeability coefficient and the O_2/N_2 permeability ratio were 4.3 Barrer and 4.9, respectively.

Ilinitch et al. (1998, 1999) studied the intrinsic micro porosity and the gas transport properties of DMPO and DPPO, as well as the random phenylene oxide copolymers containing DPPO and DMPO units in the molecular ratios of 2.5/97.5 and 25/75. Using the low-temperature nitrogen sorption technique, the authors suggested the presence of a continuous network of interconnected intermolecular micro cavities. To describe the microstructure of PPO, they used a "throat and cavity" model, in which a cavity may have several throats. The reported effective diameters of the "pore throats" were in the range of 0.4 nm at 77 K, increasing up to 0.5 nm at ambient temperature. Thus the micropores were accessible for the molecules of simple gases and vapors. The study revealed that PPO does not swell in N_2 at 77 K, but swells in propylene at room temperature. The swelling, at high relative pressures of the hydrocarbons, resulted in an increase of the effective diameter of micro pores, and gave rise to a sharp increase in the membrane permeability. Annealing of the swollen polymer membrane restored their initial pore structure and permeability.

3.5.5 Influence of molecular weight on properties of polymeric membranes

Another important aspect of polymeric membrane material is its molecular weight. In low molecular weight polymers, the polymer chains are more mobile because of less steric hindrance. As molecular weight increases, the concentration of chain ends decreases and in turn, the polymer free volume decreases. The T_g and solubility of gases in glassy polymers increase with increasing molecular weight. However, the diffusivity and solubility coefficients become insensitive to the changes in molecular weight (Ghosal & Freeman, 1993).

Chowdhury et al. (1999) prepared dense membranes from DMPOs having different intrinsic viscosities and thus different molecular weights. In addition, high molecular weight DMPO was chemically modified by bromination and sulfonation to form BrDMPO and SDMPO, respectively. The effect of the intrinsic viscosity on gas transport properties of DMPO and the effect of chemical modifications were investigated. The permeability coefficient of all studied gases (N_2, O_2, CH_4, CO_2) increased with increasing molecular weight of DMPO. On the other hand, the O_2/N_2 and CO_2/CH_4 permeability ratios were not influenced by the molecular weight of the polymer, and were 4.76-4.80 and 17.6-20.6, respectively. The observed results were consistent with the hypothesis of Kesting and Fritzsche (1993) that increases in the molecular weight, because of increases in chain entanglement and stiffness, should result in increases in the free volume of the polymer.

Permeability coefficients of high molecular weight BrDMPO were significantly greater than those of the base DMPO. At the same time, the CO_2/CH_4 and O_2/N_2 permeability ratios were also slightly greater as a result of bromination.

Sulfonation of high molecular weight DMPO brought about a significant decrease in permeability coefficient associated with an increase in the permeability ratios. This confirmed that the interaction of polar groups in polymer chains induces inter-chain interaction, with the effect being stronger in cases of sulfonated DMPO of higher degree substitution. In general, the effects of chemical modifications of high molecular weight DMPO, as reported by Chowdhury et al. (1999), were similar to those reported earlier by Perec and Li (1988) for low molecular weight DMPO.

Smid et al. (1991) prepared and studied integrally skinned hollow-fiber membranes prepared from DMPOs of different intrinsic viscosities. They reported that the O_2 permeance increased while the O_2/N_2 permeance ratio remained unchanged with the increasing intrinsic viscosity of the polymer. Polotskaya et al. (1996) also reported a similar relationship between the molecular weight and the permeability coefficients of DMPO.

PART II Methodology and Experimental Procedures

CHAPTER 4 Methodology and Experimental Procedures

This chapter includes descriptions of the materials used, experimental setups, polymer syntheses and some details of analytical methods used in this work, along with some theoretical considerations and definitions.

The experimental work was divided into the following parts:

i. Polymerization synthesis of poly(2,6-dimethyl-1,4-phenylene oxide) (DMPO) and poly(2,6-diphenyl-1,4-phenylene oxide) (DPPO)
ii. Synthesis of block copolymers with the targeted molar percentage of DPPO of 20%, 50% and 80%, respectively; and synthesis of block copolymers with the targeted molar percentage of DPPO of 25%, 50% and 75%, respectively
iii. Measurements of the intrinsic viscosity of synthesized polymers
iv. Determination of the molecular weight of polymers using a gel permeation chromatography technique and the composition of block and random copolymers using ^{1}H- NMR analysis
v. Preparation of dense membranes: determination of the best solvent for preparation of casting solutions and the optimum concentration polymer solution
vi. Characterization of the membranes from (v) in single gas permeation tests including N_2, O_2, CH_4 and CO_2
vii. Characterization of the thermal properties of the polymers using differential thermal analysis and differential scanning calorimetry analysis
viii. Development of steady-state model incorporating effects of back permeation through the membrane in constant pressure testing system

4.1 Polymer synthesis

4.1.1 Synthesis of poly- 2,6-diphenyl-1, 4-phenylene oxide (DPPO)

The DPPO was synthesized via oxidative polycondensation of 2,6-diphenylphenol (DPP). A mixture of 0.141 g (0.00061 mol) of cuprous bromide, 0.0865 g of N,N,N',N'-

tetramethyl-1,3-butanediamine (TMEDA), and 1.51 g of anhydrous magnesium sulfate was stirred at 40°C in 160 ml of benzene, with a vigorous stream of oxygen being introduced near the bottom of the flask. The solution had a yellowish color. After 5 minutes, 3.06 g (0.012 mol) of 2,6-diphenylphenol was added. The solution turned reddish. The reaction was carried out for four hours. The mixture was filtered and the polymer was precipitated in methanol. The polymer was then dissolved in chloroform and reprecipitated in methanol in order to remove the catalyst.

4.1.2 Synthesis of poly-2, 6-dimethyl-1,4-phenylene oxide (DMPO)

The DMPO was also synthesized via the oxidative polycondensation of 2,6-dimethylphenol (DMP). A mixture of 0.141 g (0.00061 mol) of cuprous bromide, 0.0865 g of N,N,N',N'-tetramethyl-1, 3-butanediamine (TMEDA), and 1.51 g of anhydrous magnesium sulfate was stirred at 25°C in 160 mL of benzene, with a vigorous stream of oxygen introduced near the bottom of the flask. The solution had a yellowish color. After five minutes, 3.06 g (0.012 mol) of 2,6-dimethylphenol was added. The solution turned reddish. The reaction was carried out for 1.5 hours. The mixture was filtered and the polymer was precipitated in methanol. The polymer was then dissolved in chloroform and reprecipitated in methanol in order to remove the catalyst.

4.1.3 Synthesis of block copolymers containing 2,6-diphenyl-1,4-phenylene oxide(DPPO) and 2,6-dimethyl-1,4-phenylene oxide(DMPO)

Block copolymers were synthesized via oxidative co-polycondensation, using 2,6-diphenylphenol and 2,6-dimethylphenol. A mixture of cuprous bromide, N,N,N',N' tetramethyl-1, 3-butanediamine and anhydrous magnesium sulfate was stirred at 25°C in 160 mL of benzene, with a vigorous stream of oxygen introduced near the bottom of the flask. The solution had a yellowish color. After five minutes, 2,6-diphenylphenol was added. The solution turned reddish. After three hours, 2,6-dimethylphenol was added and the polymerization continued for another two hours. The mixture was filtered and the polymer was precipitated in methanol. The amounts of chemicals used in the reaction are listed in Table 4.1.

Table 4.1: Quantities of chemicals used in synthesis block copolymers of 2,6-diphenylphenol and 2,6-dimethylphenol

DPPO: DMPO	DPP (g)	DMP (g)	CuBr (g)	TMEDA (g)	$MgSO_4$(g)
20:80	1.53	3.07	0.34	0.17	3.06
50:50	3.0	1.5	0.138	0.0852	1.57
80:20	3.31	0.41	0.1047	0.0852	1.52

4.1.4 Synthesis of random copolymers containing 2,6-diphenyl-1, 4-phenyleneoxide (DPPO) and 2,6-dimethyl-1, 4-phenylene oxide (DMPO)

Random copolymers were also synthesized via the oxidative co-polycondensation of 2,6-diphenylphenol and 2,6-dimethylphenol. The synthesis procedure was similar to that for the synthesis of block copolymers described above, with the molar ratios of monomers indicated in Table 4.2. Each monomer was first dissolved in benzene, and then two solutions were mixed together. The reaction time was five hours for all the copolymerization reactions. All of the chemicals were obtained from Aldrich and were used without any further treatment.

Table 4.2: Quantities of chemicals used in Random Copolymers of 2,6-diphenylphenol with 2,6-dimethylphenol

DPPO: DMPO	DPP (g)	DMP (g)	CuBr (g)	TMEDA (g)	$MgSO_4$ (g)
25:75	2.0	3.0	0.092	0.0568	1.51
50:50	3.0	1.5	0.17	0.0852	1.51
75:25	3.0	0.496	0.095	0.0866	1.51

4.1.5 Polymerization synthesis apparatus

All of the glassware used in the polymerization synthesis was sterilized in an oven at 80°C for one day prior to the experiments. The polymerization reactions were carried out in a fume hood, because benzene would evaporate during the reaction. Figure 4.1 shows the polymerization apparatus, which included a condenser, reaction flask, thermometer, hot plate, water bath, and oxygen gas cylinder. The reaction flask is used to contain the mixture of monomers. The reaction flask has three necks, and the

thermometer is placed in the first neck to monitor the temperature of the reaction mixture. The condenser consists of two concentric tubes that are mounted in second neck of the reaction flask in order to condense solvent vapors. The condensation of solvent vapors takes place in the inner tube, which is cooled by cold water flowing in the outer tube. A dispersion tube is placed in the third neck to supply oxygen. The reaction flask is placed in the water bath in order to minimize the temperature variation during the reaction. The water bath is placed on a hot magnetic plate to ensure a "good" mix during the reaction.

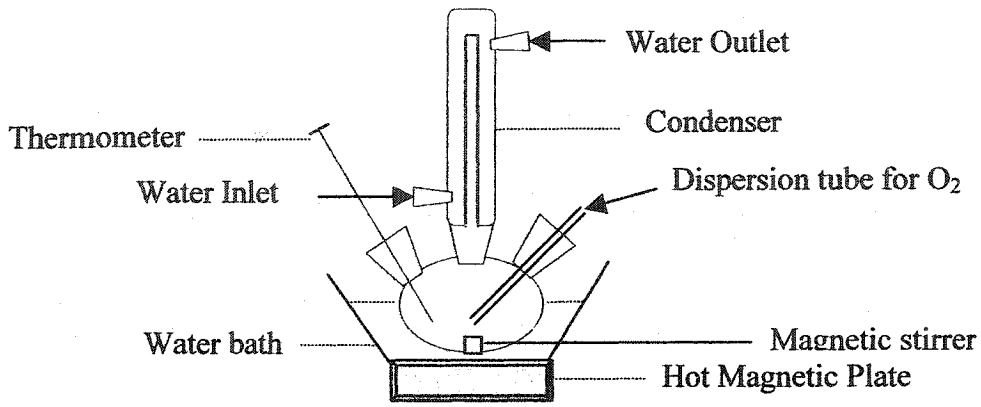

Figure 4.1: Schematic diagram of polymerization apparatus

4.2 Polymer characterization

4.2.1 Polymer-solvent interactions

Polymer-solvent interactions in polymer solutions were evaluated based on the difference between the solubility parameters of the polymer and solvent, and the intrinsic viscosity of synthesized polymers was also considered.

4.2.2 Comparison of solubility parameters

The difference between the solubility parameters was determined using the Hildebrand parameters (Δ) and the components of Hansen solubility parameters (Δ′)

$$\Delta = |\delta_P - \delta_S| \tag{4.1}$$

$$\Delta' = \sqrt{(\delta_{P,d} - \delta_{S,d})^2 + (\delta_{P,p} - \delta_{S,p})^2 + (\delta_{P,h} - \delta_{S,h})^2} \tag{4.2}$$

where subscripts P and S refer to the polymer and solvent, respectively; subscripts d, p, h refer to the dispersive, polar, and hydrogen bonding components of the Hansen solubility parameters.

The Hansen and Hildebrand solubility parameters were estimated using a group contribution approach. This method requires the decomposition of the repeat unit of the polymer into functional groups. In the cases of DMPO and DPPO, the repeat unit can be divided into phenyl, -O-, and $-CH_3$ groups. The details of determining the solubility parameters are presented in Appendix B.

4.2.3 Intrinsic viscosity measurements

Polymer was dissolved in chloroform to the concentration of 0.72 g/dL and filtered through a 3 μm pore size Teflon filter. A polymer solution sample of 4 g was placed in the Ubbelohde viscometer. The sample was kept in the viscometer for 10 minutes, to allow it to reach the temperature of the water bath (25°C). Suction was then applied to the viscometer leg containing the capillary, to force the solution about 5 mm above the upper timing mark. This step was performed very carefully, to avoid splashing of the solution in the upper bulb and the action of forming bubbles in the solution. The sample was then allowed to flow freely between the upper and lower marks indicated on the leg. The efflux time – that is, the time for the meniscus to pass from the upper to the lower mark – was recorded by a digital timer. After measuring the efflux time four times, the sample was diluted by adding a known weight of solvent. The initial polymer solution was diluted at least four times, and three efflux times were taken for each concentration. Apart from the efflux time of polymer solutions (t), the efflux time of the pure solvent (t_o) was also measured. Since the viscosity is directly proportional to the efflux time, η and η_o in Eq. (3.5) can be replaced by t and t_o, respectively, and η_{red} for each concentration of polymer solution calculated using the experimentally-measured efflux times. A plot of η_{red} *vs* c was prepared and a linear regression of the data was performed. According to Eq. (3.5), the intrinsic viscosity $[\eta]$ corresponds to the intercept – that is, to the reduced viscosity, which would exist at a zero concentration.

4.2.4 Molecular weight determination

The molecular weight of homopolymers and copolymers was determined by a gel permeation chromatography (GPC) technique. The GPC allows determination of the number average molecular weight, weight average molecular weight, Z weight average molecular weight, and molecular weight distribution. In a GPC run, macromolecules are separated strictly on the basis of their size in a solution, rather than interactions with the column packing.

The machine utilized in this project was a Waters Corporation Gel Permeation Chromatograph equipped with a 410 Refractive Index Detector (Waters Model). Three Waters Ultrastyragel packed columns were installed in a series of descending order (10^6, 10^4, 10^3 Å), as recommended by the supplier. Polystyrene narrow molecular weight distribution standards (Shodex) were used for calibration. The polymer solutions of concentration of 0.02 wt% were prepared using tetrahydrofuran as a solvent. Prior to the injection into the chromatograph columns, polymer solutions were filtered. The determination of molecular weight was performed by Ms. R. Jovanovic at the University of Ottawa.

4.2.5 ^{1}H NMR analysis

Nuclear Magnetic Resonance (NMR) spectroscopy is a technique that records transitions between the energy levels of magnetic nuclei in an external magnetic field. The percent of DPPO in the copolymers was determined from the ratio of the integrals of proton resonance at 6.22 ppm and 6.50 ppm. The former peak is characteristic of the DPPO units, while the latter of the DMPO units.

The ^{1}H-NMR spectroscopy was performed using a Bruker AMX 500 NMR spectrometer. The data were acquired with a simple one-pulse sequence and a 4.5 s acquisition time for each of 16 transient signals, averaged. The interpulse spacing was 4.5 s. A 45-degree pulse was used. The ^{1}H-NMR analysis was performed by Dr. G. Facey at the University of Ottawa.

4.3 *Preparation of homogeneous membranes from synthesized polymers*

The polymer was air-dried at room temperature for at least 24 hours. The solution was prepared by adding the solvent to the dry polymer in a glass bottle. The concentration of the solution was 4 wt%. The contents of the bottle were stirred with a magnetic stirrer for at least one day to ensure complete dissolution of the polymer. The solution was filtered through 3 μm Teflon filters from Millipore. Nitrogen at pressures of 25-50 kPa from a gas cylinder was used to force the polymer solution through the filter. The solution was then degassed for 24 hours.

A sample of approximately 2.0 cm^3 of casting solution was poured inside a 9 cm diameter aluminum ring, which was placed on a leveled glass plate in the fume hood. The polymer solution was then covered by a filter paper and the solvent was allowed to evaporate for at least one day. The plate with a dry membrane was then immersed into a water bath to facilitate the membrane removal from the plate. Such prepared homogeneous membranes, also referred to here as films, were dried in a vacuum oven for at least two days before testing.

4.4 *Single gas permeation test using constant pressure testing system*

The constant pressure method is a technique based on the gas volume gain as the gas permeates through the membrane at a constant pressure gradient. The utilized constant pressure testing system consisted of six cells, so that six membrane coupons could be tested simultaneously. The permeation rate was measured manually using a soap bubble flow meter attached to the permeate side of each cell via a flexible tube. The length and the inside diameter of the bubble flow meter were 15 cm and 2.5 mm respectively.

A coupon was mounted onto a porous mesh in the test cell. To avoid possible membrane damage, a filter paper was placed between the coupon and the porous plate. The sealing in each cell was provided by a flat metal ring in the lower part of the cell, which was in contact with a smooth metal surface on the upper part of the cell. To prevent damaging the coupon on the ring, the coupon was separated from the ring by a paraffin film. Figure 4.2 shows a schematic diagram of the cell and the order in which the paraffin film, coupon, and filter paper were arranged.

The coupons were initially tested with N_2 to check for pinholes in the films. The successful films were then tested in the following order: CO_2, N_2, O_2, and CH_4. The test with CO_2 was carried out for at least six days in order to condition the membranes, while the other gases were tested for at least two days or until the permeation rate stabilized. The permeation rate readings were taken after 24 hours of running the experiments. The schematic diagram of the constant pressure testing system, showing the arrangement of one of the testing cells, is shown in Figure 4.3.

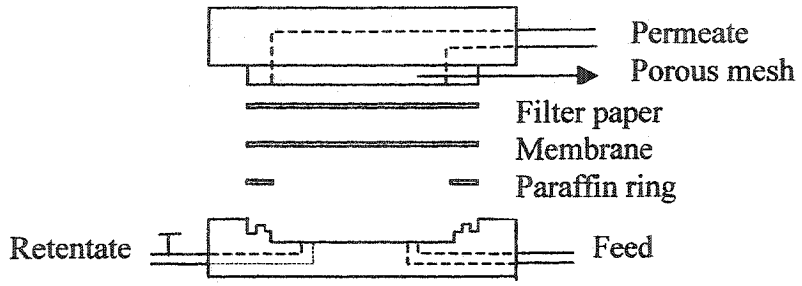

Figure 4.2: Schematic diagram of testing cell

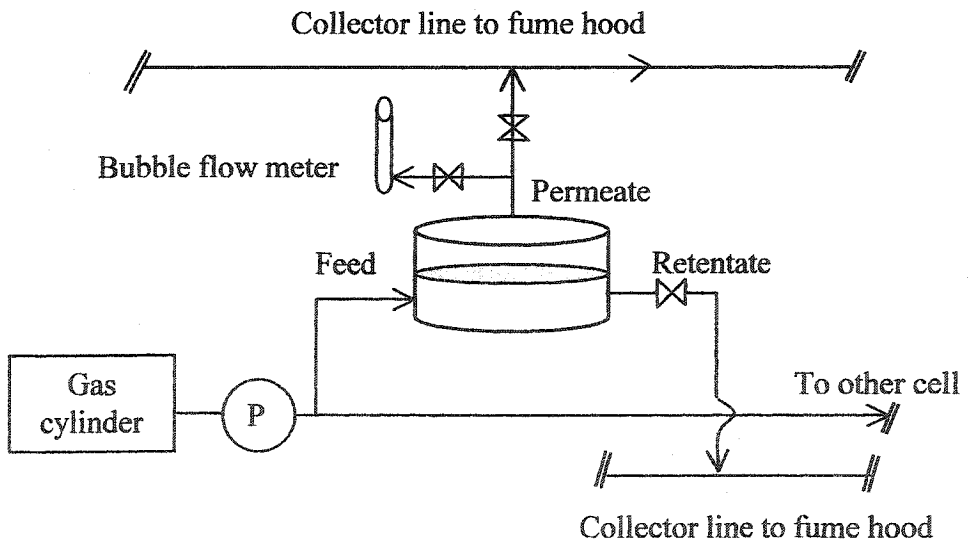

Figure 4.3: Schematic diagram of constant pressure testing system

4.5 Measurement of membrane thickness

The thickness of a membrane was determined by calculating the average from at least 10 readings taken by a Mitutoyo micrometer from the entire permeation area of the tested membrane.

4.6 *Decomposition temperature of polymers*

The decomposition temperature (T_d) of synthesized polymers was determined using a differential thermal analysis (DTA). The DTA is a thermal technique in which the temperature of a sample is compared with the temperature of a thermally inert material. The two temperatures and the mass of the sample are recorded as a function of time, as the sample is heated at a uniform rate. The analyses were performed using films previously tested with gases. A Seiko Simultaneous Thermal Analyzer (STA) TG/DTA 320 was used to measure the thermal stability of the film samples. Approximately 20 mg of sample was placed in a platinum pan and heated at a rate of 20 C/min from 25°C to 800°C under 150 mL/min Ultra High Purity nitrogen. The analyses were run by Ms. A. Delgado at the Natural Research Council of Canada (NRC) in Ottawa.

4.7 *Differential scanning calorimetry (DSC)*

The differential scanning calorimetry was used to determine the glass transition temperature (T_g) of synthesized polymers. The DSC analyses were performed using films previously tested for gas permeation. The machine used for the analyses was a 2920 Modulated Model DSC.

A sample of about 6-10 mg was placed in an aluminum pan and a cover was crimped against the pan, with the sample sandwiched in between, to ensure good heat transfer. The sample was heated from room temperature to 270°C at the rate of 10°C/min. At 270°C, the sample was kept for 1 minute, and then it was removed from the machine and quenched in liquid N_2. After quenching the sample in N_2, the machine was cooled down to 50°C using N_2. The sample was then reheated and the heating curve was recorded until all transitions were observed. The DSC experiments were performed at the Natural Research Council of Canada (NRC) in Ottawa.

4.8 *Fourier transform infrared (FTIR) spectroscopy*

The infrared spectroscopy of all the synthesized polymers was obtained. A Nicolet Magna 860 infrared spectrometer, equipped with a DTGS detector and a Spectra Tech Thunderdom attenuated total reflectance (ATR) accessory with a Germanium (GE)

crystal, was used. The analyses were performed using membranes previously tested for gas permeation.

A sample was placed over the GE crystal of the Thunderdome accessory. The collection parameters were: 32 scans, 4 cm^{-1} resolution, and 0.6329 cm/s mirror velocity. The GE crystal was carefully cleaned between each sample with a Q-tip. The sample spectrum was taken against a background collected from the GE crystal before collecting each sample spectrum. The ATR and normalization scale routines from the Omnic software (Nicolet) were applied to all spectra. All spectra were automatically baseline-corrected before plotting. The FTIR measurement was performed by A. Delgado at the Natural Research Council of Canada (NRC) in Ottawa.

4.9 Materials

The list of chemicals used in this study, together with their suppliers, is given in Table 4.3.

Table 4.3: Materials used during the course of this research

Material	Specifications	Supplier
2-Methoxylethyl ether	99% purity	Sigma-Aldrich
2,6-dimethylphenol (DMP)	99.5% purity	Sigma-Aldrich
2,6-diphenylphenol (DPP)	98% purity	Sigma-Aldrich
2-Methoxyethanol	99% purity	Sigma-Aldrich
Anhydrous magnesium sulfate ($MgSO_4$)	99% purity	Mallinck Canada Inc.
Benzene	99% purity	BDH
Carbon dioxide (CO_2)		Air Products
Cuprous Bromide (CuBr)	98% purity	Acros Organics
Ethylene glycol monobutyl ether	99% purity	Sigma-Aldrich
Methane (CH_4)	99% purity	Praxair
Omnisolv Methanol (MeOH)	99.5% purity	BDH
n- Heptane	99% purity	BDH
N, N, N', N'- tetramethyl-1, 3- butanediamine (TMEDA)	99% purity (GC)	Fluka Chemicals
Nitrogen (N_2)	99.99% purity	Praxair
Omnisolv Chloroform (CCl_3)	99.5% purity	BDH
Oxygen (O_2)	99.999% purity	Praxair

Tetrachloroethylene	99.5% purity	Sigma-Aldrich
Tetrahydrofuran(THF)	99% purity	BDH
Toluene	99.5% purity	BDH
Trichloroethylene	98% purity	Sigma-Aldrich

PART III Results and Discussion

Chapter 5 Synthesis and Characterization of Polyphenylene Oxide Homo and Copolymers

In this section, the synthesis and characterization of homopolymers, poly(2,6-dimethyl-1,4-phenylene oxide) (DMPO), and poly(2,6-diphenyl-1,4-phenylene oxide) (DPPO), as well as block and random copolymers consisting of DMPO and DPPO segments, are discussed.

5.1 Synthesis of homopolymers

The DMPO and DPPO homopolymers were synthesized by the oxidative coupling polymerization of 2,6-disubstituted phenols with oxygen in the presence of copper-amine catalysts. Scheme 1 represents the polymerization reaction. It is possible, however, that some of the 2,6-dialkylphenol will form C-C couplings, the oxidation of which would lead to the formation of diphenoquinone, following Scheme 2. Diphenoquinone is an undesirable product, because it reduces the yield of the polymer and also might degrade the polymer upon further processing at high temperatures (Viersen, 1988). It has been demonstrated by Hay (1962) that the formation of diphenoquinone is favored in oxidative coupling involving 2,6-dialkyl substituted phenols having bulky substituents such as t-butyl groups. On the other hand, with smaller substituents such as methyl groups, the reaction favors C-O coupling, resulting in high molecular weight poly(2,6-dialkyl-1,4-phenylene oxides).

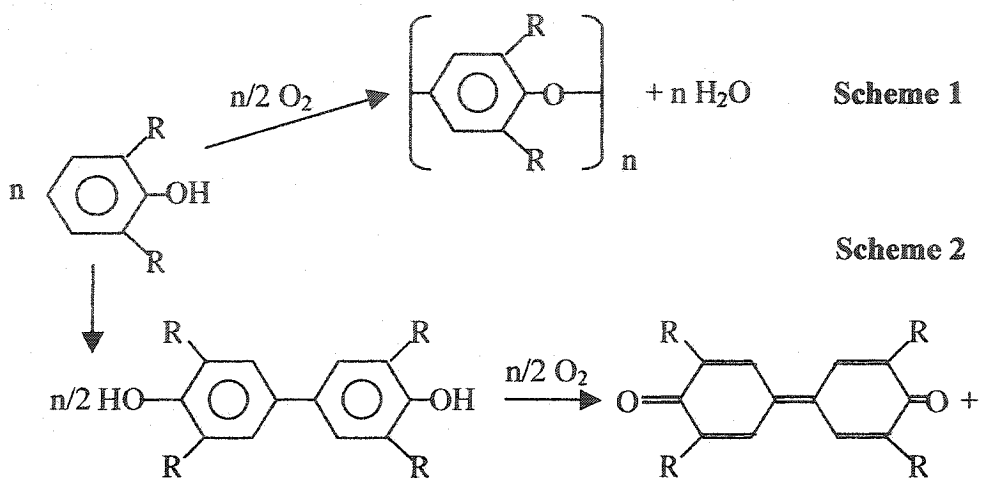

The synthesis of poly (2,6-dimethyl-1,4-phenylene oxide) is a relatively simple polymerization reaction. Hay (1998) reported that as the temperature for the synthesis of DMPO increases, the amount of undesirable diphenoquinone increases. Since in general the oxidative coupling polymerization of 2,6-dialkylphenols is an exothermic reaction, the synthesis of DMPO was carried out in a reaction flask placed in a water bath, at 25°C. According to Li (1995), the polymerization rate is very sensitive to the rate of mass transfer of oxygen through the liquid phase. Therefore, to enhance the transfer of oxygen through the liquid phase, the oxygen was dispersed under the constant pressure of 5 psig. The polymerization of DMPO was carried out for 1.5 hours. After termination of the reaction, the reactor content was dissolved in methanol. Since DMPO is insoluble in methanol, it precipitated from the solution. On the other hand, diphenoquinone (if any), which is soluble in methanol, was isolated from the polymerization products. After drying, the final DMPO product had a light yellow color.

The synthesis of DPPO using 2,6-diphenylphenol was performed following the procedure similar to the synthesis of DMPO, except the temperature and the duration of the reaction differ. In general, the synthesis of DPPO is more difficult than that of DMPO, due to the steric hindrance caused by phenyl side groups in 2,6-diphenylphenol. Also, since the phenyl groups are more bulky than the methyl groups, the synthesis of DPPO at identical conditions to the synthesis of DMPO could lead to the significant formation of undesirable diphenoquinone. Hay (1969) observed that in the synthesis of DPPO, it is desirable to carry out the reaction at elevated temperatures. Consequently, the

polymerization of 2,6-diphenylphenol was carried out at 40°C for four hours. Unlike DMPO, the final DPPO product had a reddish color due to the presence of phenyl side groups in the polymer.

5.2 Synthesis of block and random copolymers

Block copolymers containing DPPO and DMPO were synthesized following the procedures suggested by Bennett and Cooper (1969). These authors showed that block copolymers of DPPO and DMPO can be obtained by first polymerizing 2,6-diphenylphenol, and then adding 2,6-dimethylphenol and continuing the polymerization. The reverse procedure (i.e., addition of 2,6-diphenylphenol to the growing DMPO) results in a random copolymer. Similarly, oxidation of a mixture of 2,6-diphenylphenol and 2,6-dimethylphenol simultaneously also leads to a random copolymer.

Accordingly, the block copolymers were synthesized by first polymerizing 2,6-diphenylphenol for three hours at 25°C, followed by adding 2,6-dimethylphenol to the growing DPPO chains and continuing polymerization for another two hours. A relatively long time was required for the polymerization of 2,6-diphenylphenol before adding 2,6-dimethylphenol to ensure that the DPPO chains were sufficiently long to form the block copolymer. The random copolymers, on the other hand, were synthesized by simultaneous oxidation of 2,6-diphenylphenol and 2,6-dimethylphenol for five hours at 25°C. For block copolymers, three different target compositions of 20, 50 and 80% of DPPO in the copolymer, and for random copolymers of 25, 50 and 75% of DPPO in the copolymer were considered. The target composition of the copolymer is defined as a mole percent of 2,6-diphenylphenol monomer used in the synthesis of the copolymer.

In the subsequent discussion, the following codes will be used for the copolymers: B or R/XX/T or A. The letter B and R refer to the block and random structures respectively; the number XX indicates the percent of DPPO in the copolymer; and the letter T or A indicate whether the percent of DPPO refers to the target or the actual value, respectively. For example, the copolymer denoted as B/20/T indicates the block copolymer whose targeted percent of DPPO was 20%.

5.3 Characterization of synthesized homo and copolymers

There was a twofold purpose for the characterization of synthesized polymers. First of all, it was necessary to determine whether the desired products at the desired composition and structure (block versus random copolymers) were formed. The techniques utilized for these characterizations include infrared (IR) spectroscopy, ^1H NMR spectroscopy, and thermogravimetric (TG) analysis.

Secondly, the molecular structure of polymers determines the gas separation properties of polymeric membranes. Therefore, in addition to the above analysis, the synthesized polymers were characterized using gel permeation chromatography (GPC) in order to determine their molecular weight and molecular weight distribution.

5.3.1 FTIR spectroscopy

The FTIR spectroscopy was utilized to identify the synthesized polymers. The FTIR spectra of polymers were obtained using dense polymer films previously tested for gas permeation. Table 5.1 presents the theoretical ranges of the absorption frequencies for the groups, which exist in the products given by Schemes 1 and 2.

Table 5.1: Summary* of the absorption frequency for the groups in the products of oxidative polymerization of 2,6-dimethylphenol and 2,6-diphenylphenol

Group and Source	Frequency of absorption band (cm^{-1})
C—H aromatic stretch (DMPO, DPPO Diphenoquinone)	3150-3050
C—H aromatic out-of-plane bend (DMPO, DPPO Diphenoquinone)	900-690
C=C aromatic (DMPO, DPPO Diphenoquinone)	1600-1475
$-CH_3$ (DMPO)	1450-1375
C—O (DMPO and DPPO)	1300-1000
C=O (Diphenoquinone)	1725-1705

*From D.L. Pavia, G. M. Lampman and G. S. Kriz, "Introduction to spectroscopy: A guide for students of organic chemistry," Saunders College Publishing, Orlando, 1979, p. 13-73.

It will be noticed that the C=O stretching, which is characteristic of diphenoquinone, should occur in a frequency range that does not overlap with any other frequency range listed in Table 5.1. Consequently, the absence of peaks in the 1725-1705 cm^{-1} range could serve as proof of the absence of the undesirable diphenoquinone in the synthesized polymers. It is also evident that peaks resulting from the $-CH_3$ band,

characteristic for DMPO, occur in the absorption frequency range that also does not overlap with any other absorption frequency range listed in Table 5.1. Consequently, the intensity of the peaks coming from the $-CH_3$ band could serve as a measure of the actual percent of DMPO segments in the synthesized copolymers. Figure 5.1 presents the IR spectra of B/20/T. The IR spectra of other polymers synthesized in this project are shown in Appendix A.

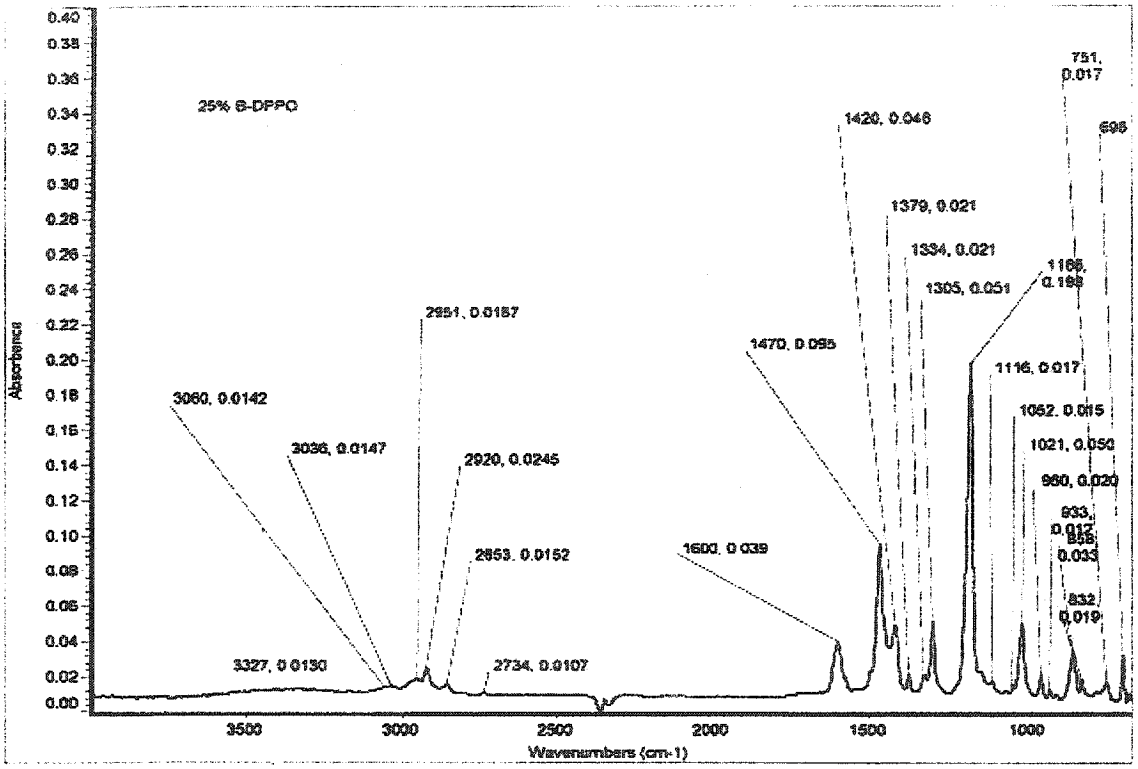

Figure 5.1: Infrared spectrum of B/20/T

Considering the ranges listed in Table 5.1, it is evident that some peaks in Figure 5.1 fall outside these ranges. For example, there are three low-intensity peaks at 933 cm^{-1}, 960 cm^{-1}, and 1334 cm^{-1} that do not belong to any frequency range listed in Table 5.1. An intermediate intensity peak at 1305 cm^{-1} and a high intensity peak at 1470 cm^{-1} are so close to the frequency absorption bands starting at 1300 cm^{-1} and 1475 cm^{-1} that it is safe to assume that they come from the C-O stretching and the aromatic C=C stretching, respectively. The most surprising feature of the IR spectra depicted in Figure 5.1 are the four peaks in the 2734-2951 cm^{-1} range and the fact that these peaks are stronger than the peaks in the 3050-3150 cm^{-1} range resulting from the aromatic C-H stretching. However,

since the intensity of the latter peaks is so low, the former peaks must also come from the aromatic C-H stretching. This is because the oxidative polymerization 2,6-disubstituted phenols cannot lead to the breakage of phenyl rings, and thus the overall intensity of the peaks resulting from the aromatic C-H stretching must be greater than that of the two peaks in the 3050-3150 cm^{-1} range appearing in Figure 5.1. It is evident that there are no peaks in the 1705-1725 cm^{-1} frequency range and its vicinity; this, according to the earlier discussion, indicates that there is no diphenoquinone in the copolymer depicted in Figure 5.1.

The examination of the FTIR spectra shown in Appendix A reveals that the intensity of peaks in the 1375-1450 cm^{-1} absorption band that originate exclusively from the

$-CH_3$ groups decreases with an increase in the percent of DPPO in copolymers. Eventually, the peaks from this band disappear completely in DPPO. Also, the FTIR spectra shown in Appendix A do not exhibit peaks in the 1705-1725 cm^{-1} frequency range and its vicinity, which indicates that there is no diphenoquinone.

5.3.2 ^1H NMR spectroscopy

The analysis of ^1H NMR spectra of copolymers was used for the determination of the actual fraction of DPPO segments in synthesized block and random copolymers. Figure 5.2 presents the ^1H NMR spectrum of B/25/T. The spectra of other copolymers synthesized in this project are shown in Appendix A. Table 5.2 summarizes the locations, intensities and the origin of the peaks observed in Figure 5.2.

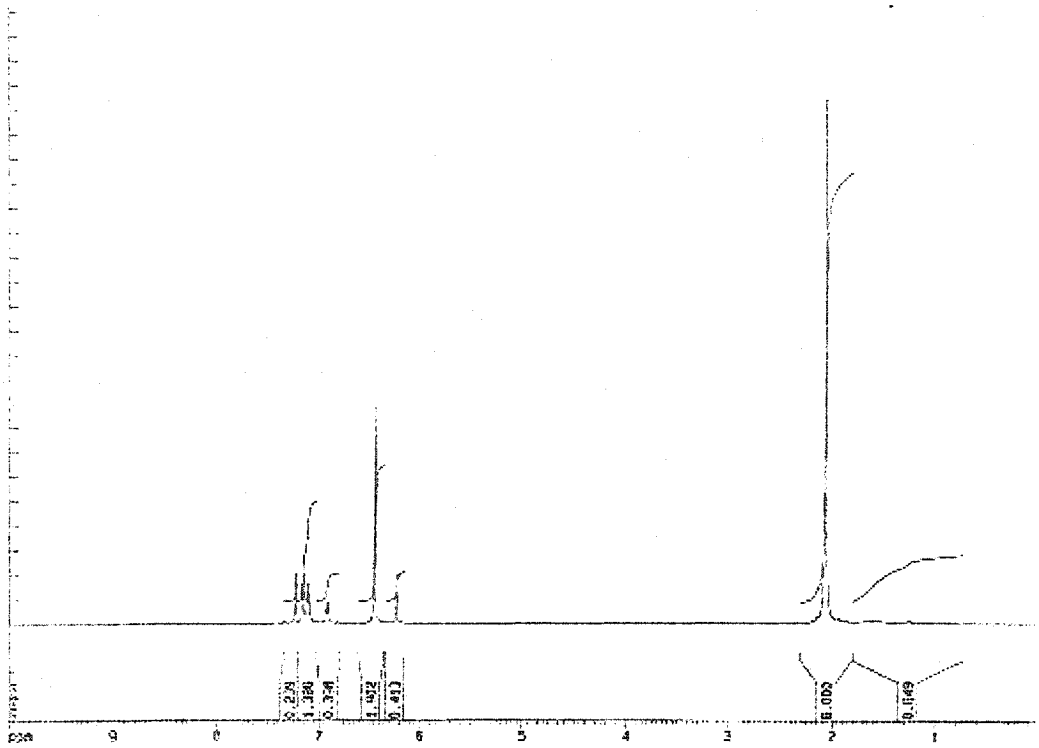

Figure 5.2: ^{1}H NMR spectrum of B/20/T

Table 5.2: Summary of the ^{1}H NMR spectrum of block copolymer.

Peak No.	Position, ppm	Intensity	Source
1	7.25	0.239	Ar-H (phenyl substitute group)
2	7.15	1.396	Ar-H (phenyl substitute group)
3	6.9	0.398	Ar-H (phenyl substitute group)
4	6.45	1.902	Ar-H (DMPO backbone)
5	6.25	0.413	Ar-H (DPPO backbone)
6	2.1	6.0	Ar-CH_3

Peaks 1, 2 and 3 come from the protons attached to the phenyl side groups of the DPPO segments. Peak 6 comes from the six protons attached to the methyl side groups of the DMPO segments. Peak 4 comes from the two protons attached to the backbone phenyl group of the DMPO segments, while peak 5 comes from the two protons attached to the backbone phenyl group of the DPPO segments.

Considering that peak intensity is proportional to the number of protons, the percent of DPPO in copolymers can be determined using one of the following two equations,

$$\%DPPO = \frac{I_5}{I_4 + I_5} 100\% \tag{5.1}$$

$$\%DPPO = \frac{\frac{I_1 + I_2 + I_3}{10}}{\frac{I_1 + I_2 + I_3}{10} + \frac{I_6}{6}} 100\% \tag{5.2}$$

where I_i is the intensity of peak i. The numbers appearing as subscript, which identify the peaks in the above equations, are consistent with those in Table 5.2.

The calculated percent of DPPO in the copolymer depicted in Figure 5.2 is 17.8% when Eq. (5.1) is used, and 16.8% when Eq. (5.2) is applied. Table 5.3 presents the comparison of the targeted %DPPO with the values calculated using equations (5.1) and (5.2) for all copolymers synthesized in this project.

Table 5.3: Calculated %DPPO using ^{1}H NMR method

Target %DPPO	Calculated %DPPO in Block Copolymer		Calculated %DPPO in Random Copolymer	
	Eq. (5.1)	Eq. (5.2)	Eq. (5.1)	Eq. (5.2)
20	17.8	16.8	-	-
25	-	-	31.4	28
50	55.6	51.4	50	53.6
75	-	-	67.5	75.6
80	71.5	75.7	-	-

It will be noticed that with the exception of R/75/T, the calculated %DPPO using equation (5.1) and (5.2) are quite similar. In general, the integration of high-intensity peaks on ^{1}H NMR spectra is more accurate than the integration of low-intensity peaks. Peaks 1-3 come from 10 protons and peak 6 comes from six protons, while peaks 4 and 5 come from the two protons each. Consequently, the %DPPO calculated using Eq. (5.2) should be more accurate than that calculated using Eq. (5.1), and the values calculated using the former equation should be used as the actual %DPPO in the subsequent discussion. It is important to note that Bennet and Cooper (1969), who studied copolymers of DMPO and DPPO, also used Eq. (5.2) for the determination of the actual %DPPO in copolymers.

As mentioned earlier, the synthesis of DMPO requires ambient temperature while the synthesis of DPPO requires an elevated temperature. Since synthesis of all copolymers was carried out at 25-30°C, one could anticipate the actual %DPPO to be less than the targeted values. Surprisingly, deviation from the targeted %DPPO is observed only in the cases of B/20/T and B/80/T. For all other copolymers, the actual %DPPO is very close to the targeted %DPPO.

5.3.3 Gel chromatography

The number average (M_n) and weight average (M_w) molecular weight of homopolymers and copolymers were determined by the gel permeation chromatography (GPC) technique. The ratio of M_w and M_n was used to calculate the polydispersity index (PDI) of the analyzed polymers. All tests were performed using tetrahydrofuran (THF) as a solvent. All synthesized polymers, except DMPO and B/16.7/A, were completely soluble in THF. The latter polymers were only partially soluble in this solvent. As a result, the reported values of M_n, M_w and PDI for DMPO and B/16.7/A might be associated with an error. Since the molecular weight of DMPO segments of 120 is significantly lower than the molecular weight of DPPO segments of 242, the experimentally-determined molecular weights do not provide an accurate picture of the average length of chains in the synthesized polymers. Therefore, in addition, the following set of equations was solved for each synthesized polymer in order to determined the average degree of polymerization (ADP):

$$120n_1 + 244n_2 = M_n \tag{5.3}$$

$$\frac{n_2}{n_1 + n_2} \times 100 = \%\text{DPPO (from Eq.5.2)} \tag{5.4}$$

where, n_1 and n_2 represent the number of DMPO and DPPO segments, respectively. The ADP is simply equal to $n_1 + n_2$. Table 5.4 provides the summary of M_n, M_w, PDI, and ADP for all polymers synthesized in this project.

Table 5.4: Summary of M_n, M_w, PDI, and ADP of homopolymers and copolymers synthesized in this project

Polymer Type	M_n	M_w	PDI	ADP
DMPO	10,054	13,357	1.38	83.78
B/16.8/A	18,663	43,862	2.35	131.08
R/28.0/A	25,470	52,505	1.49	160.83
B/51.4/A	12,674	50,072	3.95	66.91
R/53.6/A	22,558	44,544	1.98	126.48
R/75.6/A	18,663	43,862	2.35	91.34
B/75.6/A	65856	104,685	1.59	316.7
DPPO	45883	68,468	1.49	188.0

The DMPO of M_w of 40,000 is considered in the literature to be a low molecular weight polymer (Hay, 1998). Therefore, the M_w = 13,357 of DMPO synthesized in this project is even lower than the level for the low molecular polymer. Generally the molecular weights of all polymers synthesized in this project fall into the category of low and intermediate molecular weights.

Since the synthesis of DPPO is more difficult than the synthesis of DMPO (Hay, 1998) because of the bulkiness of phenyl groups, one could anticipate a decrease in the molecular weight of polymers with an increase in the targeted %DPPO. This anticipated effect is clearly evident in the case of random copolymers – in particular when the ADP is considered. On the other hand, there is no clear trend between the molecular weight and the %DPPO in the case of block copolymers. Interestingly, B/75.6/A shows the highest M_n, M_w and ADP among all polymers synthesized in this project.

Considering the PDI values listed in Table 5.4, it can noticed that generally the larger the ADP the lower the PDI. The only exception is DMPO, which shows the lowest PDI and the second lowest ADP. The DMPO might be falling outside the general pattern because of possible underestimation of the molecular weight due to only a partial solubility in THF.

5.3.4 Thermal analysis

Thermogravimetry (TG) and Differential Scanning Calorimetry (DSC) were utilized to determine the intrinsic properties of synthesized polymers, such as the

decomposition temperature (T_d) and the glass transition temperature (T_g). Figure 5.3 presents the results of thermogravimetric analysis of DMPO. There are three curves shown in the TG spectrum representing the percentage of mass loss (TG%), the derivative of the percentage of mass loss with respect to temperature (DTG), and the difference between the temperature of the sample and the temperature of the standard aluminum reference, respectively. Since each TG spectrum was obtained at the constant heating rate (20°C/min), the DTG is converted into the derivative of the percentage of mass loss with respect to time (DTG%/min). It will be noticed in Figure 5.3 that DMPO decomposes in a single stage. The decomposition begins at around 420°C; however, the highest DTG of 33.88%/min is observed at 464°C. The latter temperature is considered to be the T_d of DMPO. The T_d of DMPO is comparable to the value of 456°C reported by Karasz and Reilly (1965). Interestingly, before DMPO begins to decompose, there is an approximately 4% weight loss between 25°C and 300°C. This weight loss might be an indication of the presence of some impurities or a residual solvent in the polymer.

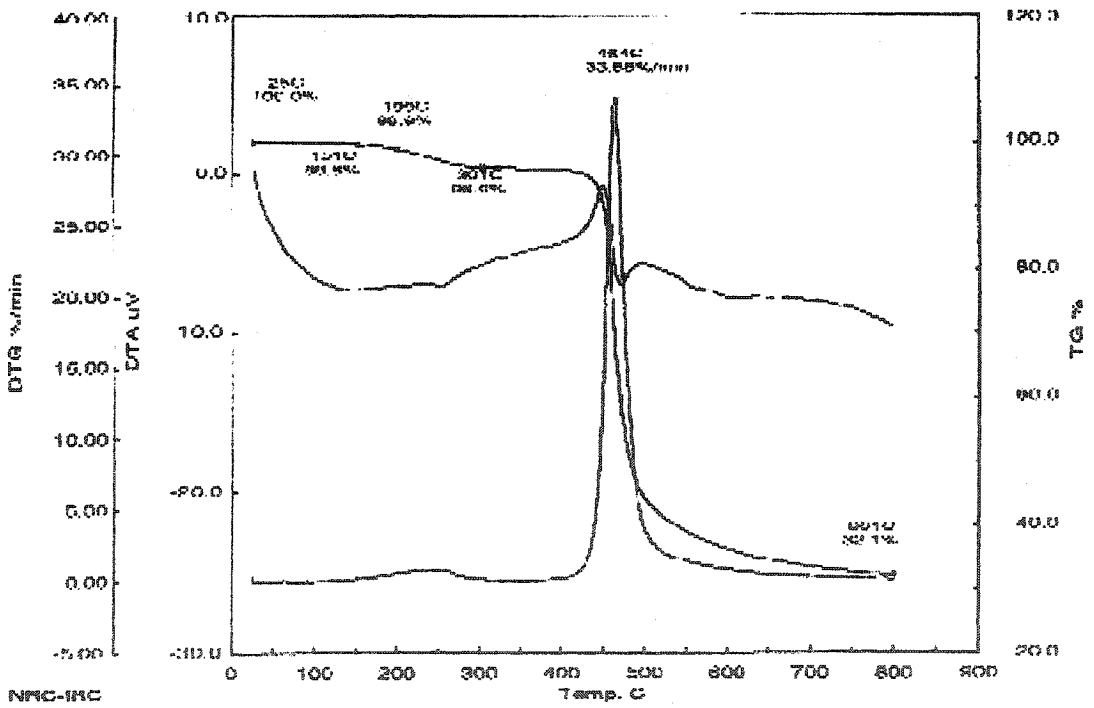

Figure 5.3: Thermogravimetric spectrum of DMPO

Figure 5.4 presents the TG spectrum of DPPO. Similar to the other homopolymers, the DPPO decomposes in a single stage. However, its T_d of 569°C is significantly greater than that of 467°C for the DMPO, which is an indication of improved thermal stability of DPPO in comparison to the DMPO. It should be emphasized that the T_d of DPPO reported here is higher than the value of 520°C reported by Hays (1968). This is probably due to the higher heating rate (20°C/min) used in this project than that used by Hays (5°C/min). The DTG at the decomposition temperature of DPPO of 18.89%/min is smaller than that for DPMO. The weight loss between 25 and 300°C of 1.65% is also less than that for DMPO.

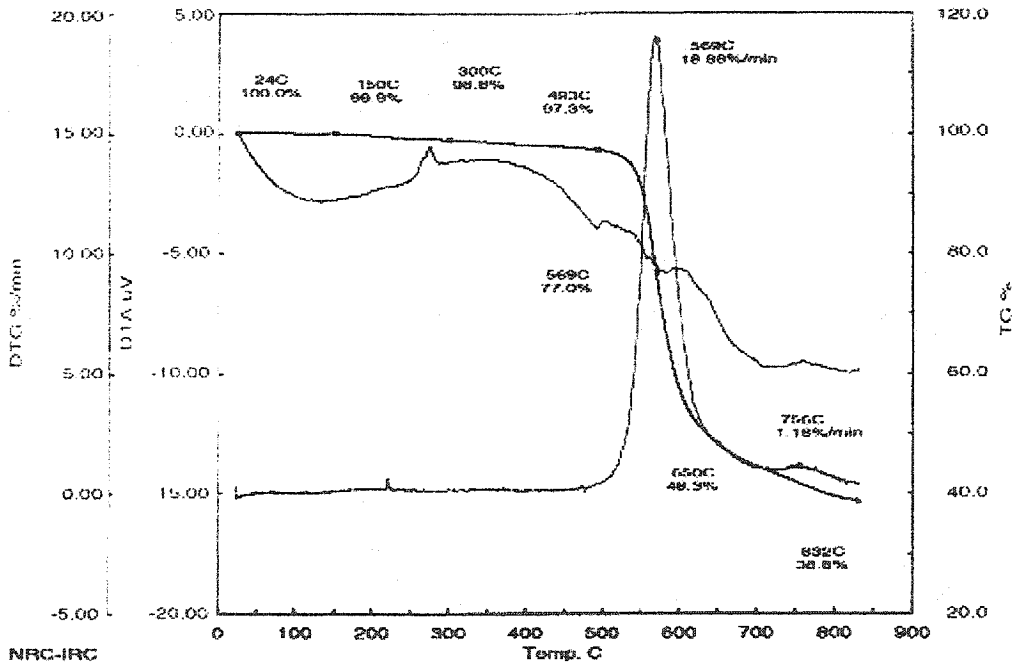

Figure 5.4: Thermogravimetric spectrum of DPPO

Figure 5.5 presents the TG spectrum of R/28/A. Similar to DMPO and DPPO, this copolymer decomposes in a single stage. The T_d of R/28/A of 484°C is between the decomposition temperatures of the two homopolymers. The DTG at the decomposition temperature of R/28/A is smaller than that of DMPO, but it is close to that of DPPO. The TG spectra of the other random copolymers can be found in Appendix A. The

examination of these spectra reveals that the T_d of random copolymers increases with the content of more thermally-stable DPPO.

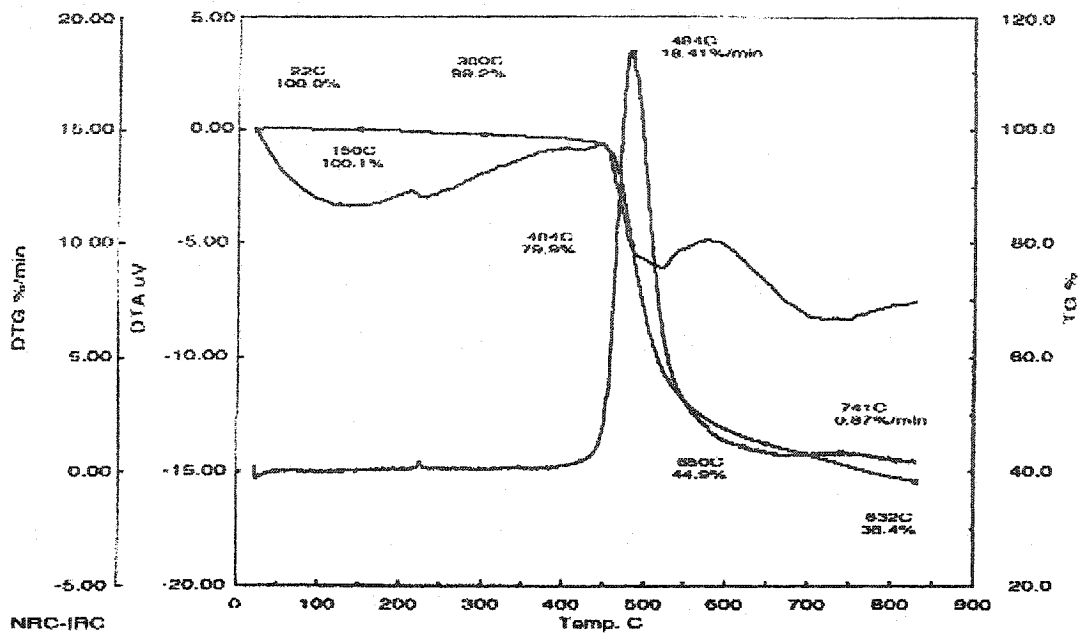

Figure 5.5: Thermogravimetric spectrum of R/28/A copolymer

Figure 5.6 presents the TG spectrum of B/16.8/A. Unlike the polymers depicted in Figures 5.3 and 5.4, this block copolymer decomposes in two stages. The first stage of decomposition occurs in a similar temperature range as that during the decomposition of DMPO, while the second stage of decomposition occurs in a similar temperature range as that during the decomposition of DPPO. At the first T_d of 467°C, the rate of weight loss of 27.81%/min is observed, while at the second T_d of 577°C, the rate of weight loss of 5.39%/min is observed. The existence of two decomposition stages confirms sufficiently long sequences of DMPO and DPPO segments, and therefore the block rather than random structure of B/16.8/A (Dawkins, 1973). Similarly, the other block copolymers, whose spectra are shown in Appendix A, also exhibit two decomposition temperatures. It is important to emphasize that the respective decomposition temperatures in block copolymers are similar, regardless of the %DPPO. On the other hand, the change in the composition affects the relative amounts of copolymer that decomposed at the two stages

– that is, the larger the %DPPO, the greater the percent of the block copolymer decomposed at the higher T_d.

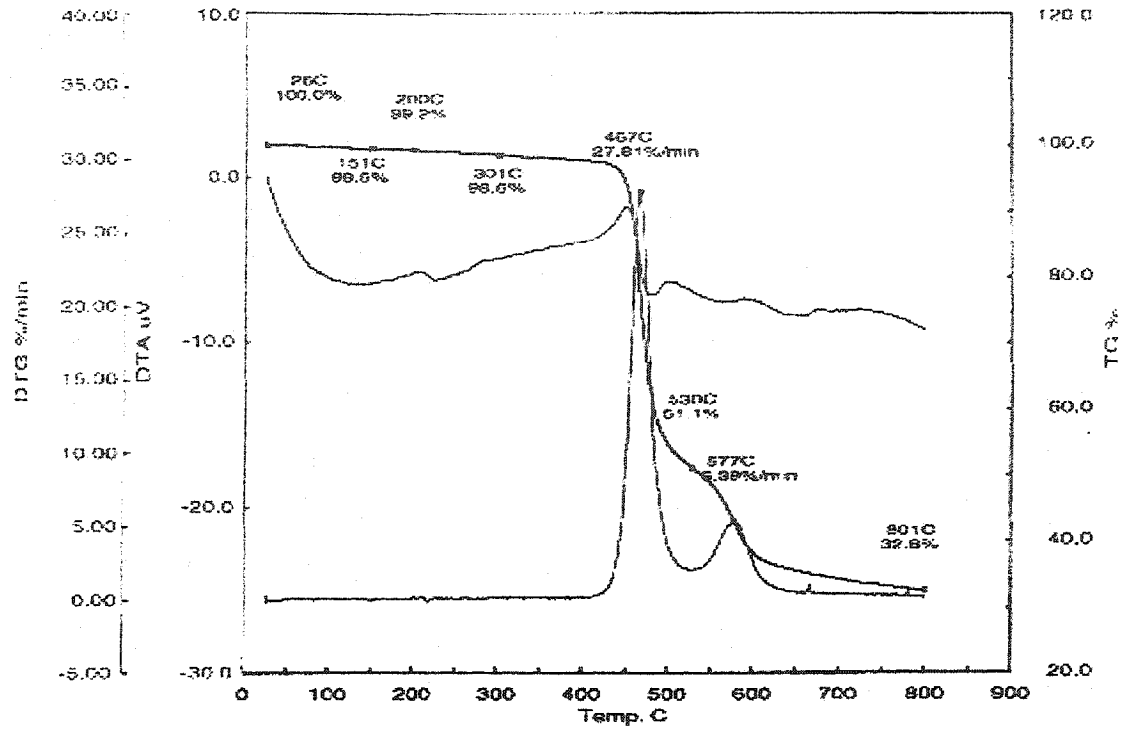

Figure 5.6: TG spectrum of B/16.8/A copolymer

Figure 5.7 presents the DSC spectrum of B/16.8/A. It will be noticed that at low temperatures, the heat flow decreases linearly with temperature. At approximately 209°C, there is a sudden change in the slope of the heat flow line; it becomes even more negative. Another step change in the slope occurs at approximately 219°C. Above this temperature, the heat flow increases with temperature. The glass transition temperature is considered to be the temperature in the middle of the range where the shift in heat flow occurs. For the polymer depicted in Figure 5.7, the T_g is estimated to be 214.08°C. A lack of peaks in the DSC spectrum of polymer is an indication of its entirely amorphous structure (Hay, 1969). It is evident that by examining the spectrum presented in Figure 5.6 and the spectra for other polymers shown in Appendix A, all polymers synthesized in this project were entirely amorphous.

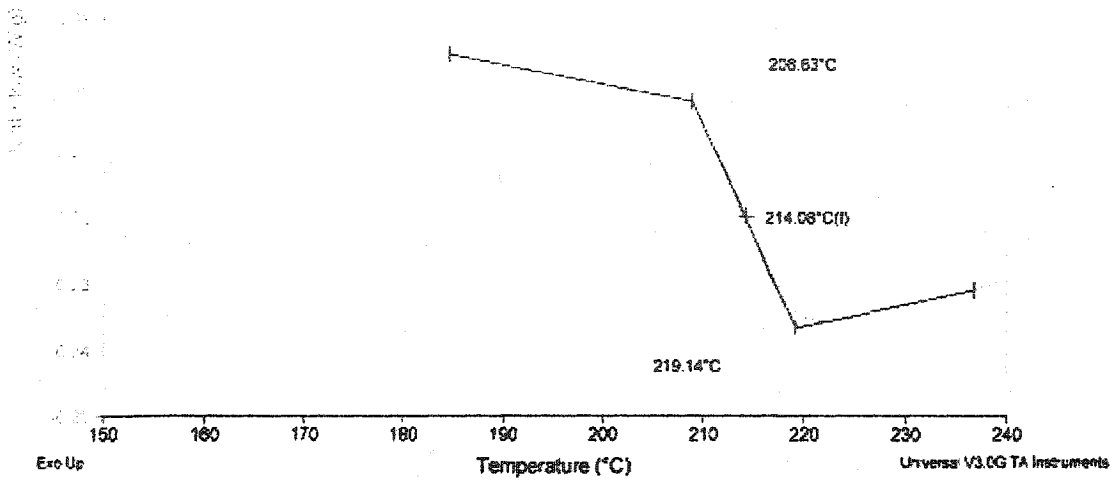

Figure 5.7: DSC spectrum of B/16.8/A copolymer

Figure 5.8 presents the percentage weight loss of hompolymers and copolymers between 25 and 300°C. The percentage weight loss of DMPO is higher than that of DPPO; this might suggest a higher content of residual solvent and impurities in the former. The percentage weight loss of block copolymer is also higher than that of random copolymer of similar %DPPO. This may be due to the presence of DMPO segments in block copolymers. For random copolymers, percentage weight loss increases with increasing %DPPO. There is no clear trend in percentage weight loss in block copolymers.

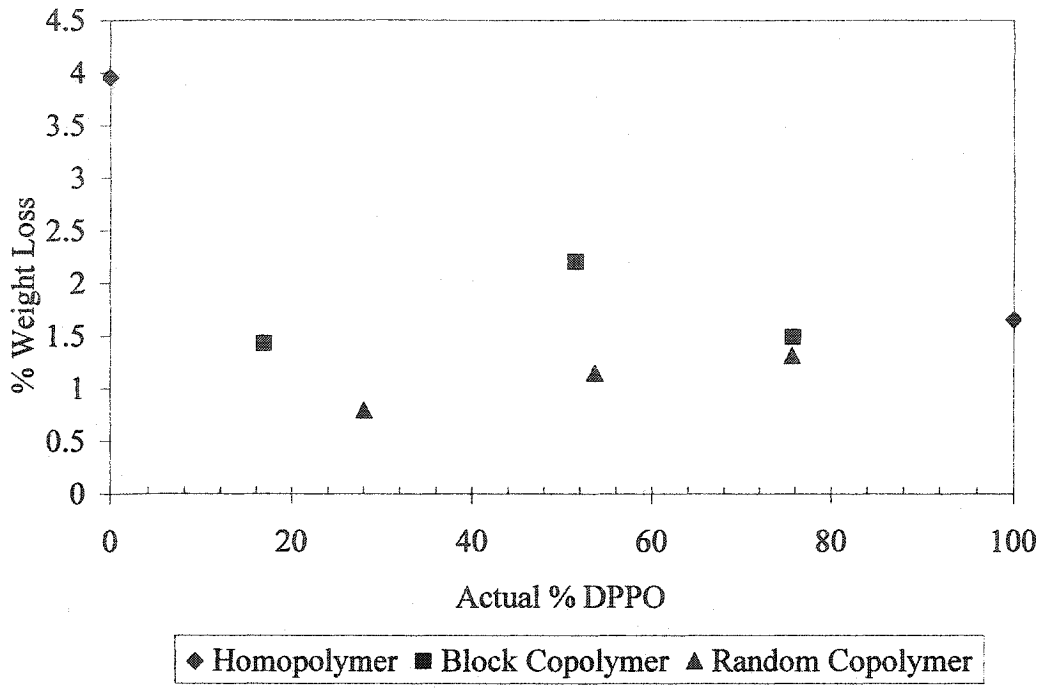

Figure 5.8: The percentage weight loss of homopolymers and copolymers between 25 and 300°C

Table 5.5 presents the summary of T_d, and T_g, along with the weight loss before the decomposition of the polymer began. For DMPO, the literature values of T_g range from 206 to 224°C, depending on the molecular weight of polymer (Hay, 1968). In general, for a given polymer an increase in the molecular weight is associated with an increase in T_g (Kesting & Fritzsche, 1993). Consequently, the T_g of 218.68°C for the DMPO synthesized in this project is surprisingly high considering its low M_w. On the other hand the T_g of DPPO of 217.12°C is rather low in comparison to the literature values of 230 and 229°C reported by Hays (1968), and Aguilar-Vegar and D.R. Paul (1993). The difference between T_g obtained in this study and literature review values could be due to the fact that the determination of T_g used in this study was carried at a different heating rate than those performed by other research group. In general, according to Wrasidlo (1972), T_g should increase with increasing %DPPO because the bulkiness of phenyl groups prevents the rotations around the ether linkages (C-O-C). However, this effect is not evident, considering the T_g values summarized in Table 5.5. Moreover, B/80/T –

which, according to Table 5.4, had the highest M_n, M_w, and ADP among the polymers synthesized in this project, and the highest actual %DPPO – has a rather low T_g of 215.31°C, which is even lower than that for DMPO.

Table 5.5: Summary of decomposition and glass transition temperatures of homo and block copolymers

Actual % DPPO	Block Copolymer[a]				Random Copolymer[b]		
	T_{d1}(°C)	T_{d2}(°C)	T_g(°C)	% Loss in (25-300°C)	T_d(°C)	T_g(°C)	% Loss in (25-300°C)
0	464	-	218.68	3.96	-	-	-
16.8	467	577	214.08	1.43	-	-	-
28	-	-	-	-	484	215	0.79
51.4	467	586	219.41	2.2	-	-	-
53.6	-	-	-	-	506	218.42	1.14
75.6	-	-	-	-	538	213.63	1.31
75.7	467	582	215.31	1.49	-	-	-
100	-	571	217.12	1.65	-	-	-

[a] T_{d1} and T_{d2} are the decomposition temperatures of DMPO and DPPO, respectively, in block copolymers.

[b] T_d is the decomposition temperature of random copolymers.

5.4 Selection of solvent

Although polymer chemistry is the most important factor governing the properties – including the gas transport properties – of polymeric membranes, there is strong evidence that properties of solution-cast membranes are also influenced by the properties of the solvent in the casting solution (Mulder, 1996). Consequently, it was desired to find a solvent capable of dissolving all synthesized homopolymers and all copolymers. The solution-cast films prepared using the selected solvent should have a sufficient mechanical integrity to withstand high-pressure gradients during gas permeation tests.

In the case of DMPO, there are a number of solvents that have been used for the preparation of solution-cast membranes and dense films. On the other hand, in the case of DPPO and copolymers of DMPO and DPPO, the information regarding the selection of solvents is rather limited. Consequently, it was decided to select the solvent for this project, starting with a list of solvents that had been previously used in the preparation of solution-cast DMPO membranes. This list includes chloroform, benzene, tetrahydrofuran (THF), and trichloroethylene (TCE).

The solubility of a polymer in a solvent can simply be verified by a solubility test. Alternatively, the strength of a solvent – and hence its potential to dissolve a given polymer – can also be assessed by the comparison solubility parameters of solvent and polymer.

The Hansen and Hildebrand solubility parameters of solvents are generally available in the literature. Table B1 in Appendix B presents the literature values of solubility parameters for chloroform, benzene, THF, and TCE. On the other hand, the solubility parameters of DMPO and DPPO had to be estimated using a group contribution method. In the case of DMPO, the repeat unit can be divided into a tetrasubstitute phenyl group, two methyl groups and one ether group. In the case of DPPO, the two phenyl groups replace the two methyl groups. Table B2 in Appendix B presents the parameters required by Eq. (3.3) and (3.4) for all functional groups appearing in both homopolymers, and the calculated Hansen and Hildebrand solubility parameters. The solubility parameters of copolymers, ($\delta_{i,cop}$), were calculated using the solubility parameters of homopolymers and the fraction of DPPO (x_i) in the copolymer using the following expression:

$$\delta_{i,cop} = x_i \delta_{i,1} + (1 - x_i)\delta_{i,2} \tag{5.5}$$

where $\delta_{i,1}$ and $\delta_{i,2}$ are the solubility parameters for DPPO and DMPO, respectively, while subscript i indicates the type of the solubility parameter.

Table 5.6: Differences (Δ) between the Hildebrand solubility parameter of polymers synthesized and solvents utilized for preparation of solution cast DMPO membranes

%DPPO	Δ,cal$^{1/2}$cm$^{-3/2}$ with various solvents below			
	Chloroform	Benzene	THF	TCE
0	2.43	2.01	2.11	2.01
16.8	2.60	2.16	2.26	2.16
28	2.69	2.27	2.36	2.26
51.4	2.91	2.47	2.57	2.47
53.6	2.93	2.49	2.58	2.48
75.6	3.13	2.71	2.81	2.71
75.7	3.13	2.71	2.81	2.71
100	3.36	2.84	3.04	2.94

It will be noticed that regardless of solvent, Δ increases with the fraction of DPPO. Considering that the strength of the solvent increases with a decrease in Δ, the strength of the solvent increases in the following order: chloroform, THF, TCE and benzene.

Alternatively, the strength of solvents can also be evaluated considering the difference between Hansen solubility parameters of polymer and solvent (Δ′), which is given by Eq. (4.2). Table 5.7 presents the summary of evaluated (Δ′) for the polymers-solvent systems considered in Table 5.6.

Table 5.7: Differences (Δ′) between the Hansen solubility parameters of polymers synthesized and solvents utilized for preparation of solution cast DMPO membranes

%DPPO	Δ′,$cal^{1/2}cm^{-3/2}$ with various solvents below			
	Chloroform	Benzene	THF	TCE
0	0.40	2.20	1.96	0.23
16.8	0.51	2.03	2.13	0.29
28	0.59	1.93	2.24	0.37
51.4	0.81	1.72	2.49	0.6
53.6	0.83	1.70	2.51	0.62
75.6	1.05	1.52	2.74	0.84
75.7	1.05	1.52	2.74	0.85
100	1.30	1.33	3.00	1.11

It will be noticed that while Δ′ does not increase with the fraction of DPPO for all solvents, in the case of benzene, Δ′ decreases with an increase in the fraction of DPPO, while in the cases of chloroform, THF and TCE, the situations are the opposite.

Consequently, the order of increasing solvent strength depends on the fraction of DPPO in a polymer. For example, for DMPO, the strength of the solvent increases in the order of benzene, THF, chloroform, and TCE, while for DPPO, it increases in the order of THF, benzene, chloroform, TCE.

It is therefore evident that considering Δ and Δ′ different conclusions can be drawn regarding to the strength of solvents. The inconsistencies in these conclusions are illustrated in Table 5.8, in which the solvent strengths – according to Δ and Δ′ – are compared for the polymer-solvent systems considered in Table 5.6 and Table 5.7. The smaller the Δ or Δ′, the stronger the solvent.

Table 5.8: The relative strength of solvents

%DPPO	Chloroform		Benzene		THF		TCE	
	Δ	Δ′	Δ	Δ′	Δ	Δ′	Δ	Δ′
0	4	2	1	4	3	3	1	1
16.8	4	2	2	3	3	4	1	1
28	4	2	1	3	3	4	1	1
51.4	4	2	1	3	3	4	1	1
53.6	4	2	1	3	3	4	1	1
75.6	4	2	1	3	3	4	2	1
75.7	4	2	1	3	3	4	2	1
100	4	2	1	3	3	4	2	1

In order to determine whether the polymer is soluble in a particular solvent, a small quantity of polymer was added to approximately 5.0 mL of solvent. The samples were then shaken and a wait of approximately 15 minutes was taken before it was visually evident whether the sample was totally soluble, swollen, or insoluble in the solvent. Table 5.9 summarizes the results of solubility tests of polymers in different solvents.

Table 5.9: Summary of solubility tests on synthesized homopolymer and copolymer PPO in various solvents

%DPPO	Solubility[a]			
	Chloroform	Benzene	THF	TCE
0	+	+	s	+
16.8	+	+	s	+
28	+	+	+	+
51.4	+	+	+	+
53.6	+	+	+	+
75.6	+	+	+	+
75.7	+	+	+	+
100	+	+	+	+

[a] + polymer was soluble in the solvent
s polymer was swollen in the solvent
- polymer was insoluble in the solvent

It will be noticed that except for DMPO and the copolymer containing the lowest fraction of DPPO, all other polymers were soluble in the four solvents considered. Interestingly, according to the Δ and Δ' values summarized in Tables 5.6 and 5.7, respectively, the solubility of PPO in THF should increase with a decrease in the DPPO content, which is exactly the opposite of what was observed in the solubility tests summarized in Table 5.9. The limited solubility of DMPO and the copolymer containing the lowest fraction of DPPO could be due to their very high molecular weight. On the other hand, according to Table 5.4, these two polymers – as determined by GPC technique – had rather low molecular weights. It should be remembered, however, that in the GPC analysis, THF was used as a solvent and as a result of incomplete solubility in THF, the parameters such as M_n, M_w, PDI and ADP listed in Table 5.4 for these two polymers might not be reliable. On the other hand, the use of Δ and Δ' values as a measure of solvent strength might not always be accurate. Because of the incomplete solubility of DMPO and B/16.8/A in THF, this solvent was dropped from the list of remaining, potential solvents. Benzene was also dropped from the list because of its potential cancergenic properties, and because other alternatives existed (i.e., TCE and

chloroform). The preliminary gas permeation tests, using the films prepared from TCE and chloroform-based polymer solutions respectively, showed a superior mechanical integrity to the latter films. Consequently, chloroform was chosen as a common solvent for all polymers synthesized in this project.

5.5 Evaluation of polymer-solvent interactions

The use of chloroform as a common solvent for all polymers synthesized in this project alleviates the potential differences in the membrane structure arising from the differences in volatility of solvent in casting solutions. On the other hand, the differences arising from different strengths of polymer-solvent interactions in casting solutions could still exist, making the assessment of the optimum chemistry of PPO for the purpose of gas separation more difficult. The strength of these interactions for different polymers and solvents could be evaluated, considering the Δ and Δ' values listed in Tables 5.6 and 5.7 respectively. Figure 5.9 shows the graphical relation between Δ and Δ' as a function of %DPPO for chloroform. It will be noticed that despite the difference in the magnitude of Δ and Δ', the same increasing trend is exhibited in the percent of DPPO, which suggests a decreasing strength of polymer solvent interactions with an increasing content of DPPO. On the other hand, a sole reliance on Δ and Δ' values as a measure of polymer-solvent interactions might be misleading, as in the case of only partial solubility of DMPO and B/16.8/A in THF.

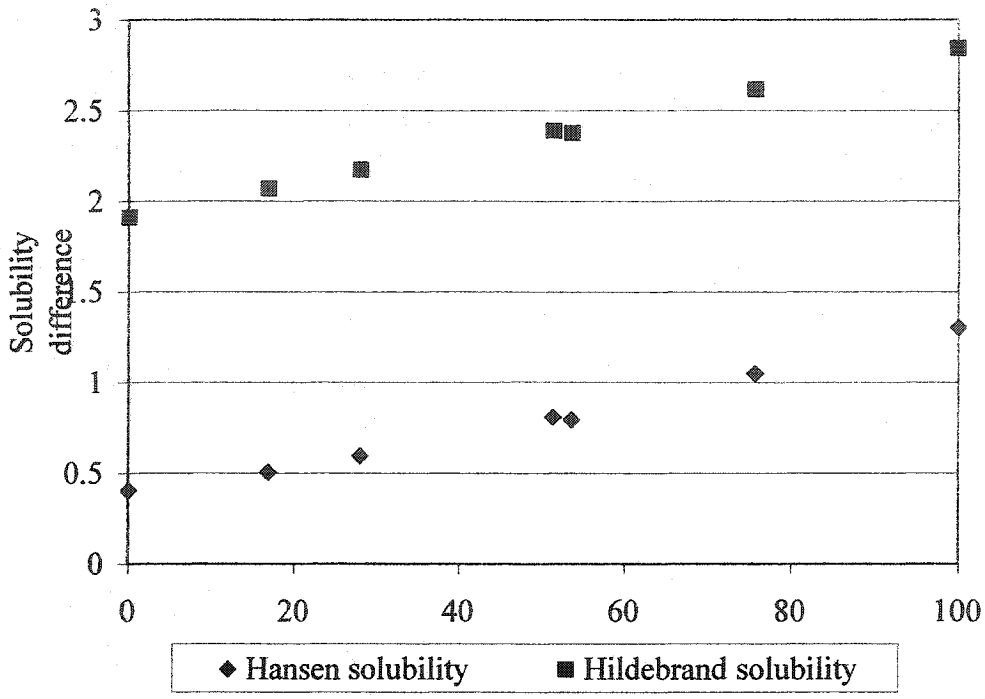

Figure 5.9: The effect of the fraction of DPPO on the difference in Hansen and Hildebrand solubility parameters of chloroform and polymers used in this study

Alternatively, the polymer-solvent interactions can also be evaluated experimentally by means of the intrinsic viscosity of polymer in a given solvent. In the presence of strong polymer-solvent interactions, polymer coils in diluted polymer solutions tend to be untangled, leading to higher viscosities. Consequently, the stronger the polymer-solvent interaction, the higher the intrinsic viscosity. Figure 5.10 shows the intrinsic viscosity of polymers in chloroform at 25°C as a function of the fraction of DPPO. It will be noticed that with the exception of DMPO, the intrinsic viscosity generally decreases with an increase of the %DPPO, suggesting that the polymer chloroform interactions decrease with the %DPPO. It is important to emphasize that intrinsic viscosity polymer-solvent systems depend not only on the polymer-solvent interaction but also on the molecular weight of polymer. The dependence of $[\eta]$ on $[M_n]$, known as the Mark-Houwink expression, is given by Eq. (3.7), and can be directly used as a measure of polymer-solvent interactions, but only when the molecular weight polymer in a given series of polymers does not change. In the situation when M_n is not constant – which is the case in this project – the value of the exponent a_n in the Mark-Houwink expression can be obtained by rearranging Eq. (3.7) as follows:

$$a_n = \frac{\ln\left[\frac{[\eta]}{K}\right]}{\ln[M_n]} \tag{5.6}$$

The bigger the a_n, the stronger the polymer-solvent interactions. With the exception of DMPO, the values of K and a_n for the polymers considered in this project are not available in the literature. Therefore, K_n of 3.8 x 10^{-4}, as reported by Hay (1967) for the DMPO-chloroform system, was assumed to be valid for other PPO-chloroform systems. Consequently, using experimentally-measured $[\eta]$ and M_n, a_n was calculated from Eq (5.7) for every PPO-chloroform system considered in this study. The experimental $[\eta]$ was determined with R^2 greater than 0.90.

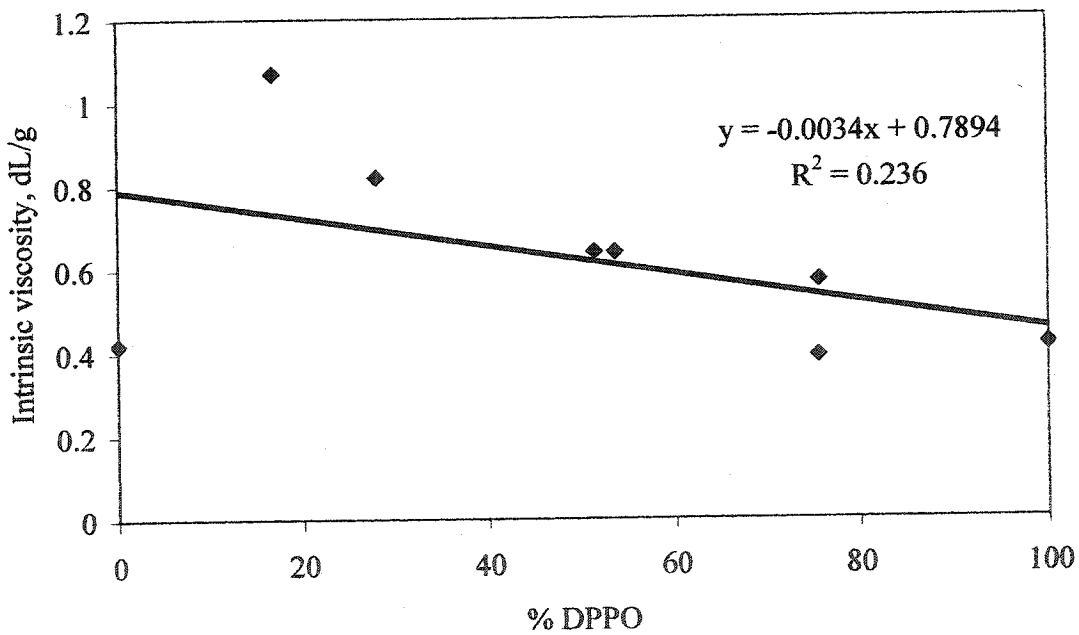

Figure 5.10: Intrinsic viscosity of PPO polymers in chloroform at 25°C as a function of DPPO content

Figure 5.11 presents the plot of a_n as a function of the %DPPO. It will be noticed that the relationship between a_n and %DPPO is similar as that between $[\eta]$ and %DPPO. The DMPO, which was clearly an outlier in Figure 5.10, is not an outlier in Figure 5.11. It is important to emphasize that a_n = 0.76, calculated for DMPO using Eq. (5.7), is similar to a_n = 0.73 reported by Hay (1967) for the DMPO-chloroform system.

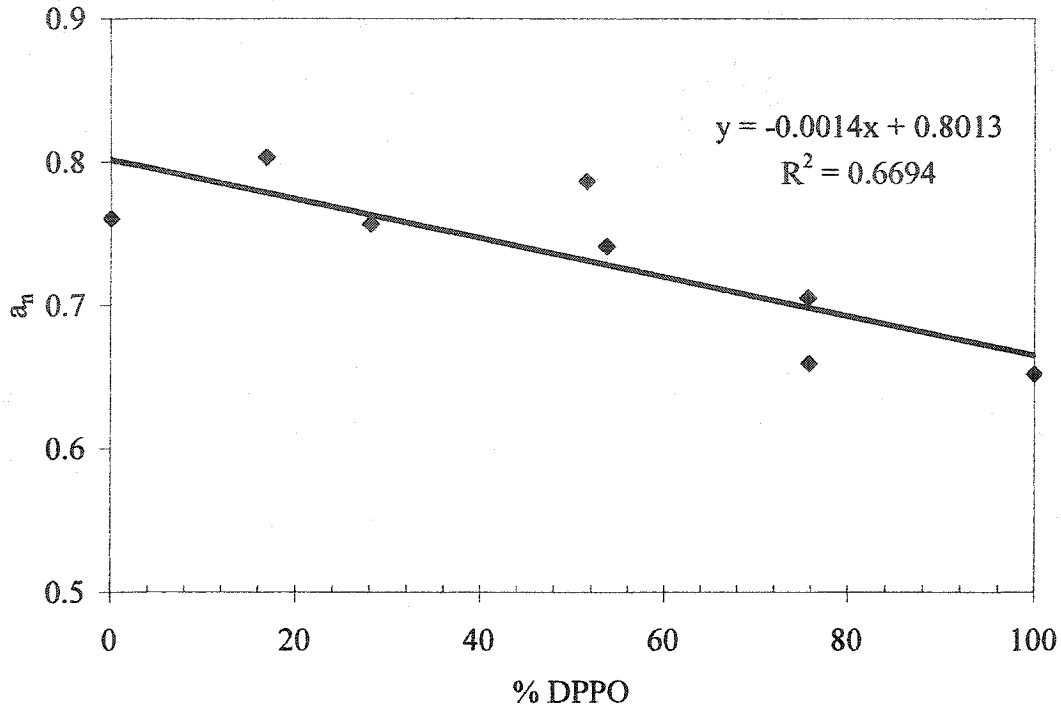

Figure 5.11: The effect of %DPPO in polymer composition on constant *a* of Mark Houwink expression

The linear regression of the data plotted in Figure 5.11 results in greater R^2 than that for the data plotted in Figure 5.10. The increase in R^2 is a result of removing the influence of the molecular weight. Although R^2 in Figure 5.11 is still significantly less than 0.95, it appears reasonable to conclude that the strength of polymer-solvent interactions decreases linearly with the %DPPO in polymer. This conclusion is consistent with the conclusion existing from considering the values of Δ and Δ' for the assessment of polymer-solvent interactions.

In general, the calculated a_n changes, depending on %DPPO, from 0.65 to 0.8. According to Barton (1983), the solvent for which a_n is in the range of 0.65-0.8 is classified as a "good" solvent, as far as the strength of solvent is concerned. Therefore, what is generally referred to as the effect of solvent – which includes volatility, size, and the strength of solvent in casting solution on gas transport properties – should be rather insignificant in the project (Kesting & Fritzsche, 1993).

CHAPTER 6 Gas Transport Properties

The gas transport properties of synthesized polymers were determined in single gas permeation tests. Gas permeation experiments were performed in a constant pressure (CP) testing system. A complete experiment for a given membrane consisted of tests with four gases in the following order: CO_2, N_2, O_2 and CH_4. The test with CO_2 was performed before the tests with other gases because of its "conditioning" properties, as it has been reported that the conditioning of membranes with CO_2 might lead to an increase in O_2 permeability without sacrificing of the O_2/N_2 selectivity (Jordan et al., 1990). The gases tested in this study represent the components of two very important gas mixtures, CO_2/CH_4 and O_2/N_2, which are of interest to membrane gas separation. However, the actual gas separation tests involving these mixtures have not been performed. The potential of synthesized polymers for separation in these binary mixtures was evaluated by considering the combination of the permeability of the faster gas from the mixture and the ratio of permeabilities of the mixture components. The method of evaluation of membranes based on gas permeabilities, as determined in single gas permeation tests, has been widely accepted in the membrane literature.

6.1 Survival of gas permeation tests

As discussed in Chapter 5, one of the criteria in selecting solvents for preparation of casting solutions was the mechanical integrity of the membrane during gas permeation experiments. While the membranes prepared using chloroform were better than those prepared using TCE, not all chloroform-based membranes survived gas permeation tests. The term "not surviving gas permeation test" means that the observed permeation rates for a given membrane were much greater, typically at least one order of magnitude, than the usual permeation rates. Membranes with such high permeation rates had no selectivity for gases.

Initially, for each polymer, six membranes were prepared for the tests with gases. If out of these six membranes at least four survived the complete experimental run, no

additional membranes were prepared, and the gas transport properties for a given polymer were determined based on performance of the successful membranes. If, however, fewer than four from the original six membranes survived the complete experimental run, additional films were prepared in order to have at least four successful membranes. In the case of some polymers, the fulfillment of this condition required up to five additional membranes.

Figure 6.1 presents the percentage of successful membranes from different polymers synthesized in this project. It is important to emphasize that because of the requirement of having at least four successful membranes, the percentages in Figure 6.1 refer to different sample sizes, varying from six to 11. Depending on the polymer, the percentage of successful membranes varied from 45.5% to 83%. Interestingly, the percentage of successful membranes made from homopolymers was lower than the percentage of successful membranes made from copolymers.

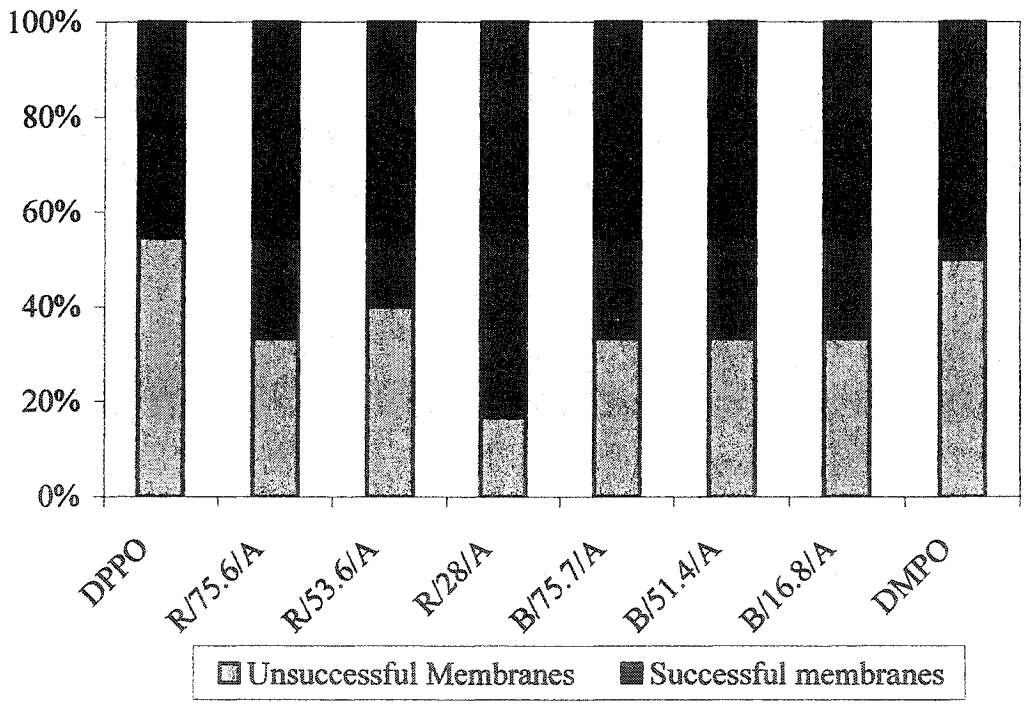

Figure 6.1: Percentage of successful and unsuccessful membranes prepared from synthesized polymers

It is well known that high molecular weight polymers are stronger than low molecular weight polymers. As shown in Table 5.4, while there are some differences in

the M_w and ADP, none of the synthesized polymers could be classified as a high molecular weight polymer; the problems with membranes surviving the entire experimental run could therefore be anticipated. Interestingly, DMPO, which had the second largest M_w and ADP, had the lowest rate of successful membranes. According to Alentiev et al. (1998), DMPO and DPPO have a greater tendency to form semi-crystalline structures than their copolymers. Under high-pressure gradients during gas permeation tests, semi-crystalline regions were the first to break, as it led to the development of defects in the membrane structure. On the other hand, according to DSC analysis, all polymers synthesized in this study were completely amorphous. It should be emphasized, however, that the DSC technique is not as sensitive for detecting semi-crystalline structures as the x-ray diffraction technique utilized by Alentiev et al. (1998).

Another reason for a lack of survival in gas permeation tests could be the existence of pinholes in the tested membranes. The pinholes could originate from micron, or even sub-micron sized solid particles in the casting solution, and/or dust particles settling on wet membranes immediately after pouring the casting solution on a glass plate. The pinholes would more likely occur in thin rather than thick membranes. The thickness of tested membranes varied from 7 to 35 μm. Figure 6.2 presents the numbers of successful and unsuccessful membranes, in different ranges of thickness. While the membranes of thickness varying from 21 to 25 μm show relatively the highest number of successful membranes[1], there is no apparent trend between the percentage of successful membranes and the membrane thickness. In particular, the percentage of successful membranes does not increase with the membrane thickness.

[1] The category, >35 μm is not included in this discussion because only one membrane in this category was tested.

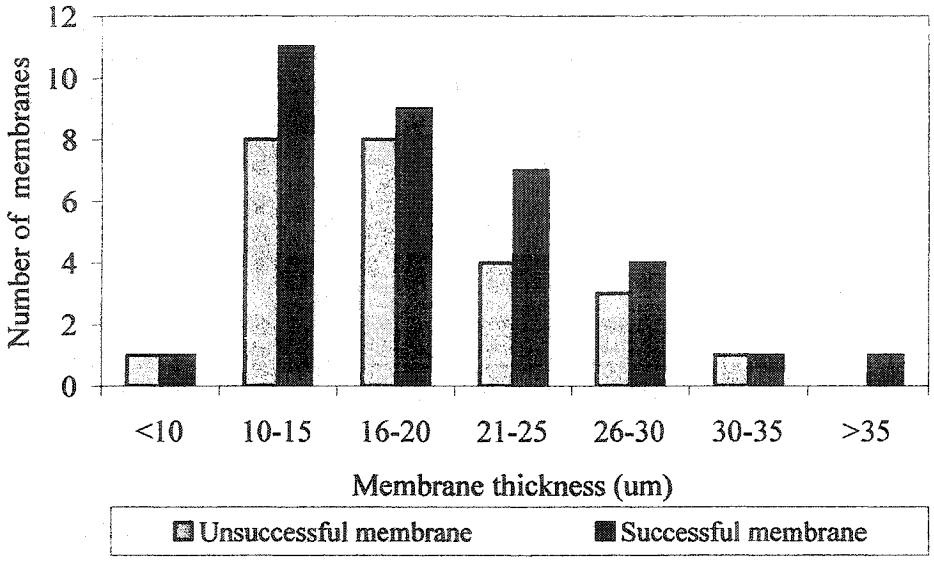

Figure 6.2: Effect of membrane thickness on its ability to survive the entire experimental run

If pinholes were responsible for membranes not surviving the entire experimental run, their presence would be evident shortly after the initiation of the first gas permeation test. However, as show in Figure 6.3, which illustrates the total percentage of unsuccessful membranes between different single gas permeation tests, some membranes ruptured during the second test (N_2) and even some during the last test (CH_4). This, in combination with a lack of relationship between the percentage of successful membranes and the membrane thickness, indicates that pinholes were not responsible for problems associated with gas permeation tests. Most likely, the problems in completing the entire experimental run for a given membrane were due to insufficient mechanical integrity resulting from relatively low molecular weight, and the tendency to form semi-crystallize structures.

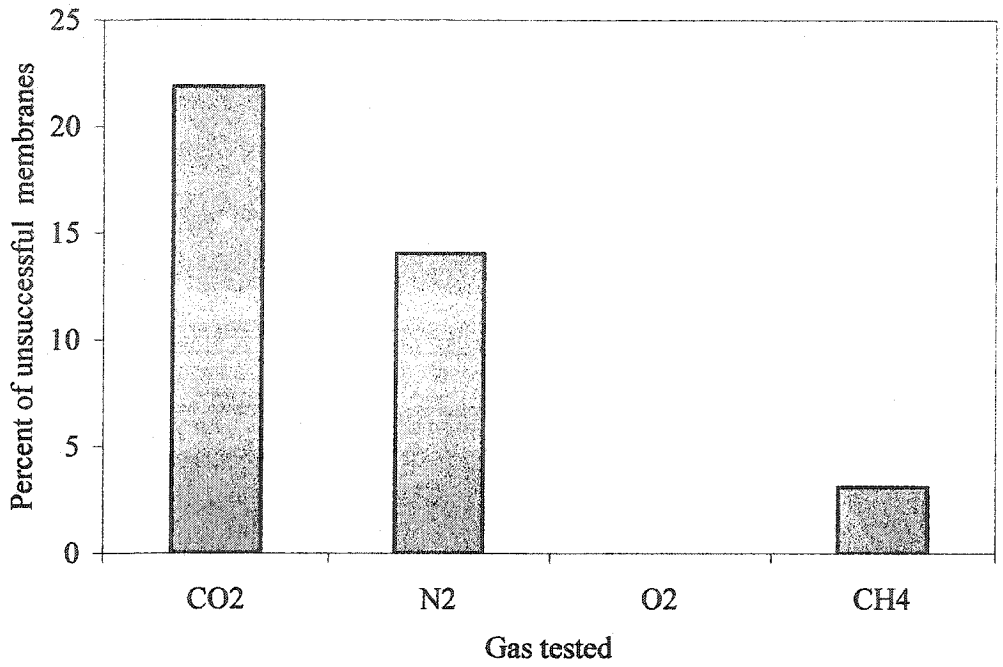

Figure 6.3: Distribution of the total percentage of unsuccessful membranes

6.2 Properties of gases and general trend in permeability coefficients

Regardless of the polymer, the permeability coefficients increase in the following order: $CH_4 \cong N_2 < O_2 < CO_2$. This order of permeability coefficients arises from the properties of tested gases – which are summarized in Table 6.1 – and the fact that synthesized polymers had high T_g. The permeability coefficient, as indicated by Eq. (2.1), is a product of the solubility coefficient (S) and diffusivity coefficient (D). Because of its highest condensibility (the highest critical temperature (T_c) (Linde, 1992)) and the highest solubility parameter (δ) (Grulke, 1989), CO_2 should have the highest S among the tested gases. At the same time, because of its lowest kinetic diameter (D_k) (Kesting & Fritzsche, 1993), CO_2 should also have the highest D. It is therefore not surprising that CO_2 has the highest permeability coefficient in synthesized polymers, among the studied gases.

Table 6.1: Some properties of gases used for testing membranes

Gas	T_c, K	δ, $Mpa^{1/2}$	D_k, Å
CO_2	304.15	12.3	3.30
CH_4	191.55	11.6	3.80
O_2	154.55	8.2	3.46
N_2	126.15	5.3	3.64

The permeability coefficients of N_2 and CH_4 are comparable to and lower than the permeability coefficient of O_2. This is despite the fact that because of its relatively high T_c and δ, CH_4 should have the second-highest solubility coefficient. In the case of glassy polymers such as those synthesized in this project, however, the permeability coefficient is influenced more by the diffusion coefficient than the solubility coefficient. Therefore, because of their smaller D_k, O_2 molecules permeate faster than the larger CH_4 and N_2 molecules. The solubility effects are not entirely negligible, as indicated by the fact that the larger but more soluble CH_4 molecules have a permeability coefficient comparable to the smaller but less soluble N_2 molecules.

6.3 Phenomenon of back permeation in constant pressure testing systems

In the testing system utilized in this study – which represents a typical constant pressure (CP) system – the permeating gas, as shown in Figure 4.2, is directed either into a collector line, or a soap bubble flow meter. Both the collector line and the soap bubble flow meter have one end open to the atmosphere. Consequently, every membrane is indirectly exposed to air during gas permeation experiments.

If not present in the permeating gas, the components of air could diffuse towards the membrane in the direction opposite to the direction of flow of the permeating gas. As a result, there could be non-zero partial pressures of N_2 and O_2 at the permeate side of the membrane. Gas permeation is driven by the partial pressure difference across the membrane; therefore, since the feed side of the membrane is continuously swept with a gas whose permeation rate is being measured, there could be a non-zero driving force for the permeation of air components from the permeate side to the feed side of the membrane. Such permeation against the total pressure gradient is referred to as a back permeation. The existence of back permeation would lead to errors in the measured

permeation rate and the driving force for permeation, and thus the permeability coefficient.

In single gas permeation tests involving CH_4 or CO_2, both O_2 and N_2 could back permeate through the membrane. In single gas permeation tests involving O_2 or N_2, only the non-tested air component could back permeate through the membrane. The phenomenon of back permeation is a fundamental mass transfer concept. Surprisingly, however, to our best knowledge, there is no quantitative model in the membrane literature taking this phenomenon into account.

6.3.1 Development of the model

A line connecting a testing cell with a soap bubble flow meter consists of two flexible tubes. The first tube has a length L_1 = 130 cm and an inside diameter d_1 = 0.635 cm. The second tube has a length L_2 = 15 cm and an inside diameter d_2 = 0.318 cm. One end of the first tube is permanently attached to the testing cell, while one end of the second tube is permanently attached into the soap bubble flow meter. During the measurement of the gas permeation rate, the open ends of two tubes are connected with each other and the permeating gas is directed to the bubble flow meter, which has a length L_3 = 15 cm and an inside diameter d_3 = 0.25 cm.

Figure 6.4 represents a schematic diagram of a path for the permeating gas to travel from the permeate side of the membrane to the atmosphere during the measurement of the permeation rate. The distance from the membrane is denoted as z, and the mole fraction of the permeating gas as x_A.

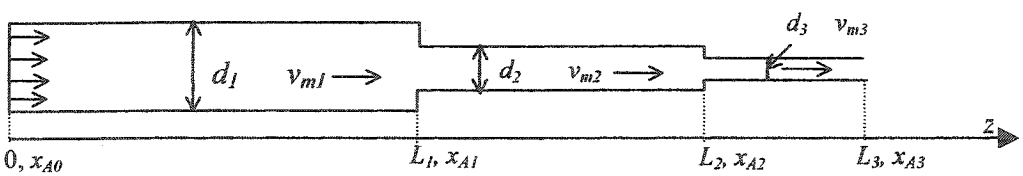

Figure 6.4: A path for the permeating gas to travel from the membrane to atmosphere during the measurement of gas permeation rate

Before initiation of the gas permeation experiment, both flexible tubes and the soap bubble flow meter are filled with air (B). After the initiation of the experiment, the tested gas (A) permeates through the membrane, and its concentration in the connecting tubes gradually increases. At the same time, because the feed side of the membrane is swept with A, the partial pressure of B at the feed side is zero and B back permeates through the membrane. Once steady-state conditions are established, the concentration profile of A, c_A (z), does not change with time, and the flux of A relative to a stationary point (N_A) is constant.

The situation described above represents a general case for the diffusion of A and B plus convection, in which steady-state N_A is given by the following expression (Geankoplis, 1993):

$$N_A = -cD_{AB}\frac{dx_A}{dz} + \frac{c_A}{c}(N_A + N_B) \tag{6.1}$$

where c (in mol/cm^3) is the total concentration of gas, D_{AB} (in cm^2/s) is the diffusion coefficient of A in B, and x_A is the mole fraction of A. The fluxes of A and B in Eq. (6.1) are in mol/cm^{2}s.

In order to measure the flow rate of the permeating gas, a soap bubble is made at z = 145 cm. The bubble is picked up by the permeating gas and moves towards the open end of the calibrated tube. The flow rate is determined from the time for the bubble to move a certain distance, corresponding to a calibrated volume, in the tube. In the case of slow gases such as N_2 and CH_4, this volume is just 0.05 cm^3, which represents one-tenth of the total calibrated volume of the bubble flow meter.

In principle, once the bubble is formed, the steady-state condition can no longer exist. Due to a continuous flux of A through the membrane and impermeability of the bubble for A and B, the concentration of A below the bubble gradually increases. On the other hand, even if the bubble were allowed to move through the entire calibrated tube and the volume of A increased by 0.5 cm^3, the concentration of A would not increase significantly, because 0.5 cm^3 represents a small fraction of the total volume of flexible tubes. Therefore, if the steady-state concentration profile of A existed before the bubble was formed, it would not be significantly disturbed during the measurement of the gas permeation rate.

The measured volumetric flow rate corresponds to the net velocity of the bulk phase (v_m) in the calibrated tube, which is given by:

$$v_m = \frac{N_A + N_B}{c} \tag{6.2}$$

Similarly, the net velocity of A can be written as:

$$v_A = \frac{N_A}{c} \tag{6.3}$$

Dividing Eq. (6.1) by c and substituting Eqs. (6.2) and (6.3) leads to:

$$v_A = -D_{AB}\frac{dx_A}{dz} + x_A v_m \tag{6.4}$$

Therefore, the net velocity of A has two components: the diffusive velocity and the convective velocity corresponding to the first and the second term on the right hand side of Eq. (6.4), respectively.

If $d_1 = d_2 = d_3$, v_A at steady state would be constant and independent of z. On the other hand, its components, because of variation of x_A with z, would depend on the position. The true permeation rate of A through the membrane corresponds to the convective term evaluated at $z = 0$. Referring to Figure 6.4, it is simply the $v_{m1}x_{A0}$ product, where $x_{A0} = x_A$ @ $z = 0$. The velocity of the bulk phase in the first tube (v_{m1}) can be determined from the measured flow rate (Q):

$$Q = \frac{\pi d_1^2}{4} v_{m1} \tag{6.5}$$

6.3.2 Application of the model

The application of the model will be presented, assuming that the permeating gas is either N_2 or O_2, and that these two gases are the only components of air.

Integration of Eq. (6.4) leads to:

$$\ln\left[x_A - \frac{v_A}{v_m}\right] = \frac{v_m}{D_{AB}} z + const \tag{6.6}$$

Taking x_A at $z = L_1$ as x_{A1}, the concentration profile in the first tube is given by:

$$x_A = \frac{v_{A1}}{v_{m1}} + \left[x_{A1} - \frac{v_{A1}}{v_{m1}} \right] e^{-\frac{v_{m1}}{D_{AB}}(L_1 - z)} \tag{6.7}$$

At $z = 0$, Eq. (6.7) becomes:

$$x_{A0} = \frac{v_{A1}}{v_{m1}} + \left[x_{A1} - \frac{v_{A1}}{v_{m1}} \right] e^{-\frac{v_{m1}}{D_{AB}}L_1} \tag{6.8}$$

There are two unknowns on the right-hand side of Eq. (6.8), v_{A1} and x_{A1}. The latter unknown can be eliminated by recognizing that Eq. (6.6) is also applicable for the second tube and the bubble flow meter. Taking x_A at $z = L_2$ as x_{A2} and x_A at $z = L_3$ as x_{A3}, the following two equations can be written as:

$$x_{A1} = \frac{v_{A2}}{v_{m2}} + \left[x_{A2} - \frac{v_{A2}}{v_{m2}} \right] e^{-\frac{v_{m2}}{D_{AB}}(L_2 - L_1)} \tag{6.9}$$

and

$$x_{A2} = \frac{v_{A3}}{v_{m3}} + \left[x_{A3} - \frac{v_{A3}}{v_{m3}} \right] e^{-\frac{v_{m3}}{D_{AB}}(L_3 - L_2)} \tag{6.10}$$

if A is N_2, $x_{A3} = 0.79$, while if A is O_2, $x_{A3} = 0.21$. The continuity equation requires that

$$v_{A1} d_1^2 = v_{A2} d_2^2 = v_{A3} d_3^2 \tag{6.11}$$

and

$$v_{m1} d_1^2 = v_{m2} d_2^2 = v_{m3} d_3^2 \tag{6.12}$$

Consequently, substituting x_{A2} from Eq. (6.10) with Eq. (6.9), and the resulting equation for x_{A1} with Eq. (6.8) allows for the elimination of x_{A1}.

The elimination of v_{A1} from Eq. (6.8) is more challenging. First of all, one must recognize that:

$$\frac{dx_A}{dz} \approx 0 \text{ at } z = 0 \tag{6.13}$$

The above equation implies that at the membrane surface, the diffusive velocity of A is negligible compared to the convective velocity of A. Since the convective velocity at $z = 0$ is entirely due to the permeation of A through the membrane, v_{A1} can be expressed in terms of the permeability coefficient of A, (P_A) in the tested membrane using the definition of permeability coefficient:

$$v_{A1} = \frac{P_A\left(p_f - p_0 x_{A0}\right)}{t}\left(\frac{d_m}{d_1}\right)^2 C_f \tag{6.14}$$

where p_f and p_0 are the total feed side and permeate side pressures, measured in cmHg, respectively; the latter is equal to the atmospheric pressure, t (in cm) is the membrane thickness, d_m (also in cm) is the membrane diameter, and C_f is a correction factor defined as:

$$C_f = 1\times10^{-10}\frac{T}{273.15}\frac{76}{p_0} \tag{6.15}$$

where T [K] is the absolute temperature at which the gas permeation test is performed. If P_A in Eq. (6.14) is expressed in Barrer, the use of C_f allows obtaining v_{A1} in cm/s. Substitution of Eq. (6.14) into Eq. (6.8) eliminates v_{A1}, but at the same time introduces P_A, which is also unknown. The net velocity of the bulk phase in the first tube can be written as

$$v_{m1} = v_{A1} + v_{B1} \tag{6.16}$$

where v_{B1} is the net velocity of B in the first tube, and v_{B1} is entirely due to the diffusion of B towards the membrane surface. At steady state,

$$v_{B1}d_1^2 = v_{Bm}d_m^2 \tag{6.17}$$

where v_{Bm} is the velocity of B through the membrane due to the back permeation. Similar to v_{A1}, v_{B1} can be expressed in terms of the permeability coefficient of B in the tested membrane:

$$v_{B1} = \frac{P_B\left(0 - p_0\left(1 - x_{A0}\right)\right)}{t}\left[\frac{d_m}{d_1}\right]^2 C_f = -\frac{P_B p_0\left(1 - x_{A0}\right)}{t}\left[\frac{d_m}{d_1}\right]^2 C_f \tag{6.18}$$

In the above equation, it is assumed that the partial pressure of B at the feed side of the membrane is zero, which is reasonable considering that in the actual experiments the feed side is continuously swept with A. The negative sign in Eq. (6.17) indicates that B is transported in a direction opposite to that of A.

Substituting Eq. (6.14) and Eq. (6.18) with Eq. (6.16) yields:

$$v_{m1} = \frac{P_A\left(p_f - p_0 x_{A0}\right)}{t}\left[\frac{d_m}{d_1}\right]^2 C_f - \frac{P_B p_0 (1 - x_{A0})}{t}\left[\frac{d_m}{d_1}\right]^2 C_f \tag{6.19}$$

The permeability coefficient P_B can be expressed in term of P_A,

$$P_B = P_A \alpha \tag{6.20}$$

where α is the ideal selectivity (permeability ratio) of B over A. Substituting Eq. (6.20) with Eq. (6.19) leads, after rearrangement, to

$$P_A = \frac{v_{m1} t}{[p_f - p_0 x_{A0} - \alpha p_0 (1 - x_{A0})] C_f}\left[\frac{d_1}{d_m}\right]^2 \tag{6.21}$$

The above equation is very important, because it expresses P_A in terms of v_{m1}, which can be determined from the experimental Q. On the other hand, elimination of P_A is associated with the introduction of α, which is also unknown. Substitution of Eq. (6.21) with Eq. (6.14), and the resulting equation with Eq. (6.8), yields one equation with two unknowns, x_{A0} and α.

The original assumption was that the permeating gas was either N_2 or O_2. If it was performed with N_2 and, in another experiment using the same membrane, O_2 was the permeating gas, Eq. (6.21) could also be used for the determination of the permeability coefficient of O_2, but in a slightly different form,

$$P'_A = \frac{v'_{m1} t}{\left[p'_f - p'_0 x'_{A0} - \frac{1}{\alpha}\left(1 - x'_{A0}\right)\right] C'_f}\left[\frac{d_1}{d_m}\right]^2 \tag{6.22}$$

The parameters with "primes" could be different from the corresponding parameters in Eq. (6.21). On the other hand, since the two tests involve N_2 and O_2, the permeability ratio in Eq. (6.21) is represented by the reciprocal of the permeability ratio from Eq.

(6.20). Substituting Eq. (6.22) with the equation for v'_{A1} similar to Eq. (6.14), and then the resulting equation with the equation for x'_{A0} similar to Eq. (6.8), results in one equation with two unknowns, x'_{A0} and α. Therefore, considering the experimental results obtained in two separate single gas permeation tests – one with N_2 and the other one with O_2 – two independent equations with three unknowns (x_{A0}, x'_{A0} and α) are obtained. The third independent equation is obtained by dividing Eq. (6.22) by the Eq. (6.21). The ratio of these two equations represents the unknown parameter α.

To obtain the actual permeability coefficient of N_2 and O_2 in a given membrane, the following iterative procedure is used. In the first iteration, the experimental data and an estimated value of α are used to determine the composition profiles in tests with N_2 and O_2, respectively. In the first iteration, α is taken as a ratio of permeability coefficients obtained without correcting the experimental data. The determined mole fractions x_{A0} and x'_{A0} allow for correcting the permeability coefficients P_A and P'_A, respectively. In turn, the corrected permeability coefficients are used to determine α for the second iteration. The procedure continues until the α values obtained in two consecutive iterations are the same.

In the case of experiments with CO_2 and CH_4, the actual three-component system is simplified into a two-component system by treating the back permeating air (B) as a single gas. The permeability coefficient of air (P_B) is estimated from the corrected permeability coefficients of N_2 and O_2 in membrane,

$$P_B = 0.79P_{N_2} + 0.21P_{O_2} \tag{6.23}$$

Once P_B is known, the analytical procedure for obtaining P_A is simplified. Rearranging Eq. (6.19) leads to:

$$P_A = \frac{v_{m1} + \dfrac{P_B p_0 (1 - x_{A0})}{t}\left(\dfrac{dm}{dt}\right)^2 C_f}{\left(\dfrac{p_f - p_0 x_{A0}}{t}\right)\left(\dfrac{dm}{dt}\right)^2 C_f} \tag{6.24}$$

Consequently, the expression for v_{A1} becomes:

$$v_{A1} = v_{m1} + \frac{P_B p_0 (1 - x_{A0})}{t} \left(\frac{dm}{dt} \right)^2 C_f \tag{6.25}$$

Substitution of Eq. (6.25) with Eq. (6.8) results in an equation in which x_{A0} is the only unknown. The corrected P_A is determined by back substitution of the calculated x_{A0} into Eq. (6.24).

6.3.3 Quantitative results

Figure 6.5 presents the relative error (denoted as a percentage) in the apparent permeability coefficient for different gases, due to back permeation of air component(s) through the membrane, as a function of the measured permeation rate. The error in Figure 6.5 is calculated from:

$$\text{Error} = \frac{P_A(\text{Eq.2.5}) - P_A\text{corrected}}{P_A(\text{Eq.2.5})} 100\% \tag{6.26}$$

The corrected P_A was determined from Eqs. (6.21) and (6.22) for the experiments with N_2 and O_2, respectively, and from Eq. (6.24) for the experiments with CH_4 and CO_2.

For permeation rates greater that 0.05 cm^3/min, the error is less than 1%. In the case of experiments with CO_2, the permeation rates were always greater that 0.1 cm^3/min. Consequently, the error in P_{CO2} was considered negligible, and is not included in Figure 6.5.

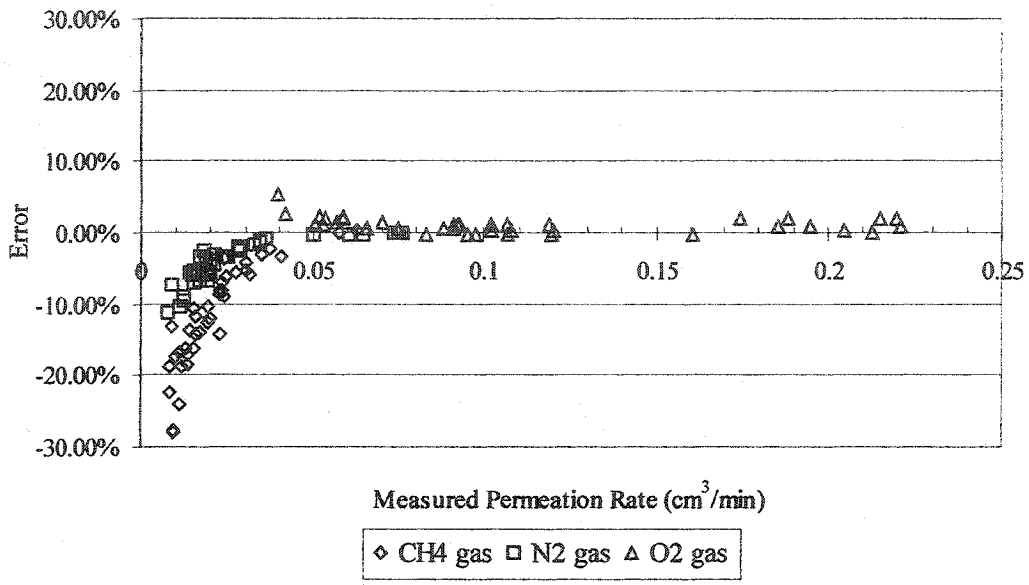

Figure 6.5: Error in experimentally-determined permeability coefficients due to the phenomenon of back permeation

It will be noticed that depending on the gas, the error is positive or negative. Back permeation of air component(s) always leads to underestimation of the actual flow rate of the permeating gas. Therefore, if the actual permeation rate were the only parameter affected by the phenomenon of back permeation, the error in the apparent permeability coefficient, if any, would always be negative. On the other hand, as shown in Figure 6.5, the error in the apparent permeability coefficient of O_2 is positive. This is because the phenomenon of back permeation also affects the driving force, which is required in the calculation of the permeability coefficient.

As x_{A0} decreases from unity, the driving force, $p_f - p_o x_{A0}$, increases. Since the permeability coefficient is inversely proportional to the driving force, neglecting back permeation – that is, assuming $x_{A0} = 1$ – leads to underestimation of the driving force and hence to overestimation of the permeability coefficient. Therefore, on one hand, because of the actual permeation rate, neglecting the phenomenon of back permeation leads to underestimation of the permeability coefficient; on the other hand, because of the of the actual driving force, it leads to overestimation of the permeability coefficient. If the relative error in the permeation rate is greater than the relative error in the driving force, the permeability coefficient calculated from Eq. (2.5) will underestimate the actual

permeability coefficient. If the relative error in the driving force is greater than the relative error in the permeation rate, the permeability coefficient calculated from Eq. (2.5) will overestimate the actual permeability coefficient.

The relative error in the permeation rate increases with an increase in the permeability coefficient of the back permeating gas, relative to the permeability coefficient of the tested gas. In tests with N_2, the back permeating O_2 is at least five times more permeable that N_2; in the case of tests with CH_4, the back permeating air is also more permeable than CH_4; as shown in Figure 6.5, the uncorrected permeability coefficients of N_2 and CH_4 underestimate the actual values. In the case of tests with O_2, the back permeating N_2 is less permeable than O_2, and the uncorrected permeability coefficient of O_2 overestimates the actual value.

The relative error in driving force depends on the feed pressure. At high feed pressures, the relative error in driving force will tend to be small, even when x_{A0} is significantly less than unity. In order for the permeation rates to be greater than 0.01 cm^3/min – that is, the minimum detectable flow of the utilized bubble flow meter – the tests with N_2 and CH_4, because of their low permeability coefficients, were carried out at feed pressures ranging from 120 to 175 psig. On the other hand, the experiments with O_2, because of their moderate permeability coefficient, were carried out at feed pressures ranging from 50 to 90 psig.

For the experiments with N_2 and CH_4, the negative error is a strong function of the measured permeation rate. As the measured permeation rate approaches 0.01 cm^3/min, the error increases rapidly, reaching values as high as 30%. It will be noticed that for similar experimental permeation rates of N_2 and CH_4, the error in the permeability coefficient of CH_4 is greater than the error in the permeability coefficient of N_2. This indicates that the back permeation rate in the experiments with CH_4 is greater than the back permeation rate in the experiments with N_2. Similar to the permeation rate, the back permeation rate is proportional to the permeability coefficient of the back permeating gas in the membrane, and the driving force for back permeation.

On one hand, because the permeability coefficient of O_2 is at least five times greater that the permeability coefficients of N_2, the permeability coefficient of air determined from Eq. (6.22) is always less than the permeability coefficient of O_2.

Consequently, the permeability coefficient of the back permeating gas in experiments with N_2 is greater than the permeability coefficient of the back permeating gas in experiments with CH_4. On the other hand, because there is no CH_4 in the air while the mole fraction of N_2 in the air is 0.79, the maximum possible driving force for back permeation is 1.0 atm in the experiments with CH_4 and 0.21 atm in the experiments with N_2. Therefore, for the errors in the apparent permeability coefficients of N_2 and CH_4, as shown in Figure 6.5, the difference in the driving force for the back permeating gases must be greater than the difference in their permeability coefficients.

The effects of steady-state back permeation are minimized when x_{A0} approaches to unity. In turn, according to Eq. (6.8), x_{A0} depends on v_m, L, and D_{AB}. In particular, x_{A0} increases with an increase in v_m and L, and a decrease in D_{AB}. Of these three parameters, only the first two are controllable. For a given permeation rate of tested gas, decreasing the diameter of flexible tube connecting the membrane with the bubble flow meter would increase v_m. It is also possible to increase the permeation rate by increasing the feed pressure. This however, might not always be a feasible solution, because of a limited mechanical strength of tested membranes. Another simple solution would be to increase the length of flexible tube between the testing cell and the bubble flow meter. A drawback of this solution would be a longer time required to establish a steady-state composition profile of the permeating gas and thus the steady-state permeation rate.

6.4 Parameters affecting gas transport properties

It is widely accepted in the field of membrane gas separation that the permeability coefficient of a gas in a given material is a material property. This assumption implies that gas transport properties of homogeneous polymeric membranes, such as those prepared in this project, are entirely determined by the polymer chemistry. On the other hand, there is evidence in the literature that while polymer chemistry is the most important factor, it is not the sole factor determining the microstructure and hence the gas transport properties of membranes. The other parameters include molecular weight and molecular weight distribution, method of film preparation, polymer-solvent interactions and the volatility of the solvent in casting solution, and the content of residual solvent in membranes (Kesting & Fritzsche, 1993). As already discussed, all membranes in this

project were prepared following the same protocol; casting solutions for all polymers were prepared in chloroform to the same concentration of the polymer. Moreover, polymer-chloroform interactions in all casting solutions were comparable. Consequently, the effects related to the method of preparation and the solvent in casting solution are eliminated or minimized in this project. Except for DMPO, the weight loss between 25°C and 300°C, which could be an indication of the presence of residual solvent in membranes, was in the range of 2% or less. Therefore, while the presence of residual solvent in tested membranes could play some role, its effect is assumed to be negligible.

For the synthesized homopolymers and copolymers, the effect of chemistry is represented by the actual percentage of DPPO units in the polymer (%DPPO). The use of the molecular weight as a parameter affecting gas transport properties might be misleading, because of different molecular weight in the repeat units of DMPO and DPPO. Consequently, the average degree of polymerization (ADP) rather than the molecular weight, is used as a parameter in the following discussion. The third factor that potentially influences gas transport properties of synthesized polymers is the structure (random versus block) of copolymers.

To decouple the effects related to polymer chemistry from those related to molecular weight, Figure 6.6 plots ADP versus %DPPO for the synthesized polymers. While the ADP varies from 67 for B/51.4/A to 317 for B/75.7/A, there is no clear relationship between the ADP and the %DPPO, when all polymers are considered. The B/75.7/A had the highest ADP value because it had the highest average molecular weight. On the other hand, in considering only random copolymers, the ADP decreases with increases in the %DPPO.

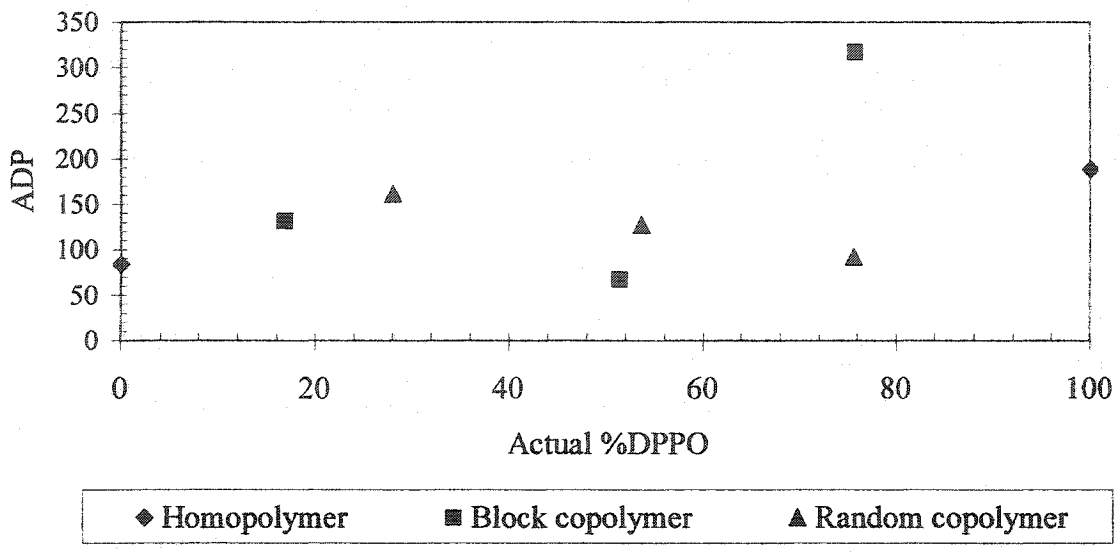

Figure 6. 6: Effect of %DPPO on the *ADP* of synthesized polymers

According to Chowdhury et al., the permeability coefficients of N_2, O_2, CH_4, and CO_2 in DMPO increase, while the O_2/N_2 and CO_2/CH_4 permeability ratios decrease with increases in the molecular weight of polymers (1999). The observed result was explained on the basis of increasing chain entanglement and chain stiffness, which led to lower packing density in high molecular weight DMPO. In turn, lower packing density is responsible for higher free volume in polymers, and hence increases in the permeability of gases. It is important to note, however, that the differences in ADP of DMPOs considered by Chowdhury et al. were significantly greater than the differences in ADP of polymers studied in this project. Moreover, the ADP of the DMPO having the lowest molecular weight in Chowdhury et al.'s work was greater than 317, which is the highest ADP in this project. Consequently, the synthesized polymers might have too low an ADP for the above-mentioned effects related to the length of macromolecules. Therefore, while there are some variations in the ADP among the synthesized polymers, they are not expected to have any major influence on the gas transport properties. This means that the %DPPO should be the main factor determining these properties.

6.4.1 Effect of DPPO content on gas transport properties of block copolymers

Figure 6.7 presents the effect of %DPPO on the permeability coefficients of CO_2 (Figure 6.7a) and O_2 (Figure 6.7b) in block copolymers. For comparison, the figure 6.7 also includes the experimental data for homopolymers and the literature data for homopolymers and copolymers. The experimental data presented in Figure 6.7 and in all subsequent figures were corrected for the effects of back permeation discussed in section 6.3. The error bars in Figure 6.7 and in all subsequent figures represent standard deviation from the permeation data of at least four identical membranes.

It will be noticed that for DMPO, the CO_2 permeability coefficient is comparable, while the O_2 permeability coefficient is significantly greater than the values in respective literature. In the case of the synthesized DPPO, the permeability coefficients CO_2 and O_2, although slightly greater, are comparable to the literature data. Generally, the O_2 and CO_2 permeability coefficients decrease with the DPPO content. The largest drop in permeability coefficient occurs between DMPO and B/16.8/A. The O_2 permeability coefficient of B/16.8/A is comparable to the O_2 permeability coefficients of random copolymers reported in the literature (Alentiev et al., 1999). It is important to emphasize that apart from the data for two random copolymers of relatively low %DPPO reported by Alentiev et al., there is no other gas permeation data related to copolymers of DMPO and DPPO in the literature.

Interestingly, while the permeability coefficient generally decreases with an increase in %DPPO, the CO_2 and O_2 permeability coefficients of B/75.7/A are lower than those of DPPO. This is despite the fact that B/75.7/A had the highest ADP among the synthesized polymers, which confirms the anticipated lack of influence of the length of macromolecule on gas transport properties.

(a) CO_2

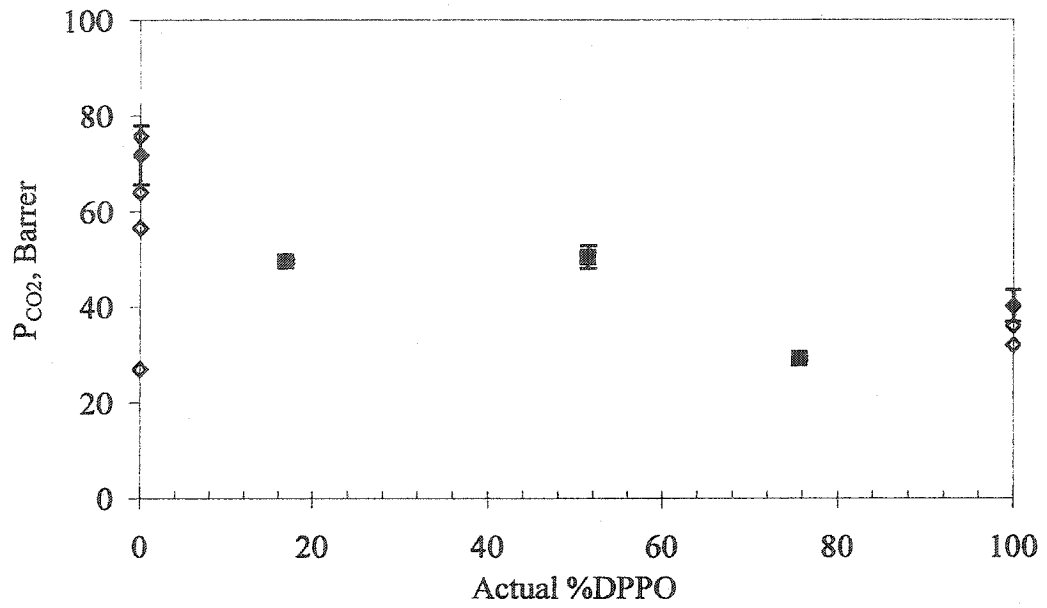

(b) O_2

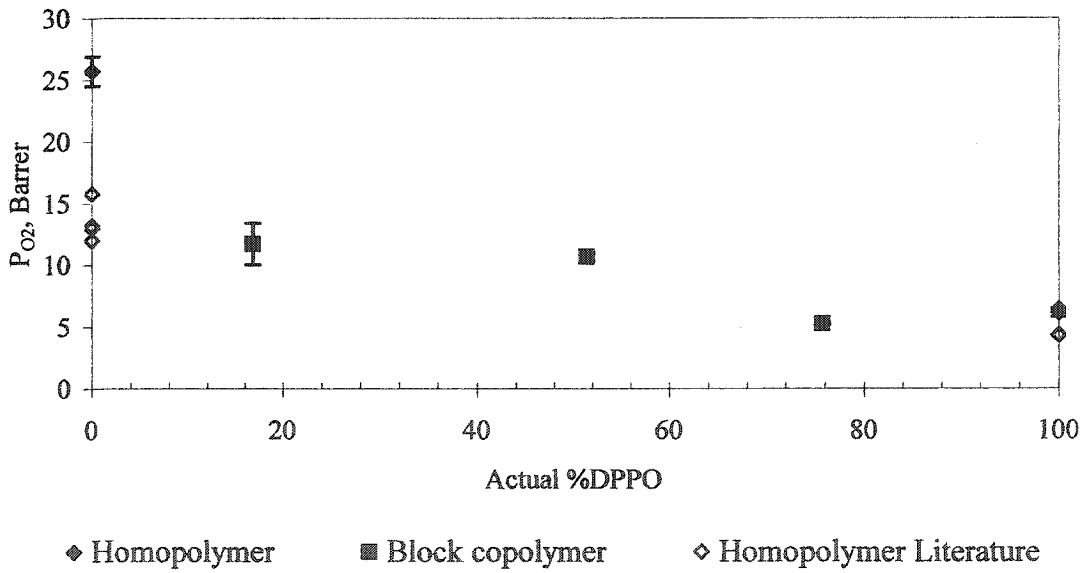

Figure 6.7: Permeability coefficients of (a) CO_2 and (b) O_2 in DMPO, DPPO and their block copolymers

The observed decrease in permeability coefficients with increases in DPPO content can be explained considering the work of Tonelli (1973), who found by conformational energy analysis that pendent phenyl groups in DPPO have energy minima at 90° and 270° to the plane of the backbone phenyl groups. This implies that the pendent phenyl groups in DPPO have a preferential perpendicular orientation to the plane of backbone phenyl rings. In turn, this could lead to reduction in the intermolecular spacing, thus reducing the free volume for diffusion and hence the permeability coefficient.

The minimum permeability coefficient of gases in B/75.7/A can be explained considering interactions between permeating species and the pendent phenyl groups. While the increase in DPPO content leads to a decrease in the free volume of a polymer and the diffusion coefficient, the strength of interactions between permeating species, in particular CO_2, and a polymer should increase. This, in turn, could lead to an increase in the solubility coefficient. Since the permeability coefficient in glassy polymers is influenced more by the diffusion coefficient than by the solubility coefficient, it generally decreases with the DPPO content. However, since the solubility effects are not entirely negligible, this decrease is not monotonic. The minimum in permeability coefficient for B/75.7/A is more evident for CO_2 in Figure 6.7a than for O_2 in Figure 6.7b, because CO_2 is more polar than O_2.

Figure 6.8 presents the effect of %DPPO on CO_2/CH_4 (Figure 6.8a) and O_2/N_2 (Figure 6.8b) permeability ratios in block copolymers. For comparison, the figure also includes the experimental data for homopolymers and the literature data for homopolymers and copolymers. The CO_2/CH_4 and O_2/N_2 permeability ratios increase drastically between DMPO and B/16.8/A. As the DPPO content increases beyond 16.8%, its influence on the permeability ratios appears to be rather weak. While the CO_2/CH_4 permeability ratio of B/75.7/A and DPPO are slightly greater than the CO_2/CH_4 permeability ratio of B/16.8/A, the O_2/N_2 permeability ratio of B/16.8/A is actually greater than the O_2/N_2 permeability ratio of any other homopolymer or block copolymer. It should be emphasized, however, that the reported O_2/N_2 permeability ratio of B/16.8/A is associated with a significant uncertainty, as indicated by the size of the error bar.

Considering the inverse relationship between permeability and selectivity (Robeson, 1991), one could anticipate a clearer increases in the permeability ratios with

%DPPO.

(a) CO_2/CH_4

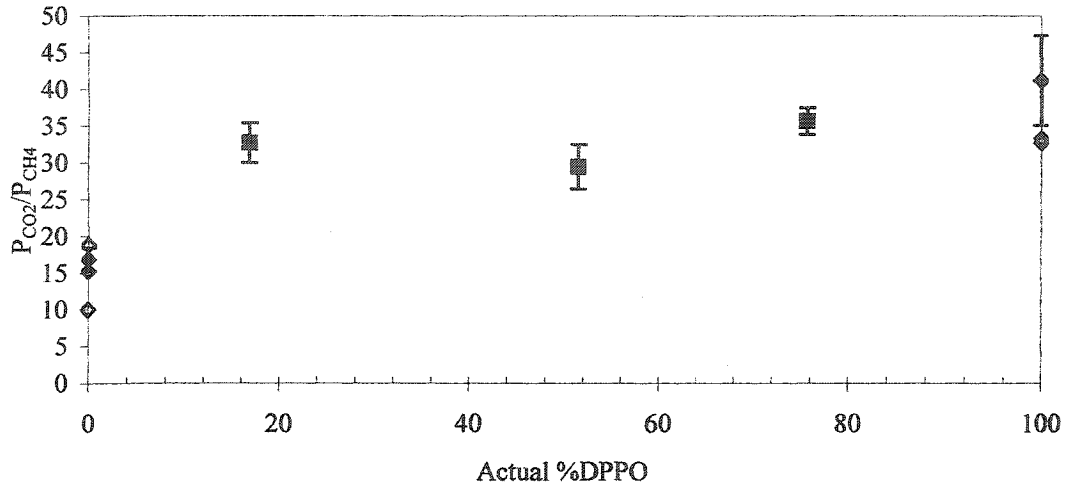

(b) O_2/N_2

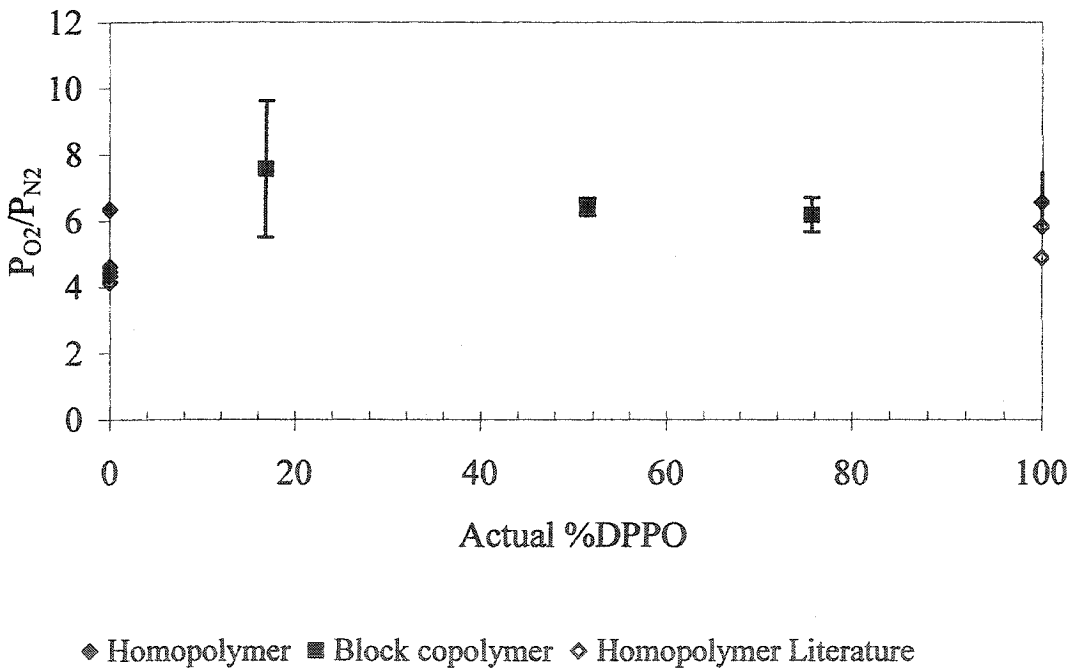

Figure 6.8: Permeability ratios of (a) CO_2/CH_4 and (b) O_2/N_2 in DMPO, DPPO, and their block copolymers

A decrease in the permeability coefficient with %DPPO, as shown in Figure 6.7, was attributed to decreases in the diffusion coefficient resulting from the decrease in free volume of polymer. Normally, a decrease in the diffusion coefficient is associated with an increase in the diffusion selectivity. Since the diffusion effects dominate the solubility effects in glassy polymers, it appears that after an initial jump in the diffusion selectivity resulting from the introduction of a small fraction of side phenyl groups, this parameter is not affected by further introduction of these groups. The fact that in the case of CO_2/CH_4 the permeability ratio slightly increases with %DPPO beyond B/16.8/A is probably due to solubility effects, arising from strong interactions between CO_2 and the pendent phenyl groups.

6.4.2 Effect of DPPO content on gas transport properties of random copolymers

Figure 6.9 presents the effect of %DPPO on the permeability coefficients of CO_2 (Figure 6.9a) and O_2 (Figure 6.9b) in random copolymers. Figure 6.9, similar to Figure 6.7, includes the experimental and literature data for homopolymers. Unlike block copolymers, the minimum permeability coefficient for the random copolymer with the largest DPPO content is not evident in Figure 6.9. The influence of the DPPO content on the CO_2 and O_2 permeability coefficients is strong when the %DPPO varies from 0 to 50%. On the other hand, the permeability coefficients in R/53.6/A, R/75.6/A and DPPO are comparable.

Figure 6.10 presents the effect of %DPPO on the CO_2/CH_4 (Figure 6.10a) and O_2/N_2 (Figure 6.10b) permeability ratios for random copolymers. For comparison, the figure also includes the experimental and literature data for both homopolymers. Generally, for random copolymers, the uncertainty in the permeability ratio data is quite significant, as indicated by the size of the error bars. Similar to block copolymers, the CO_2/CH_4 permeability ratio in random copolymers increases drastically between DMPO and the copolymer with the lowest content of DPPO (R/28.0/A). In the case of O_2/N_2, the increase in the permeability ratio between DMPO and R/28.0/A is modest. Similar to block copolymers, the influence of DPPO content beyond R/28.0/A on the permeability ratios is rather weak. In the case CO_2/CH_4, the permeability ratio increases with the %DPPO, reaching the maximum value for DPPO. In the case of O_2/N_2, the permeability

ratio increases with %DPPO for copolymers but then drops for DPPO. The O_2/N_2 permeability ratio in DPPO is lower than in random copolymers.

(a) CO_2

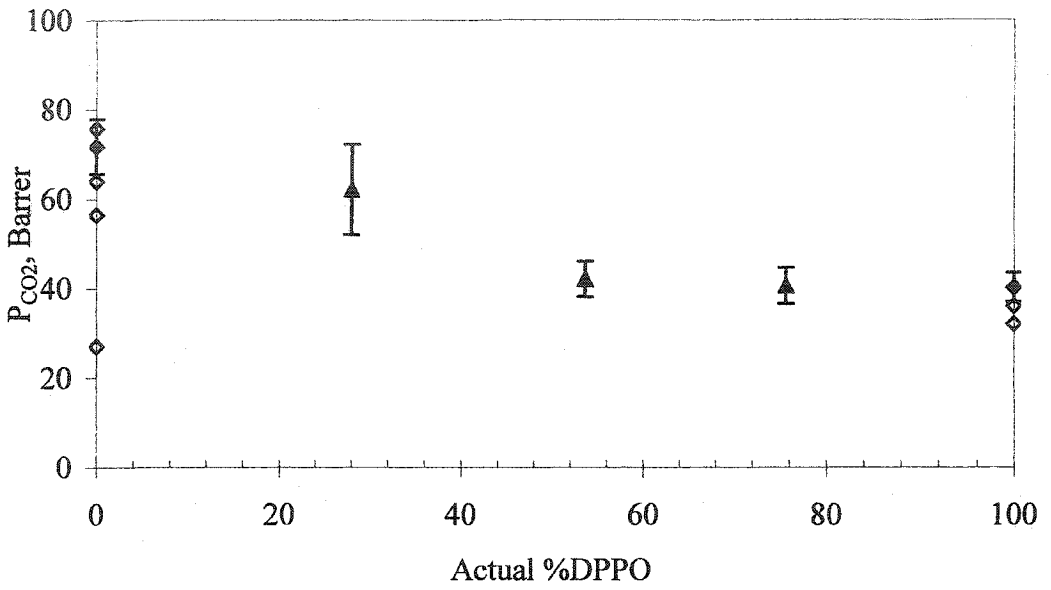

(b) O_2

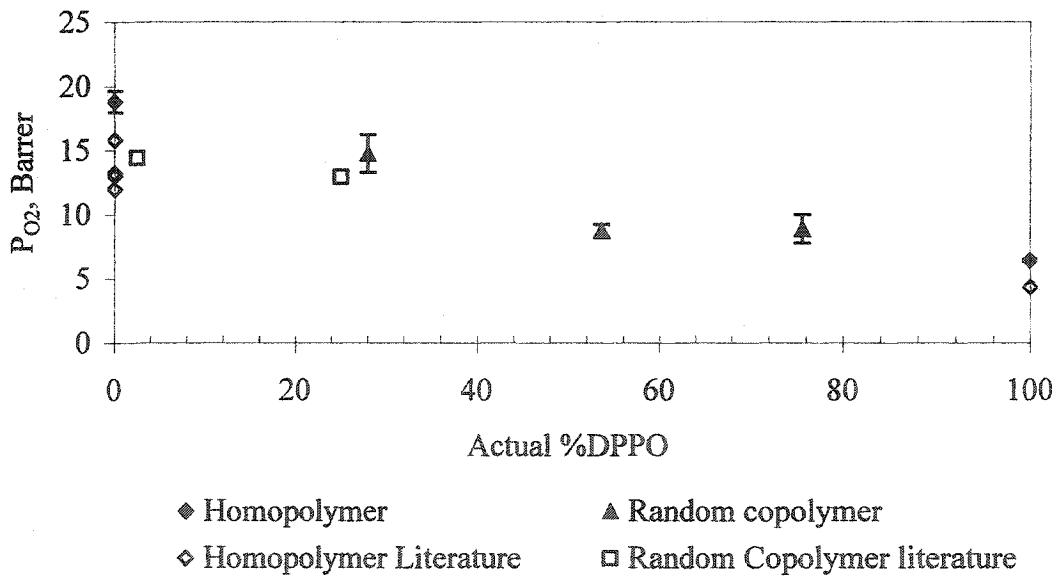

Figure 6.9: Permeability coefficient of (a) CO_2 and (b) O_2 in DMPO, DPPO and their random copolymers

(a) CO_2/CH_4

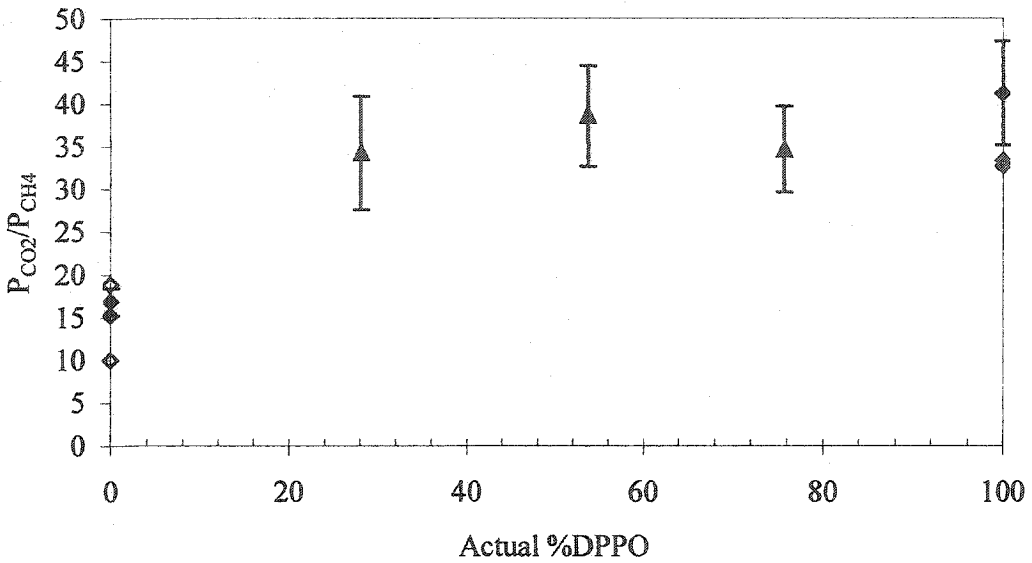

(b) O_2/N_2

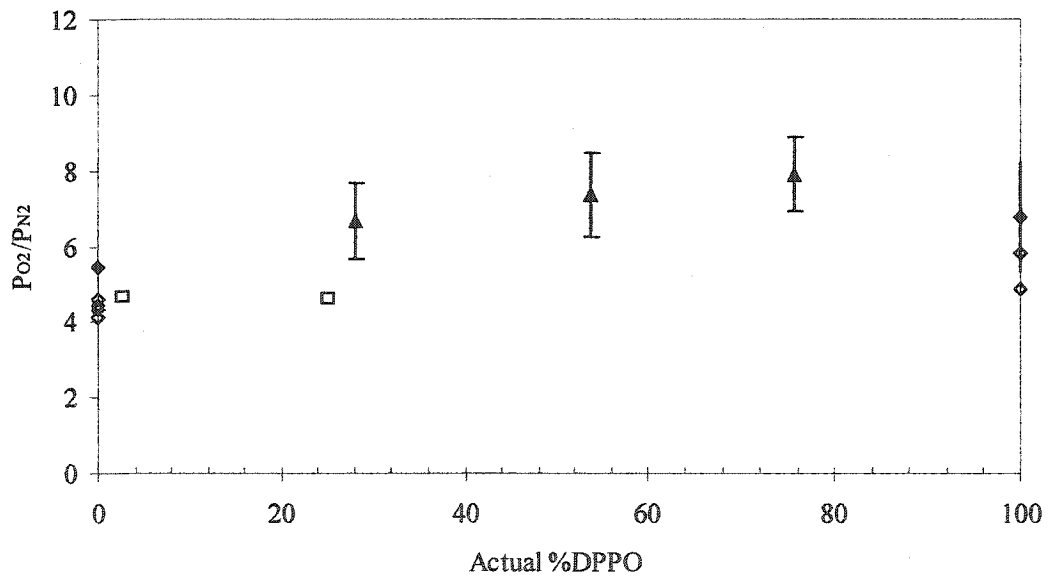

Figure 6.10: Permeability ratios (a) CO_2/CH_4 and (b) O_2/N_2 in DMPO, DPPO and their random copolymers

6.4.3 Effect of structure of copolymers and assessment of potential of synthesized polymers for gas separation

Figure 6.11 summarizes the average gas transport properties of synthesized polymers: Figure 6.11a presents the plot of CO_2/CH_4 permeability ratio versus CO_2 permeability coefficient, and Figure 6.11b presents the plot of O_2/N_2 permeability ratio versus O_2 permeability coefficient. In both figures, an upper-bound line for the respective pairs of gases is also included. The position relative to the upper-bound line can be used to assess the potential of membrane materials for the separation of a given pair of gases. It is desired for a membrane material that the combination of its permeability and selectivity falls above the upper-bound line.

Figure 6.11 can also be used in the comparison of block and random copolymers. The data for block and random copolymers of similar DPPO content are presented, using symbols of the same shape. The symbols for block copolymers, however, are filled while the symbols for random copolymers are not filled.

Considering Figure 6.11a, it will be noticed that for a given shape, unfilled symbols representing random copolymers fall closer to the upper-bound line than the filled symbols representing block copolymers. This indicates that for a given %DPPO, random copolymers have a better potential than block copolymers for separation of CO_2/CH_4 mixtures. For the symbols falling above the upper-bound line – as in the case of Figure 6.11b – it is desired that they be as far from the upper-bound line as possible. With the exception of copolymers with the lowest DPPO content – for which the distances from the upper-bound line for block and random copolymers are comparable – the random copolymers have a better potential for O_2/N_2 separation than their block counterparts. For copolymers with the low and higher targeted DPPO content, the more favorable gas transport properties of random copolymers are due to their higher permeability for gases. For copolymers with the targeted DPPO content of 50%, the more favorable gas transport properties of random copolymers are, on the other hand, due to their higher selectivity.

(a) CO_2/CH_4

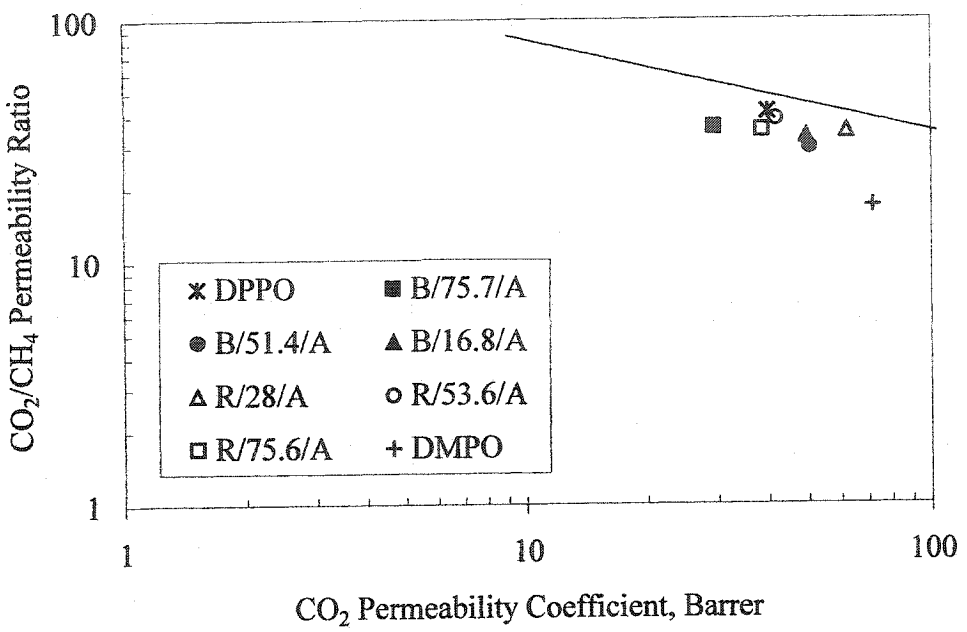

(b) O_2/N_2

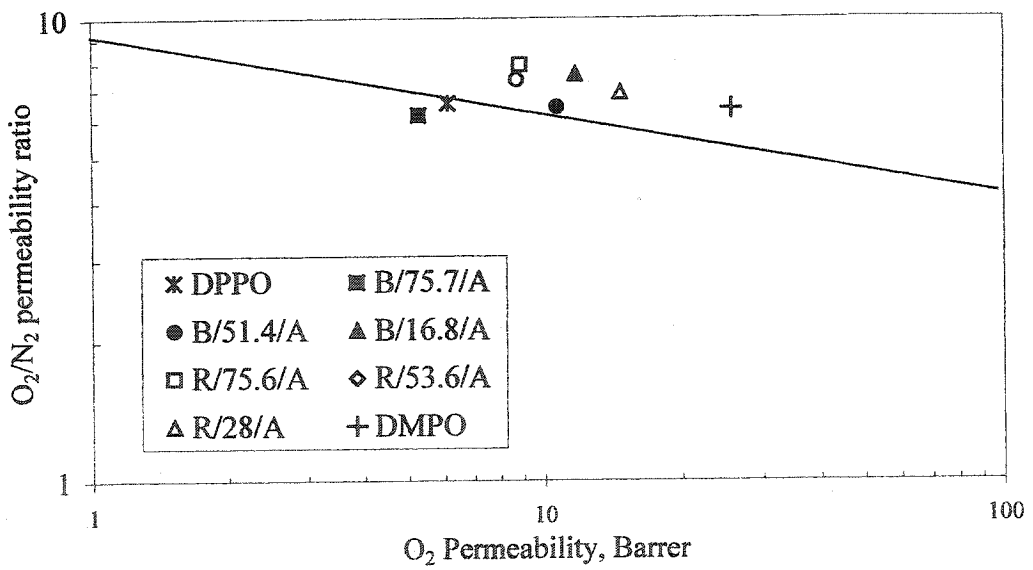

Figure 6.11: Performance of hompolymers, and block and random copolymers in comparison to upper-bound line for (a) CO_2/CH_4 and (b) O_2/N_2

It should be emphasized that according to Robeson (1991), who proposed the concept of the upper-bound line, 12 years ago there were no polymers above the upper-bound line. While in the mean time the original upper bound has been shifted up – because of the development of new high-performance polymers – the results presented in Figure 6.11b should be taken with caution. This is because the polymers falling above the upper-bound line include DMPO which, according to the literature data, should fall below the line.

It is important to note that the correction factor for back permeation has been included in the data presented in Figure 6.11. Without the incorporation of this correction factor, the performance of synthesized polymers would appear even more favorable. As a matter of fact, it was this extraordinary performance that led the author of this paper to re-examine the method of measurement of gas permeation rates in constant pressure systems, and the development of the model incorporating the effect of back permeation.

The model discussed in section 6.3 assumes the existence of a steady-state composition profile in the bubble flow meter at the time of making the bubble. In reality, however, this may not be the case. The flow path for the permeating gas, presented in Figure 6.4, exists only during the measurement of the gas permeation rate. Otherwise, the flexible tube of length L_1 is connected to a long collector line. Because the total length of tubing between the permeate side of the membrane and the atmosphere is considerably greater when the cell is connected to the collector line (as compared to the situation depicted in Figure 6.4), the steady-state mole fraction of the permeating gas at L_1 must also be greater in the former arrangement. Consequently, immediately after connecting the cell to the bubble flow meter, there is an excess of the permeating gas in the flexible tube and an excess of air in the bubble flow meter. As a result, before the steady-state composition profile is established, the net diffusive flow of the back permeating gas toward the membrane will be greater than the back permeation rate. At the same time, transient back permeation rate is less than the steady-state back permeation rate. Without a systematic model describing these transient effects, it is difficult to speculate on their impact on the measured gas permeation rates. If they led to a greater error in the measured permeation rates of slow gases than the one estimated from the steady-state

model, the actual N_2/O_2 and CO_2/CH_4 permeability ratios would decrease, shifting down the points shown in Figure 6.11.

To eliminate possible errors due to unsteady-state effects, a bubble flow meter must be connected to the testing cell at all times, rather than only during the measurement of the permeation rate. This means that a testing system consisting of six testing cells – such as the one utilized in this project – would require six bubble flow meters rather than only one. It would also be interesting to develop a model to quantitatively assess the transient effects on the measured gas permeation rates through the membrane.

CHAPTER 7 Conclusions

The following is the list of conclusions that have been drawn from this study. The conclusions are presented in two parts. The first part summarizes findings concerning material development aspects, and the second part summarizes the conclusions concerning membrane formation and the gas transport properties of synthesized polymers.

7.1 Material development

- Two homopolymers – DMPO and DPPO – as well as three different block and three different random copolymers have been successfully synthesized. The presence of the desired functional groups and the absence of undesired by-products in synthesized polymers were confirmed by the infrared analysis.
- For block copolymers, the targeted contents of DPPO were 20%, 50% and 80%. The actual DPPO contents, as determined by ^{1}H NMR analysis, were 16.8%, 51.4%, and 75.7%. For random copolymers, the targeted contents of DPPO were 25%, 50% and 75%. The actual DPPO contents were 28.0%, 53.6% and 75.6%.
- The existence of block and random structures in synthesized copolymers was confirmed by thermogravimetric analysis. Block copolymers showed two distinct decomposition temperatures corresponding to the decomposition temperatures of DMPO and DPPO. On the other hand, random copolymers showed a single decomposition temperature that increased with the DPPO content.
- The synthesized polymers fall into the category of low molecular weight polymers. The average degree of polymerization, which because of the difference in the molecular weight of repeat units in DMPO and DPPO better describes the size of synthesized macromolecules, varied from 67 to 317. No relationship was observed between the average degree of polymerization and the DPPO content in synthesized polymers.

- Differential Scanning Calorimetry was used to determine the glass transition temperature of polymers. The anticipated increase in the glass transition temperature with the DPPO content has not been observed.

7.2 *Membrane formation and gas transport properties of polymers*

- Chloroform, TCE and benzene were identified as potential solvents for the preparation of solution-cast membranes from synthesized polymers.
- For chloroform, which was selected as a solvent for the preparation of membranes, the polymer-chloroform interactions in casting solutions were evaluated using the concept of solubility parameters, and experimentally measured intrinsic viscosities of synthesized polymers. It was established while using both methods the polymer-chloroform interactions decrease with increases in the DPPO content. Based on the numerical value of the exponent in the Mark Houwink expression, it is concluded that despite some differences in the polymer-chloroform interactions with the %DPPO, chloroform can be classified as a strong solvent for all synthesized polymers.
- Homogeneous membranes from all synthesized polymers were tested with single gases in a typical constant pressure testing system. The percent of membranes that survived the entire experimental run, which consisted of tests with four different gases, varied from 45.5% to 83.3%. Problems with surviving the entire experimental run were attributed to a limited mechanical integrity of membranes, arising from the low molecular weight of the polymers and the tendency to form semi-crystalline structures.
- Regardless of polymer, the permeability coefficients of four tested gases in membranes from synthesized polymers increased in the following order: $CH_4 \cong N_2 < O_2 < CO_2$.
- The permeability coefficients and the ratios of permeability coefficients (CO_2/CH_4 and O_2/N_2) depend on the DPPO content. The strongest effect of %DPPO is observed between DMPO and copolymers of low-DPPO content: in particular, the permeability coefficients of O_2 and CO_2 increase while the O_2/N_2 and CO_2/CH_4 permeability ratios decrease with increases in DPPO content.

- Considering block and random copolymers of similar DPPO content, random copolymers show generally more favorable gas transport properties.
- Considering the concept of the upper-bound line, synthesized polymers are more suitable for the separation of O_2/N_2 mixtures than CO_2/CH_4 mixtures.
- Most synthesized polymers fall above the upper-bound line for O_2/N_2 separation. However, these very exciting results should be taken with caution, because the polymers above the upper-bound line include DMPO which, according to the literature data, should be below the upper-bound line.
- The performance of synthesized polymers above the upper-bound line has led to a re-examination of the method of measurement of gas permeation in constant pressure-type systems. A steady-state model, which includes the possible effects of the back permeation of air components through the membrane, has been developed.
- The model indicates that permeability coefficients of slow gases such as CH_4 and N_2 could be underestimated by up to 30% when the measured permeation rates approach the minimum detectable flow of the bubble flow meter (i.e., 0.01 cm^3/min). Consequently, an application of the proposed model shifts down the experimentally-determined gas transport properties of synthesized membranes, but a number of polymers for O_2/N_2 separation remain above the upper-bound line.

CHAPTER 8 Recommendations

The following are the recommendations formulated, based on the results of the present work:

- The experimental procedures related to the synthesis of copolymers should be modified in order to increase their degree of polymerization. For example, the temperature during oxidation of 2,6-diphenylphenol could be increased to 60°C, and and decreased to 25°C during the oxidation of 2,6-dimethylphenol. Increasing molecular weight would allow for the improvement of the mechanical integrity of membranes, and probably their permeability for gases.
- Gas transport properties from newly-prepared copolymers should be re-examined, both in a testing system similar to the one utilized in this work, and in a constant volume testing system. In addition, the actual gas separation experiments involving CO_2/CH_4 and O_2/N_2 mixtures should be performed.
- Thin film composite membranes could be prepared from the most promising polymers (i.e. R/28/A, R/53.6/A, B/16.8/A, B/51.4/A) and DPPO, by coating diluted polymer solutions in appropriate substrate(s). The gas transport properties of thin composite membranes should be determined and compared with those of homogeneous membranes.
- The transient effects in measurement of membrane gas permeation rates in constant pressure-type systems should be evaluated by developing the appropriate mathematical model. The transient effects could also be evaluated experimentally in a series of carefully-designed experiments.

Bibliography

Aguilar-Vega, and Paul, D. R, "Gas Transport Properties of Polyphenylene Ethers", J. Polymer Science, Part B: Polymerr Physics, **31**, 1577(1193).

Alentiev, A., Drioli, E., Gokzhaev, M., Golemme, G., Ilinich, O., Lapkin, A., Volkov, V., Yampolskii, Y., "Gas Permeation Properties of Phenylene Oxide Polymers", J. Membrane Science, **138**, 99 (1998).

Baesjou, P. J., Driessen, W. L., Challa, G., Reedijk, J., " A Kinetic study of the copper catalysed oxidative coupling of 2,6-dimethylphenol. The role of copper, base and phenol concentrations", J. Molecular Catalysis A: Chemical, **135**, 273 (1998)

Baesjou, P. J., Driessen, W. L., Challa, G., Reedijk, J., "Kinetics and Selectivity of the Copper –catalysed oxidative coupling of 4-(2',6'-dimethylphenoxy)-2,6-dimethylphenol", J. Molecular Catalysis A: Chemical, **140**, 241 (1999).

Baesjou, P. J., Driessen, W. L., Challa, G., Reedijk, J., "Kinetics and spectroscopic study on the copper catalyzed oxidative coupling polymerization of 2,6-dimethylphenol. X-ray structure of the catalyst precusor tetrakis (N- methylimidazole)bis(nitrato)copper (II)". J. Molecular Catalysis A: Chemical, **110**, 195 (1996).

Baker, R. W., Cussler, E.L, Eykamp, W., Koros, W.J., Riley, R.L., Strathmann, H., "Membrane Separation Systems. Recent Developments and Future Directions", Noyes Data Corporation, New Jersey, (1991).

Borisov, S., Khotimsky, V. S., Rebrov, A. I., Rykov, S. V., Slovetsky, D. I., Pashunin, Y. M., "Plasma Fluorination of Organosilicon Polymeric Films of Gas Separation Applications", J. Membrane Science, **125**, 319 (1997).

Chao, H.S-I, Whalen, J. M., "Poly(2,6-dimethyl-1,4-phenylene ether) (PPO) Capping and Its Significance in the Preparation of PPO/Epoxy Laminate", J. Applied Polymer Science, **59**, 473 (1996).

Chern, R. T., Sheu, F.R, Jia, L., Stannett, V. T., Hopfenberg, H.B., "Transport of Gases in Unmodified and Arylbrominated 2,6-Dimethyl-1,4-Poly(Phenylene Oxide), J. Membrane Science, **35**, 103 (1987).

Chern, R. T., Brown, N. F., Macromolecule, **23**, 2370 (1990).

Chowdhury, G., Vujosevic, R., Matsuura, T., Laverty, B., "Effect of Polymer Molecular Weight and Chemical Modification on the Gas Transport Properties of Poly (2,6-dimethyl-1,4-phenylene oxide), J. Applied Polymer Science, **77**, 1137 (2000).

Cooper, G. D., Blanchard, H. S., Endres, G. F., Finkbeiner, H. L., J. Am. Chem. Soc., **87**, 3996 (1965)

Cohen, M. H., Turnbull, D. J., J. Chem. Phys, 1959, **31**, 1164.
Ebewele, R. O., "Polymer Science and Technology", CRC Press, (2000).

Endres, G. F., Hay, A. S., Eustance, J. W., "Polymerization by Oxidative Coupling. V Catalytic Specificity in the Copper-Amine- catalyzed Oxidation of 2,6- Dimethylphenol", J. of Organic Chemistry, **28**, 1300 (1963).

Finkbeiner, H., Hay, A. S., Blanchar, H. S., Endres, G. F., J. Org. Chem., **31**, 549, 1966.

Flory, P. J., J. Chem. Phys, **10**, 51 (1942).

Fritzsche, A. K., Kurz, J. E., "Handbook of Industrial Membrane Technology", M.C. Porter, Noyes Publication (1990).

Fujita, H., Kishimoto, A., Matsumoto, K., Trans. Faraday Soc., 1960, 56, 424.

Gagne, S., Chowdhury, G., Matsuura, T., Laverty, B., "Optimization of CO_2- CH_4 Separation Performance of Integrally Skinned Asymmetric Membranes Prepared form Poly(2,6-dimethyl-1,4-phenylene oxide) by Factorial Design, J. Applied Polymer Science, **72**, 1601 (1999).

Goodman, I., "Developments in Block Copolymers-2", Elsevier Applied Science, London, New York, 1982.

Gordon, M., Taylor J. S., J. Appl. Chem., **2**, 493, 1952

Ghosal, K., and Freeman, B. D., "Gas Separation Using Polymer Membranes: An Overview", Poymers for Advanced Technologies, **5**, 673 (1993).

Graham, T. G., Phil. Mag. J. Sci., **32**, 401 (1866).

Groenewoud, W.M, "Characterisation of Polymers by Thermal Analysis", Elsevier Science B.V., Netherlands, 2001.

Gu, Y., Huang, Y., Liao, B., Zhao, S., Cong, G., "The Effect of Solvent Polarity on Phase Inversion Process for Emulsification of Poly (phenylene Oxide) (PPO) ionomer", European Polymer J., **36**, 1477 (2000).

Hay, Allan S., "Reflection on Polymerization by Oxidative Coupling. II . Oxidation of 2,6-Disubstituted Phenols", J. Polymer Science, **58**, 1369 (1996).

Hay, A. S., "Polymerization by Oxidative Coupling. Oxidation of 2,6-Disubstituted Phenols", J. Polymer Science, **58**, 581(1962).

Hay, A. S, "Polymerization by Oxidative Coupling: Discovery and Commerciallization of PPO and Noryl Resin", J. Polymer Science, **36**, 505 (1998).

Hay, A. S., U. S. Patent 3306875, 1967.

Hay, A. S., US Patent 3306874, 1967.

Hay, A. S., Macromolecules, **2**, 107 (1969)

Huggins, M. L., J. Am. Chem. Soc, **64**, 1712, 1942.

Ilinich, O., Yampolskii, Y., Volkov, V., Lapkin, A., Alentiev, A., Gokzhaev, M., Plate, N., Drioli, E., "Gas Permeation and Diffusion In and Free Volume of Methyl- and Phenyl- Substituted Phenylene Oxides Polymers", Japan ICOM, 375 (1996).

Ilinich, O., Lapkin, A.A., Zamaraev, K.I., "Rapid Communication: Propylene in Polyphenylene Oxides Membranes: Unusual Permeability vs. Pressure Behaviour", J. Membrane Sciences, **98**, 287 (1995).

Ilinitch, O.M, Fenelonov, V. B., Lapkin, A. A., Okkel, L. G., Terskikh, V.V., Zamaraev, K.I., "Intrinsic Microporosity and Gas Transport in Polyphenylene Oxide Polymers", J. Microporous and Mesoporous Materials, **31**, 97 (1999).

Oguchi, T., Tawaki, S-I., Uyama, H., Kobayashi, S., "Synthesis of a Soluble Polyphenol by Peroxidase-Catalyzed Oxidative Polymerization",

Kesting, R. E. and Fritzsche, A. K., "Polymeric Gas Separation Membranes", Wiley-Interscience, New York, 1993.

Khulbe, K.C., Matsuura, T., "Characterization of PPO Membranes by Oxygen Plasma Etching, Gas Separation and Atomic Force Microscopy", J. Membrane Science, **171**, 273 (2000).

Koros, W. J., Hellums, M. W., "Encyclopedia of Polymer Science and Engineering", 724 (1989).

Krause, S, Paul, D. R., Newman, S., "Polymer Blends I", Academic Press Inc, Orlando, Florida, 1978, p6.

Lapkin A.A., Roschupkina, O.P., Ilinitch, O.M., "Transport of C_1-C_3 Hydrocarbons in Poly(phenylene oxices) membranes, J. Membrane Science, **141**, 223 (1998).

Li, K-T, "Polymerization of 2,6- Dimethylphenol with Mixed- Ligand Copper Complexes", J. Ind. Eng. Chemistry, **33**, 1107 (1994).

Li, K-T, "Oxidative polymerization of 2,6-dimethylphenol catalyzed by copper-mixed amine system", Polymer Bulletin, **34**, 419 (1995).

Li, X. G., "High-Resolution Thermogravimetry of Poly(2,6- Dimethyl-1,4- phenylene oxide)", J. Applied Polymer Science, **71**, 1887 (1999).

Morgan, C.R., Blinka, T. A., Chen, C.C., "Crosslinked Polyphenylene Oxide Polymers for Gas Separations", Japan Icom, 827 (1990).

Park, J. Y., Paul, D. R., "Correlation and Prediction of Gas Permeability in Glassy Polymer Membrane Materials via a Modified Free Volume Based Group Contribution Method", J. Membrane Science, **125**, 23 (1997).

Percec, S., Li, G., "Chemical Modification of Poly(2,6- dimethyl-1,4-phenylene oxide) and Properties of the Resulting Polymers", ACS Symp. Seri. 364, American Chemical Society, Washington, DC, 16, 1988.

Ravve, A, "Principles of Polymer Chemistry", 2nd edition Kulert Academic, New York, 2000.

Robeson, L. M., Smith, C. D., Langsam, M., "A Group Contribution Approach to Predict Permeability and Permselectivity of Aromatic Polymers", J. Membrane Science, **132**, 33 (1997).

Robeson, L.M., "Correlation of Separation Factor versus Permeability for Polymer Membranes", J. Membrane Science, **62**, 165 (1991).

Salame, M., "Prediction of Gas Barrier Properties of High Polymers", J. Polymer Engineering and Science, **26**, 1543 (1986).

Schauer, J., Albrecht, W., Weigel, T., "The Preparation of Microporous Membranes from Blends of Poly(2,6-dimethyl-1,4-, phenylene oxide) and Sulfonated Poly(2,6-dimethyl-1,4-phenylene oxide)", J. Applied Polymer Science, **73**, 161 (1999).

Scott, K., "Handbook of Industrial Membranes", Elsevier Advanced Technology, UK, (1997).

Servens, E., Lowik, D., Bosman, A., Nelissen, L., Lemstra, P.J., "Synthesis and characterization of poly[(2,6-dimethyl-1,4-phenylene oxide)-block isoprene] diblock copolymers.", Macromolecule Che. Phys.,**198**, 379 (1997).

Sperling, L. H, "Introduction to Physical Polymer Science", 3rd editions, John Willey & Sons Inc., New York, 2001

Story, B. J., and Koros, W. J., "Sorption of CO_2/CH_4 Mixture of Poly(phenylene Oxide) and a Carboxylated Derivative", J. Applied Polymer Science, **42**, 2613 (1991).

Stannett, V. , "Diffusion in Polymers", J. Crank and G.S. Park, Academic Press (1968).

Story, B. J., and Koros, W. J., "Comparision of Three Models for Permeation of CO_2/CH_4 Mixtures in Poly(phenylene oxide)", J. Polymer Science, PartB: Polymer Physics, **27**, 1927 (1989).

Suzuki, T., Miyauchi, M., Takekawa, M., Yoshimizu, H., Tsujita, Y., Kinoshita, T., "Characterization of the Microvoids in Poly(2,6-dimethyl-1,4-phenylene oxide) by Means of ^{129}Xe NMR Spectroscopy", J. Macromolecules, **34**, 3805 (2001).

Takeshi, K., Okuyama, K-I, Ohba, Y., Ueda, M, " New Positive Type Photosensitive Poly(phenylene ether): Poly(2-hydroxy-6-methylphenol-co-2,6-dimethylphenol) with Diazonaphthoquinone", J. Photopolymer Science and Technology, **12**,353 (1999).

Van Amerogen, G. J., J. Polym. Sci, **5**, 307, 1950.

Viersen, F.J., "PhD Thesis", Groningen University, 1988

Volkov, V.V., "Free Volume Structure and Transport Properties of Glassy Polymers-Materials for Separating Membranes", J. Polymer, **23**, 457 (1991).

Won, J, Kim, M. H., Kang, Y. S., Park, H. C., Kim, U. Y., Choi, S. C., Koh, S. K., "Surface Modification of Polyimide and Polysulfone Membranes by Ion Beam for Gas Separation", J. Applied Polymer Science, **75**, 1554 (2000).

White, D. M., Loucks, G.R, "Coupling and Capping Reaction on Poly(2,6-dimethyl-1,4-phenylene oxide)"

Winston Ho, W. S., Sirkar, K.K., "Membrane Handbook", Van Nostrand Reinhold, New York, (1992).

APPENDIX A Characterization of Polymers

A.1 IR SPECTROCOPY

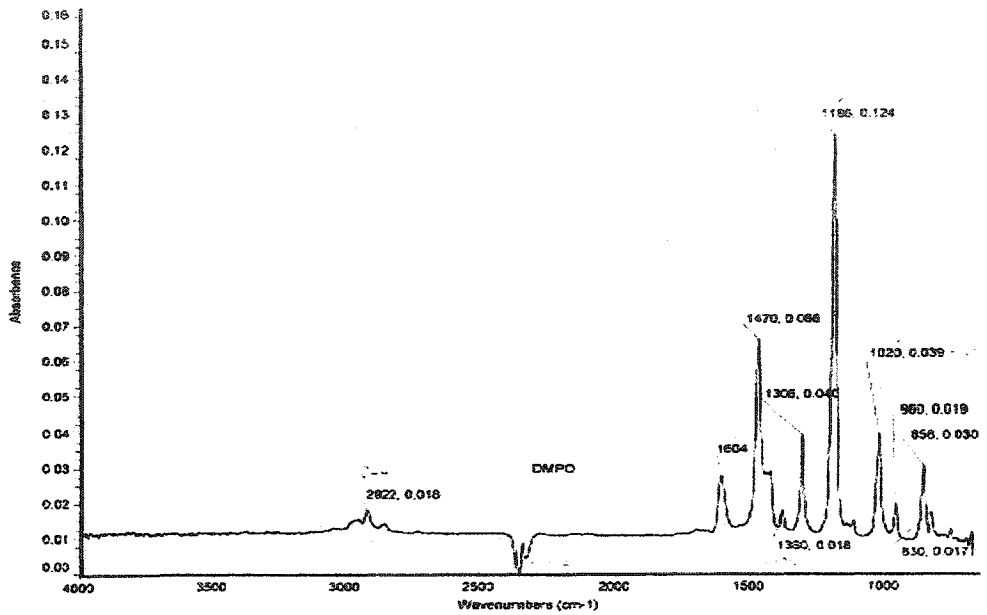

Figure A.1.1: Infrared spectrum of DMPO.

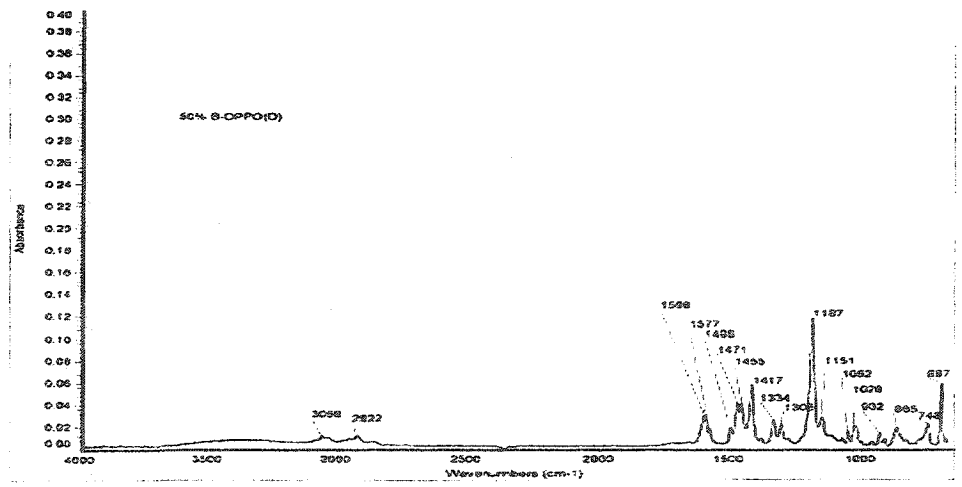

Figure A.1.2: Infrared spectrum of B/50/T.

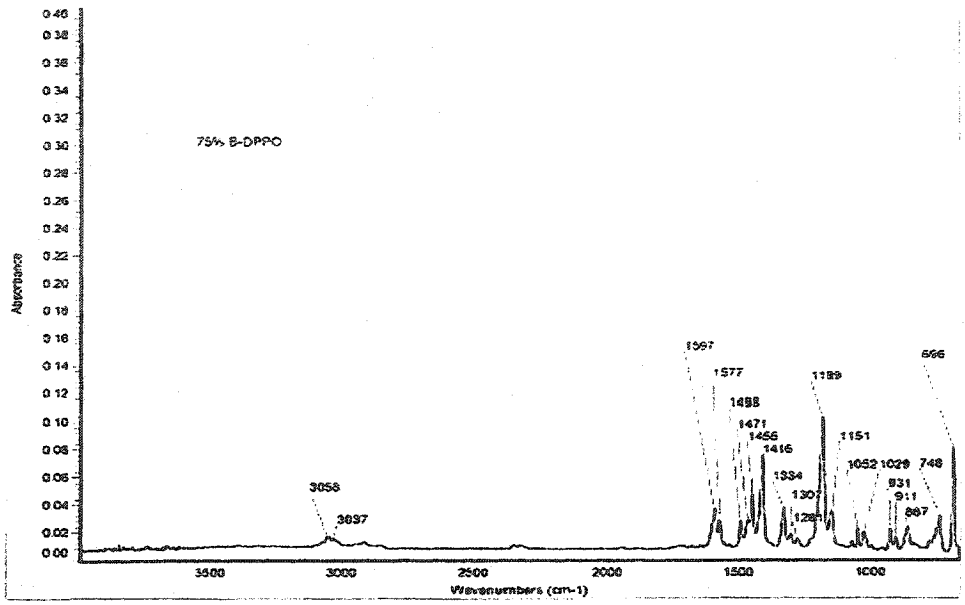

Figure A.1.3: Infrared spectrum of B/80/T.

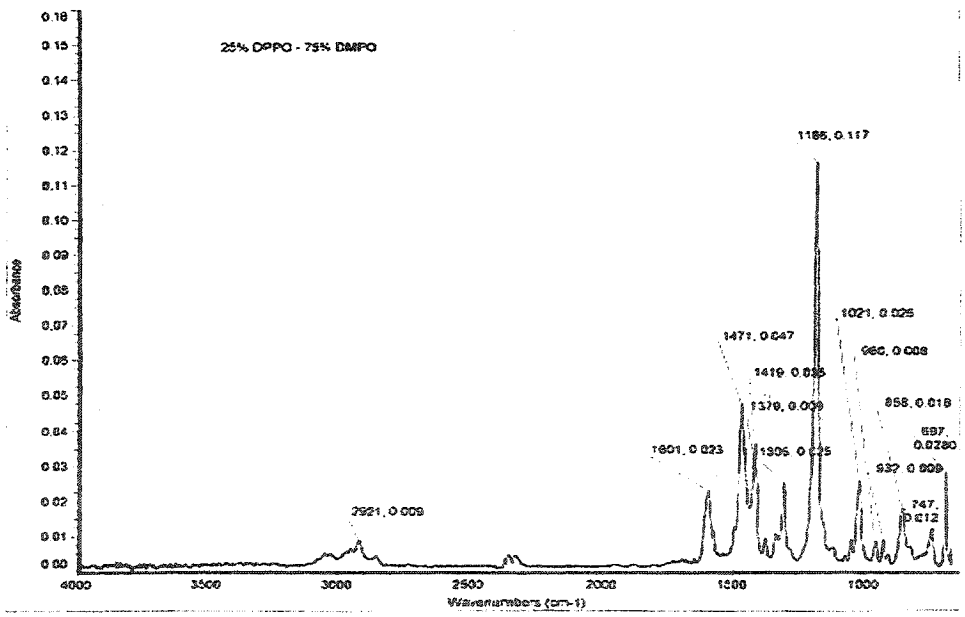

Figure A.1.4: Infrared spectrum of R/25/T.

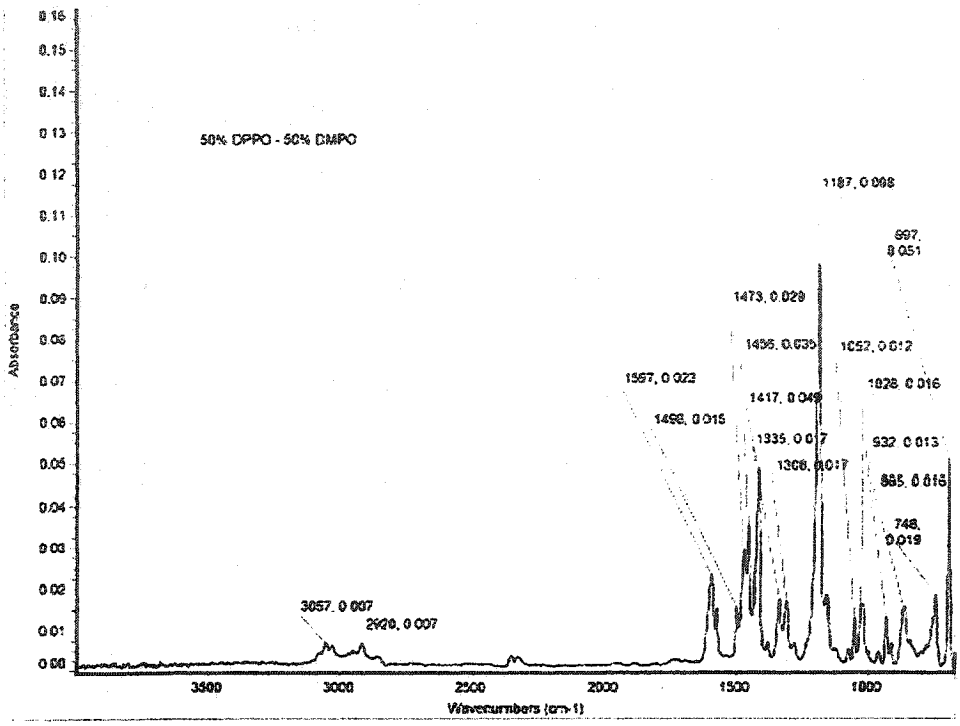

Figure A.1.5: Infrared spectrum of R/50/T.

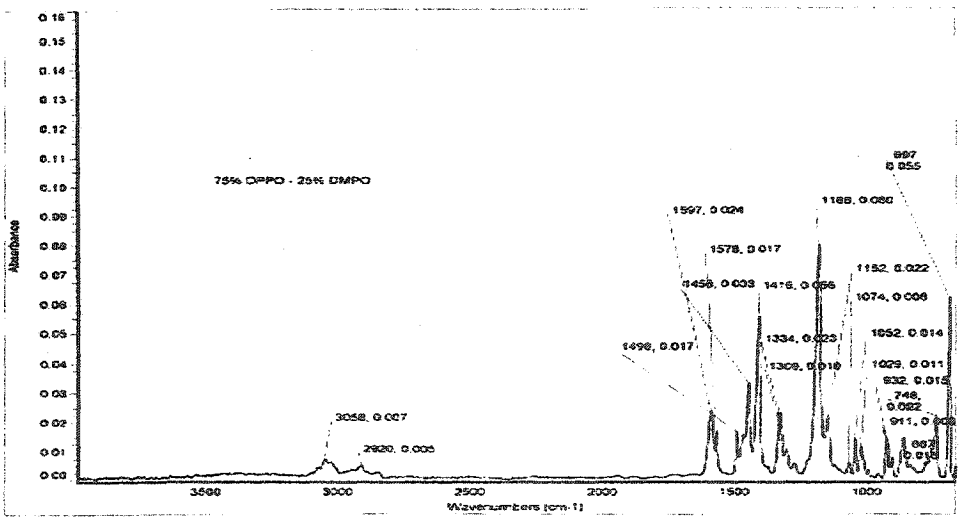

Figure A.1.6: Infrared spectrum of R/75/T.

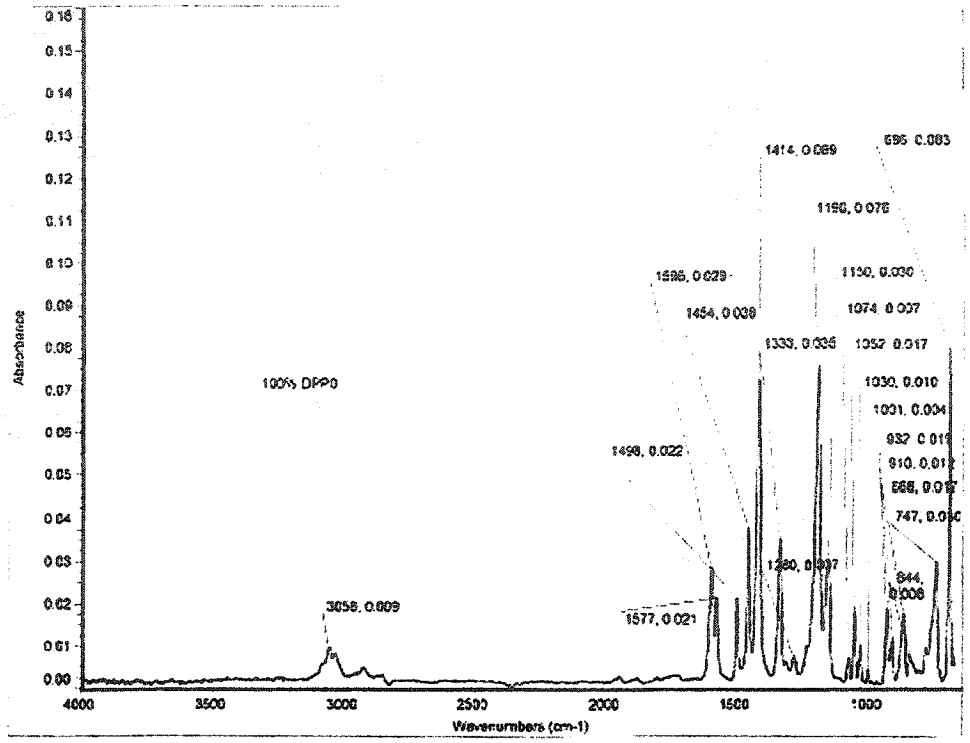

Figure A.1.7: Infrared spectrum of DPPO.

A.2 Thermogravimetric Spectrocopy

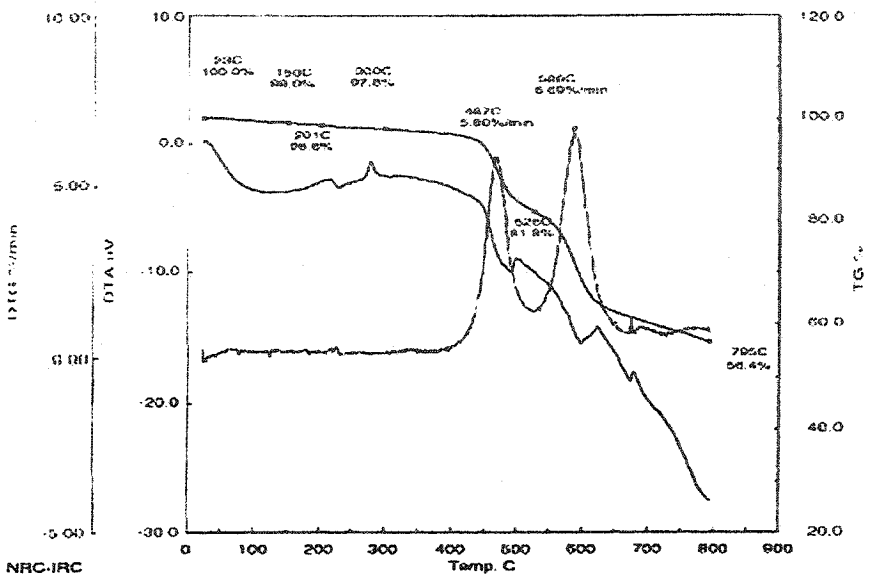

Figure A.2.1: TG spectrum of B/50/T.

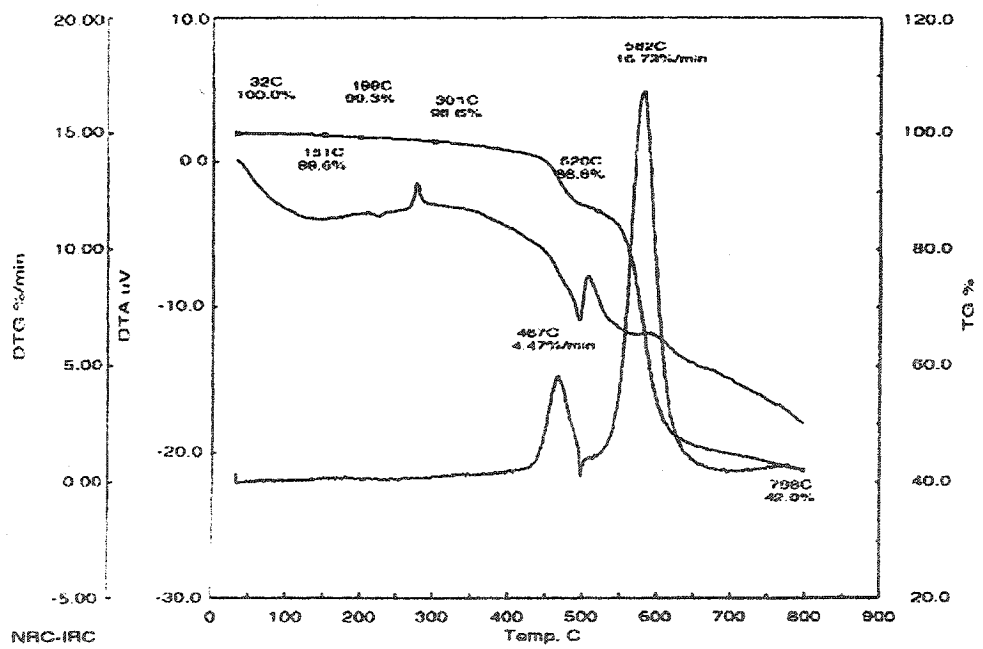

Figure A.2.2: TG spectrum of B/80/T.

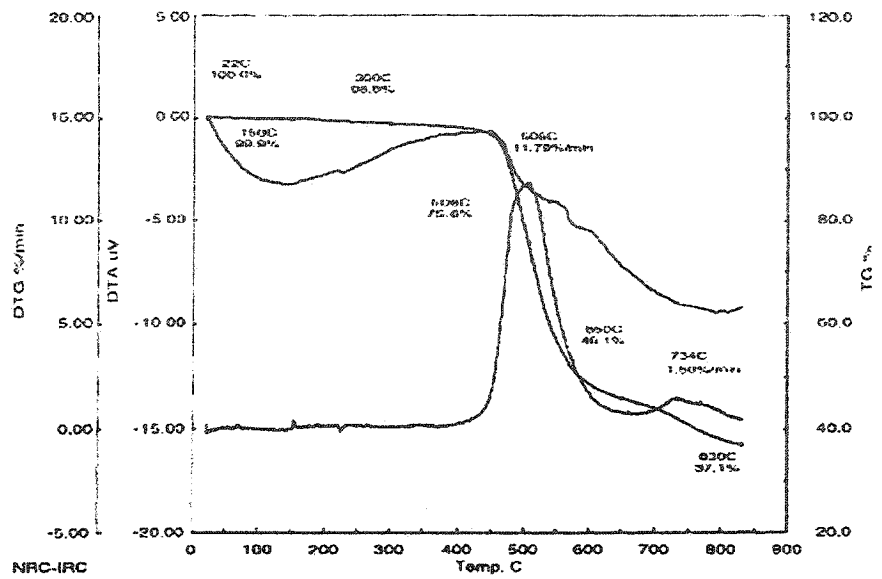

Figure A.2.3: TG spectrum of R/50/T.

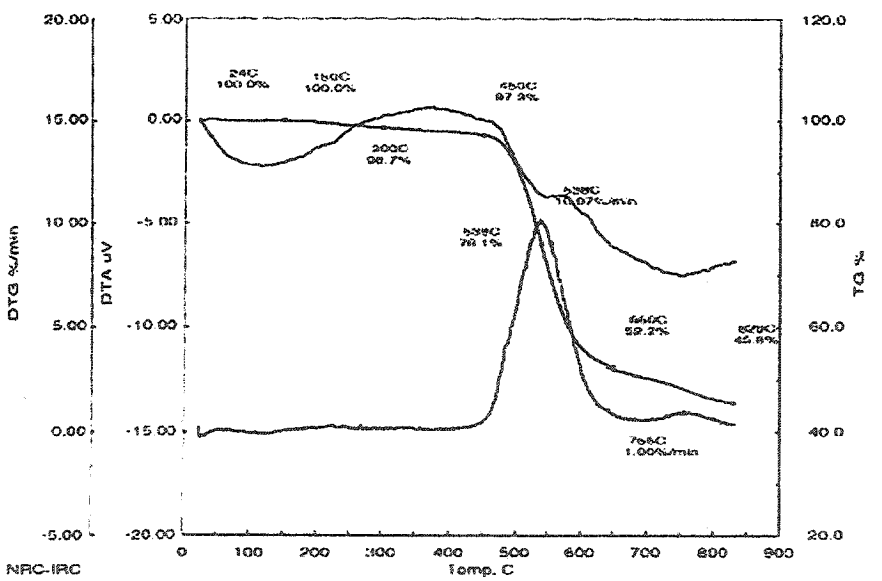

Figure A.2.4: TG spectrum of R/75/T.

A.3 ^{1}H-NMR SPECTROCOPY

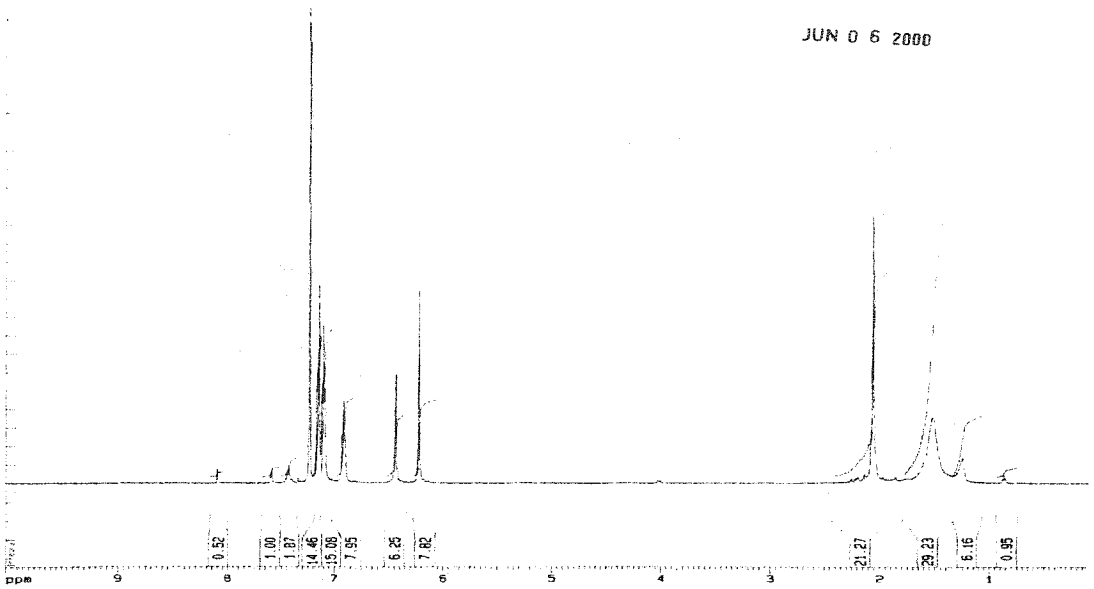

Figure A.3.1: ^{1}H NMR spectrum of B/50/T.

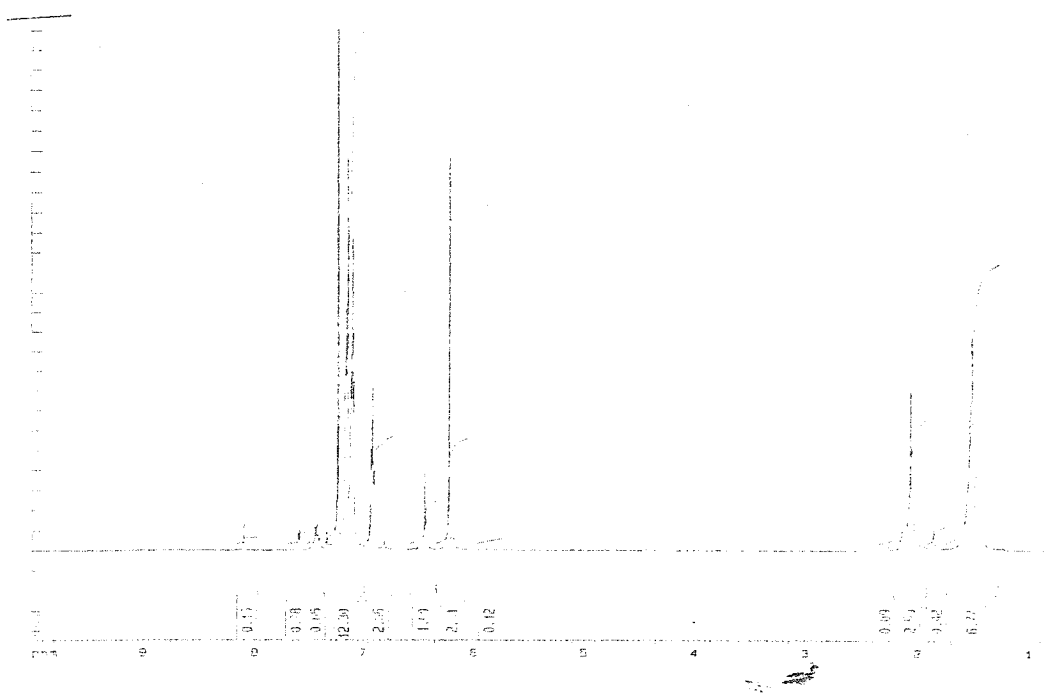

Figure A.3.2: ^{1}H NMR spectrum of B/80/T.

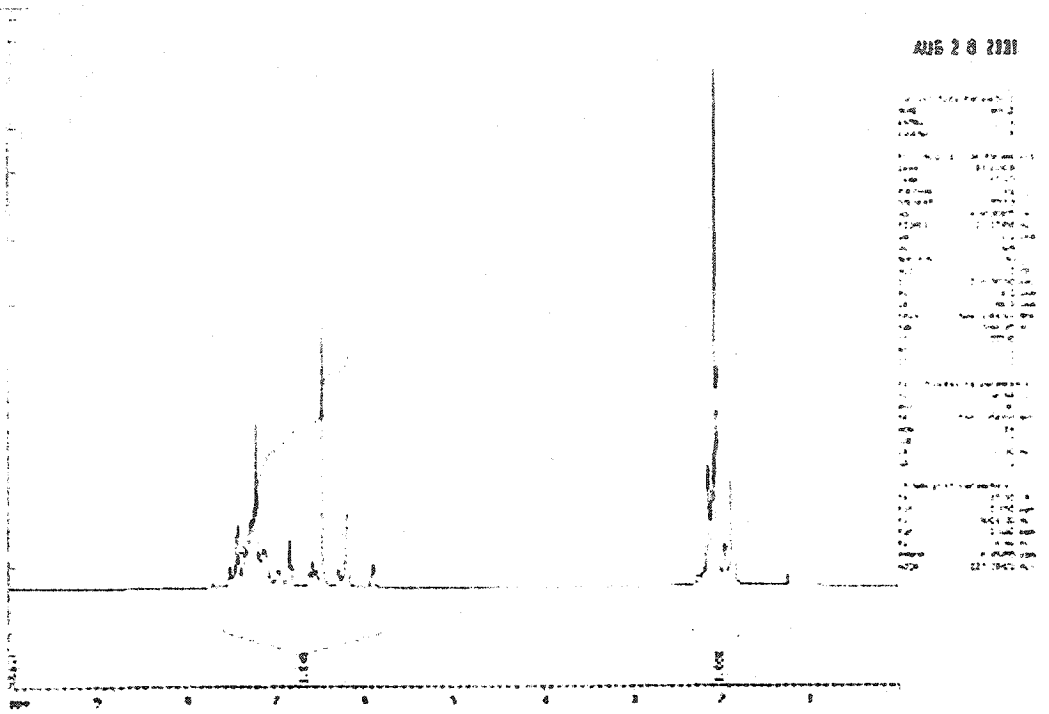

Figure A.3.3: ^{1}H NMR spectrum of R/25/T.

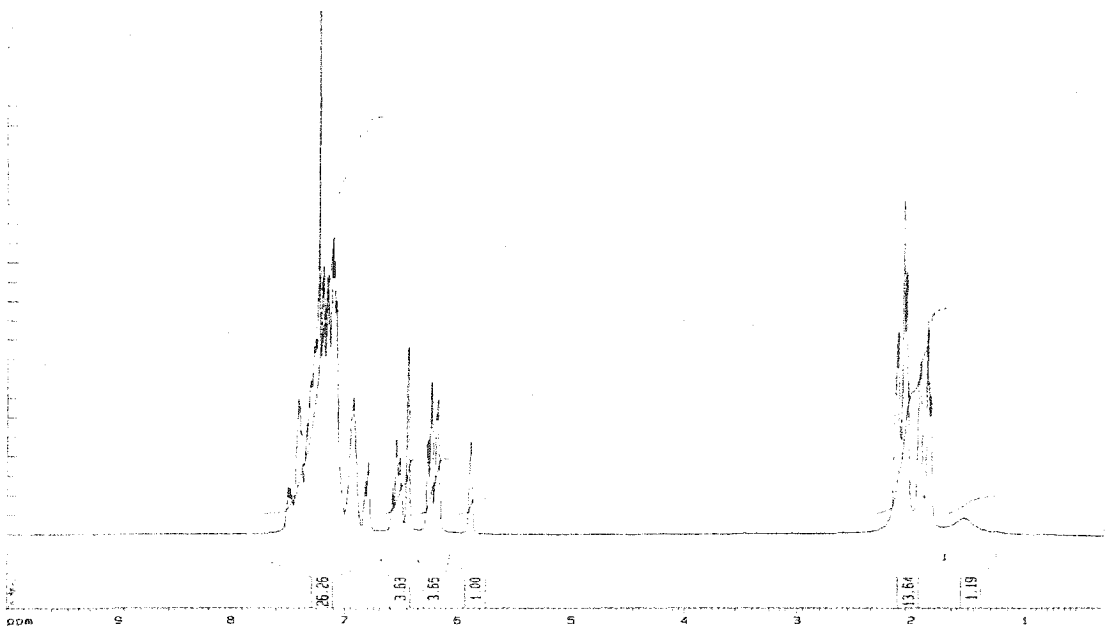

Figure A.3.4: ^{1}H NMR spectrum of R/50/T.

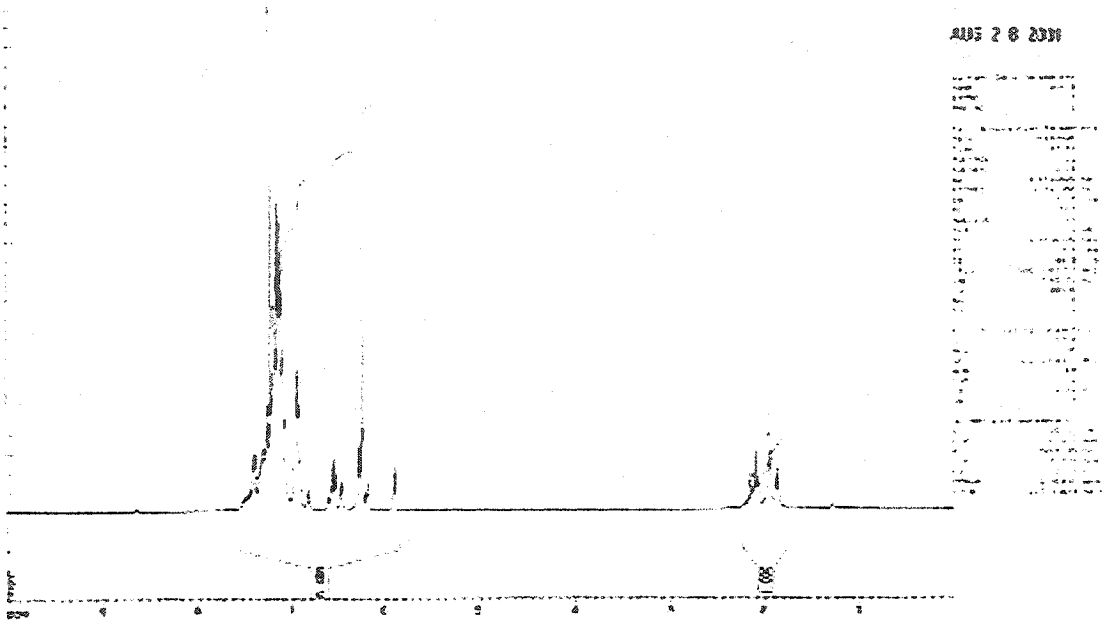

Figure A.3.5: ^{1}H NMR spectrum of R/75/T.

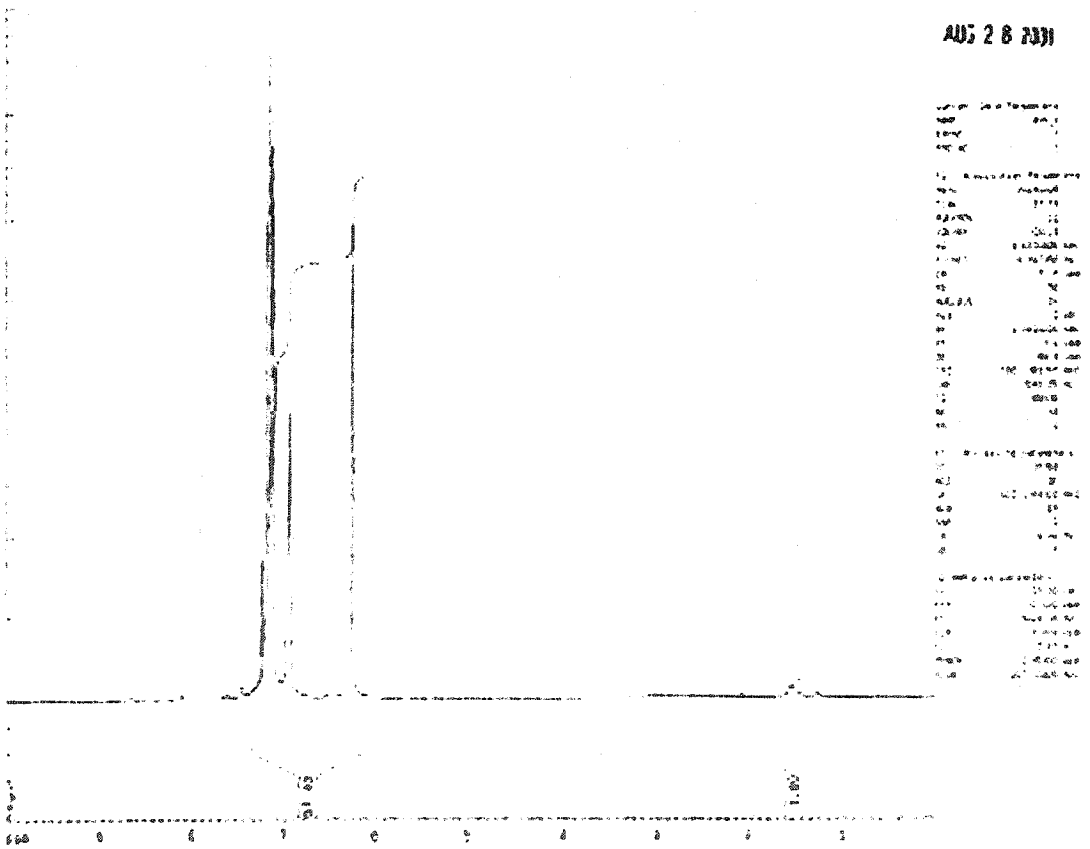

Figure A.3.6: ^{1}H NMR spectrum of DPPO.

A.4 DSC SPECTROCOPY

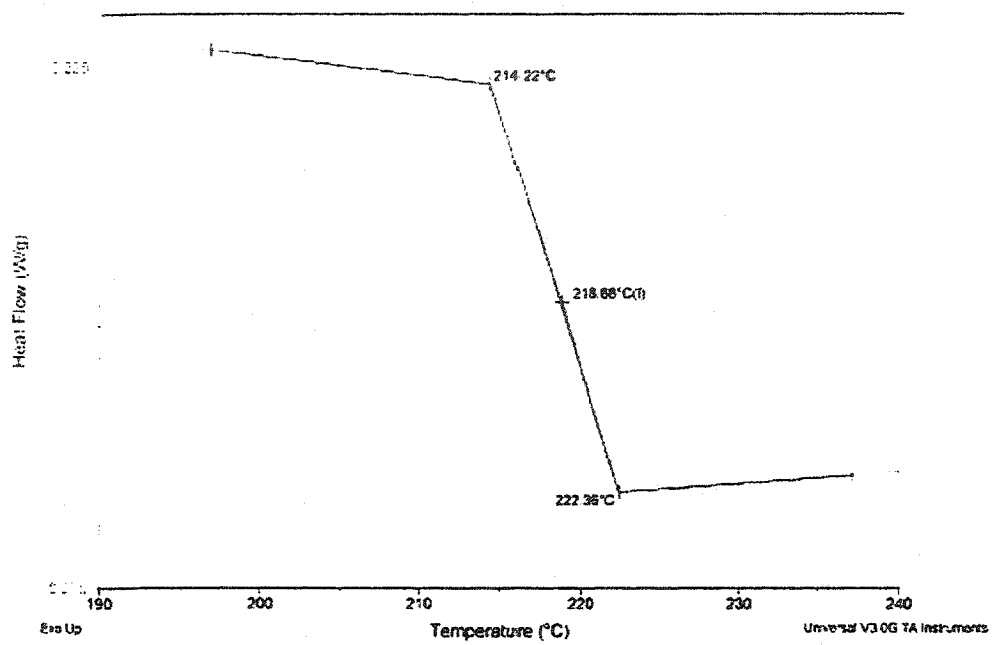

Figure A.4.1: DSC spectrum of DMPO.

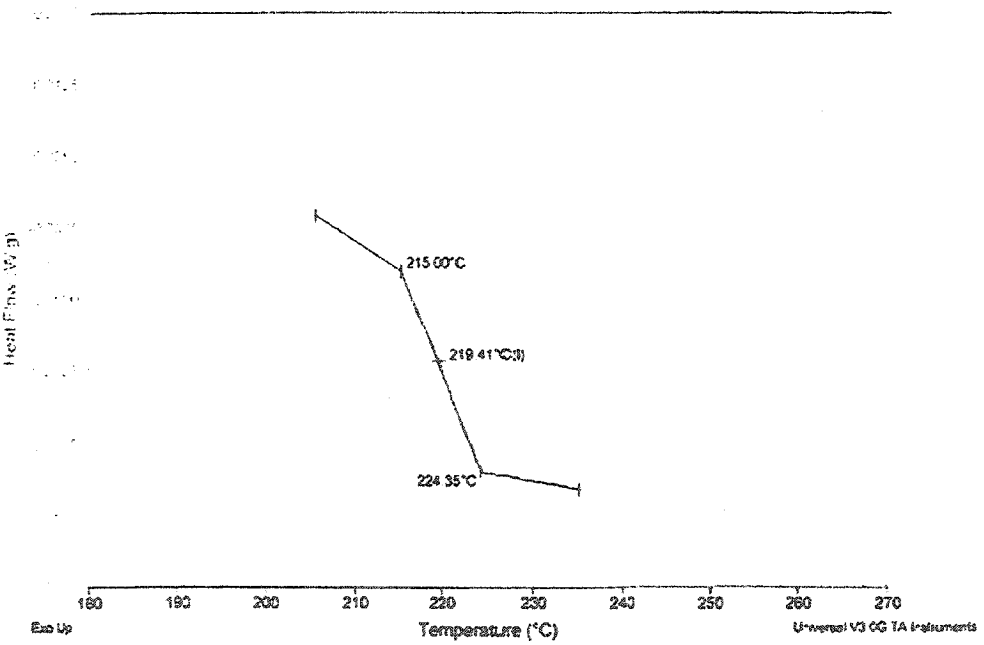

Figure A.4.2: DSC spectrum of B/50/T.

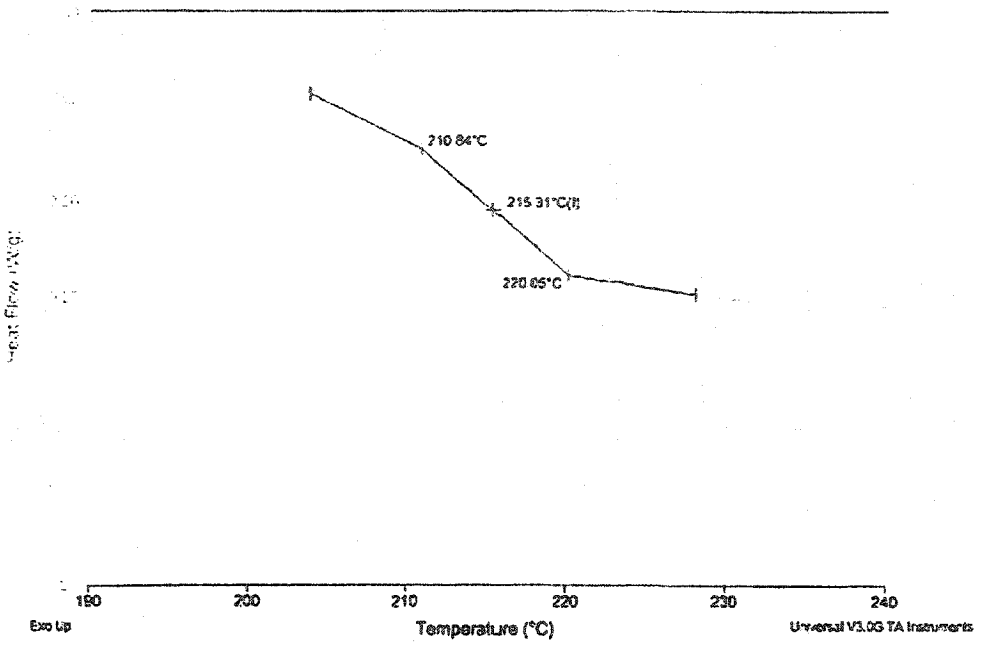

Figure A.4.3: DSC spectrum of B/80/T.

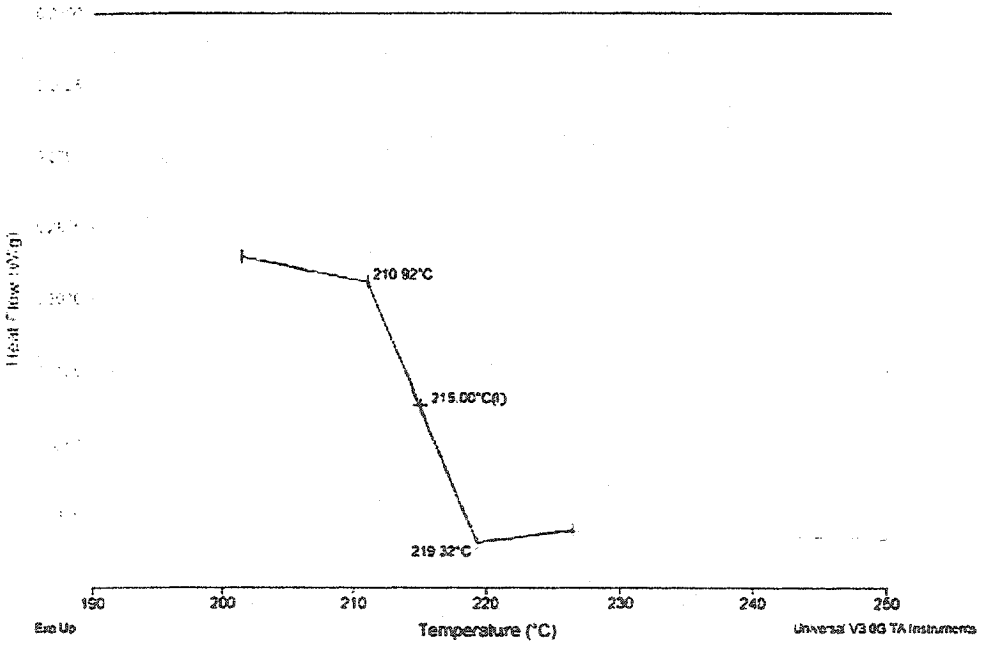

Figure A.4.4: DSC spectrum of R/25/T.

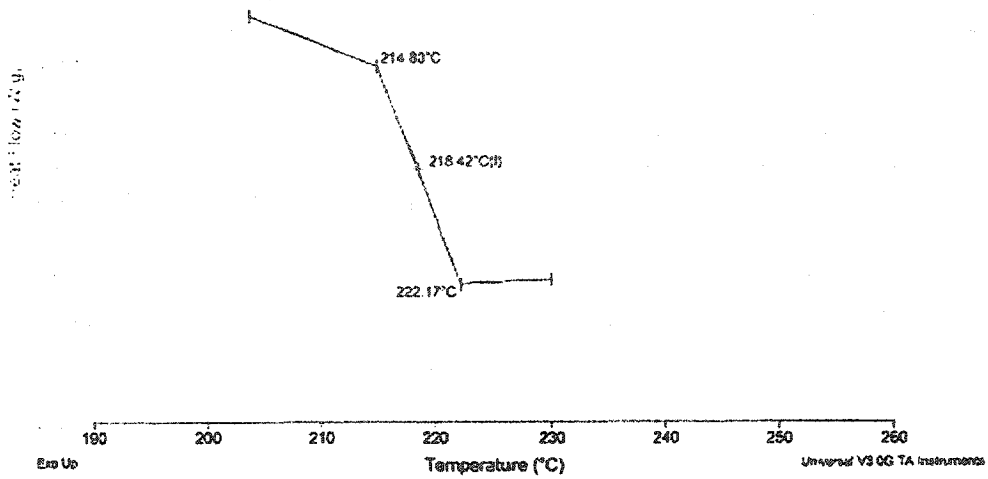

Figure A.4.5: DSC spectrum of R/50/T.

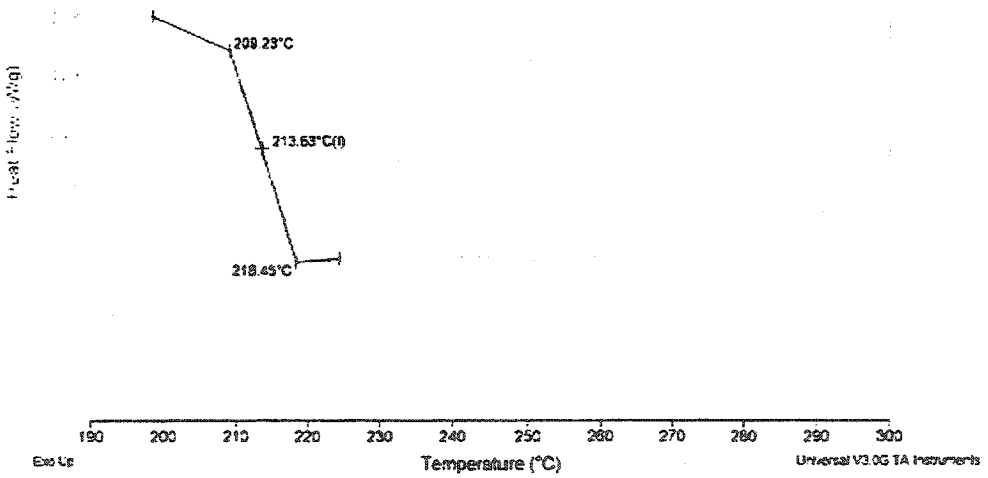

Figure A.4.6: DSC spectrum of R/75/T.

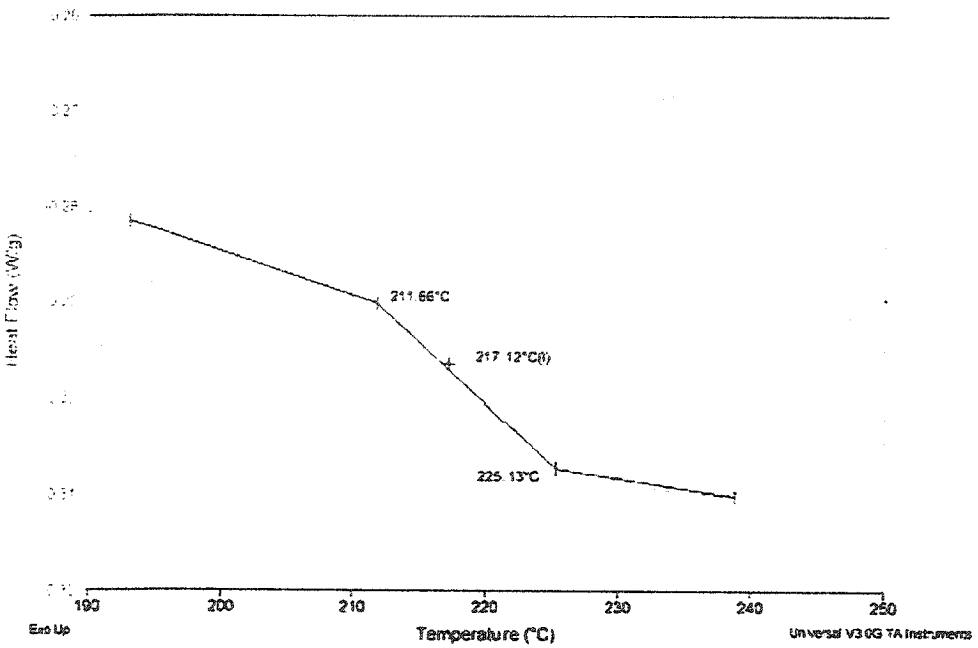

Figure A.4.7: DSC spectrum of DPPO.

APPENDIX B Evaluation of Solubility Parameters

Solubility parameter data is available for a wide variety of solvents and some polymers. It can also compute using group contribution method. The difference of the solubility parameters of polymer and solvent provides the basis for the evaluation of the polymer-solvent interactions.

B.1 Solubility parameters of solvents and polymers

The Hansen and Hildebrand solubility parameter of solvents considered for dissolution of polymer are presented in Table B-1. The total solubility parameter (δ_{sp}) is calculated from Eq. (B.1) using the Hansen solubility parameters, and its value is compared with the Hildebrand parameter (δ).

$$\delta_{sp}^2 = \delta_d^2 + \delta_p^2 + \delta_h^2 \qquad \text{(B.1)}$$

where δ_d is the dispersive term, δ_p is the polar term, and δ_h is the hydrogen bond term.

There is only a limiting Hansen and Hildebrand solubility parameters. For the rest of available polymer, Hansen and Hildebrand solubility parameters can be calculated using group contribution methods. This method requires decomposition of the repeat unit of polymer into functional groups. In case of DMPO, the repeat unit can be divided into: phenyl (tetrasubstituted), methyl and oxygen. In case of DPPO, the repeat unit can be divided into phenyl (tetrasubstituted), phenyl and oxygen. Table B.2 shows the components of the repeat unit of both DMPO and DPPO along with the cohesion

parameters and molar volumes for each group. The cohesion parameters for phenyl (tetrasubsituted) is not available; hence phenylene (o,m,p) is used instead. The numerical values presented in Table B-2 are based on the data listed by Matsuura (1993).

Table B.1: Hansen and Hildebrand solubility parameter for selected organic solvents [Barton, 1983].

	δ_d $cal^{1/2}cm^{-3/2}$	δ_p $cal^{1/2}cm^{-3/2}$	δ_h $cal^{1/2}cm^{-3/2}$	δ_{sp} $cal^{1/2}cm^{-3/2}$	δ $cal^{1/2}cm^{-3/2}$
Chloroform	8.70	1.51	2.79	9.29	9.29
Benzene	8.90	0	0.98	9.09	9.19
n-heptane	7.48	0	0	7.48	7.38
Toluene	8.80	0.68	0.98	8.90	8.90
Tetrahydrofuran	8.21	2.79	3.91	9.48	9.09
Trichloroethylene	8.80	1.52	2.59	9.29	9.19

Table B.2: Group contributions to the Hildebrand (V_i and $E_{coh,i}$) and Hansen ($V_{g,i}$, $F_{d,i}$, $F_{p,i}$, $E_{h,i}$) solubility parameter [Matsuura, 1993].

Group	V_i cm^3/mol	$E_{coh,i}$ cal/mol	$V_{g,i}$ cm^3/mol	$F_{d,i}$ $cal^{1/2}cm^{3/2}/mol$	$F_{p,i}$ $cal^{1/2}cm^{3/2}/mol$	$E_{h,i}$ cm^3/mol
Phenyl (tetrasubstituted)	14.4	7630	65.5	621	54	0
Methyl	33.5	1125	23.9	205	0	0
Oxygen	3.8	800	10	49	196	717
Phenyl	71.4	7630	72.7	699	54	0

Table B.3: Hansen and Hildebrand solubility parameter for homopolymers, copolymers, and chloroform, calculated by group contribution method.

% DPPO	δ_d $cal^{1/2}cm^{-3/2}$	δ_p $cal^{1/2}cm^{-3/2}$	δ_h $cal^{1/2}cm^{-3/2}$	δ_{sp} $cal^{1/2}cm^{-3/2}$	δ $cal^{1/2}cm^{-3/2}$
0 (DMPO)	8.76	1.65	2.41	9.23	11.2
16.8	8.86	1.54	2.30	9.20	11.356
28	8.93	1.46	2.24	9.32	11.46
53.6	9.08	1.29	2.08	9.41	11.68
51.4	9.10	1.27	2.07	9.42	11.70
75.6	9.21	1.15	1.95	9.49	11.90
75.7	9.21	1.15	1.95	9.49	11.90
100 (DPPO)	9.36	0.98	1.80	9.58	12.13
Chloroform	10.1	6.7	2.04	12.29	8.77

Appendix C Summary of Permeation data

Table C.1: Summary of gas transport data before correction for back permeation.

	Coupons	Date	Test duration [hr]	thickness [cm]	Feed p_{CO2} [psig]	CO_2 perm. [Barrer]	Feed p_{CH4} [psig]	CH_4 perm. [Barrer]	Feed p_{O2} [psig]	O_2 perm. [Barrer]	Feed p_{N2} [psig]	N_2 perm. [Barrer]	CO_2/CH_4
	R/53.6/A-1	4/10/01	264	0.0022	100	42.263	95	0.751	115	8.206	130	1.081	56.310
	R/53.6/A-3	4/10/01	264	0.00123	100	36.832	95	0.753	115	8.145	130	0.835	48.906
	R/53.6/A-6	4/10/01	264	0.00205	100	36.412	95	1.023	115	7.979	130	1.227	35.581
	R/53.6/A-4	7/9/01	264	0.00226	45	44.580	135	0.922	90	9.290	95	1.228	48.370
	R/53.6/A-5	7/9/01	264	0.00257	45	44.763	135	0.914	90	9.529	95	1.211	49.000
	R/53.6/A-6	7/9/01	264	0.00238	45	44.944	135	0.903	90	9.512	95	1.159	49.767
Average			**264**			**41.632**		**0.878**		**8.777**		**1.124**	**47.989**
Std			**0.000**			**4.004**		**0.107**		**0.739**		**0.152**	**6.758**
Successful rate:			**60% (6 out of 10)**										

	Coupons	Date	Test duration	thickness	Feed p_{CO2}	CO_2 perm.	Feed p_{CH4}	CH_4 perm.	Feed p_{O2}	O_2 perm.	Feed p_{N2}	N_2 perm.	CO_2/CH_4
	R/75.6/A-1	9/5/01	216	0.00218	50	41.23614	115	0.96	50	9.6389	105	1.00147	42.9498
	R/75.6/A-3	9/5/01	216	0.00167	50	35.61482	115	0.91	50	8.825	105	1.06143	39.1989
	R/75.6/A-5	9/5/01	216	0.00239	50	33.61565	115	1.01	50	11.187	105	1.12681	33.4005
	R/75.6/A-6	9/5/01	216	0.00207	50	45.33606	115	0.88	50	7.5832	105	1.10636	51.4743
	R/75.6/A-3	9/19/01	192	0.00418	48	39.89116	130	0.99	50	7.5477	130	1.05513	40.1389
	R/75.6/A-4	9/19/01	192	0.00226	48	35.58072	130	0.89	50	10.866	130	0.94376	40.0151
Average	**R/75.6/A**					**38.54576**		**0.93981**		**9.2747**		**1.04916**	**41.1963**
Std						**4.401004**		**0.0544**		**1.5728**		**0.06763**	**5.93277**
Successful rate:	**67% (6 out of 9)**												

	Coupons	Date	Test duration	thickness	Feed p_{CO2}	CO_2 perm.	Feed p_{CH4}	CH_4 perm.	Feed p_{O2}	O_2 perm.	Feed p_{N2}	N_2 perm.	CO_2/CH_4
	R/28/A-1	8/1/01	216	0.0022	60	77.2047	120	1.47	65	16.324	95	1.87052	52.409
	R/28/A-3	8/1/01	216	0.00246	60	58.64522	120	1.76	65	14.657	95	2.04019	33.2466
	R/28/A-4	8/1/01	216	0.00262	60	55.32626	120	1.76	65	13.984	95	1.9381	31.3936
	R/28/A-5	8/1/01	216	0.00236	60	66.77568	120	2.07	65	17.074	95	2.23301	32.3305
	R/28/A-6	8/1/01	216	0.00273	60	52.06551	120	1.27	65	12.309	95	2.17619	40.8647
Average	**R/28/A**					**62.00347**		**1.66778**		**14.87**		**2.0516**	**38.0489**
Std						**10.10541**		**0.3038**		**1.8948**		**0.15349**	**8.86278**
Successful rate:	**83.3 % (5 out of 6)**												

Coupons	Date	Test duration	thickness	Feed p_{CO2}	CO_2 perm.	Feed p_{CH4}	CH_4 perm.	Feed p_{O2}	O_2 perm.	Feed p_{N2}	N_2 perm.	CO_2/CH_4
DPPO-1	5/24/01	192	0.00266	55	39.312	135	0.669	95	6.269	175	1.105	58.783
DPPO-6	5/24/01	192	0.00242	55	38.134	135	0.643	95	5.687	175	0.820	59.276
DPPO-1	6/21/01	192	0.0017	55	41.450	131	1.086	100	6.4683	125	0.86835	38.164
DPPO-5	6/21/01	192	0.00193	55	43.79832	131	1.211	100	6.3398	125	1.0078	36.171
DPPO-6	6/21/01	192	0.00321	55	36.17489	131	0.726	100	6.201	125	0.70418	49.803
Average	**DPPO**				**39.774**		**0.867**		**6.193**		**0.901**	**48.439**
STD					**2.952**		**0.262**		**0.300**		**0.158**	**10.981**
Successful rate:		**45.50%**			**(5 out of 11)**							

Coupons	Date	Test duration	thickness	Feed p_{CO2}	CO_2 perm.	Feed p_{CH4}	CH_4 perm.	Feed p_{O2}	O_2 perm.	Feed p_{N2}	N_2 perm.	CO_2/CH_4
B/75.7/A-1	9/26/00	288	0.00173	55	29.762	110	0.718	75	5.289	110	0.865	41.446
B/75.7/A-2	9/26/00	288	0.00093	55	29.199	110	0.701	75	5.150	110	0.857	41.633
B/75.7/A-3	9/26/00	288	0.00149	55	29.546	110	0.727	75	5.326	110	0.804	40.655
B/75.7/A-6	9/26/00	288	0.00125	55	28.670	110	0.730	75	5.408	110	0.739	39.271
Average	**B/75.7/A**				**29.294**		**0.719**		**5.293**		**0.817**	**40.751**
STD					**0.476**		**0.013**		**0.108**		**0.058**	**1.074**
Successful rate:		**66.70%**			**(4 out of 6)**							

Coupons	Date	Test duration	thickness	Feed p_{CO2}	CO_2 perm.	Feed p_{CH4}	CH_4 perm.	Feed p_{O2}	O_2 perm.	Feed p_{N2}	N_2 perm.	CO_2/CH_4
B/16.8/A-1	10/18/00	312	0.00212	68	49.27834	110	1.49	75	12.057	145	1.93518	33.068
B/16.8/A-2	10/18/00	312	0.00212	68	49.24718	110	1.24	75	13.103	145	1.2299	39.705
B/16.8/A-3	10/18/00	312	0.00153	68	50.30059	110	1.37	75	13.5	145	1.93944	36.816
B/16.8/A-4	10/18/00	312	0.00176					75	9.0204	145	1.80996	
B/16.8/A-5	10/18/00	312	0.00217	68	49.20058	110	1.39	75	12.04	145	1.635	35.523
B/16.8/A-6	10/18/00	312	0.00168	68				75	10.458	145	1.05011	
Average					**49.507**		**1.370**		**11.697**		**1.600**	**36.278**
STD					**0.530**		**0.102**		**1.684**		**0.377**	**2.763**
Successful rate:		**66.7% (4 out of 6)**										

Coupons	Date	Test duration	thickness	Feed p_{CO2}	CO_2 perm.	Feed p_{CH4}	CH_4 perm.	Feed p_{O2}	O_2 perm.	Feed p_{N2}	N_2 perm.	CO_2/CH_4
B/51.4/A-2	7/22/00	240	0.00162	100	49.02274	100	1.51	100	11.249	95	1.63616	32.5365
B/51.4/A-3	7/22/00	240	0.00126	100	50.44346	100	1.67	100	10.465	95	1.53901	30.1942
B/51.4/A-5	7/22/00	240	0.00143	100	53.79817	100	1.57	100	10.608	95	1.63429	34.1969
B/51.4/A-6	7/22/00	240	0.00124	100	48.5139	100	1.87	100	10.698	95	1.72768	25.8971
Average					**50.445**		**1.656**		**10.755**		**1.634**	**30.706**
STD					**2.380**		**0.160**		**0.343**		**0.077**	**3.602**
Successful rate:		**66.7% (4 out of 6)**										

Coupons	Date	Test duration	thickness	Feed p_{CO2}	CO_2 perm.	Feed p_{CH4}	CH_4 perm.	Feed p_{O2}	O_2 perm.	Feed p_{N2}	N_2 perm.	CO_2/CH_4
DMPO-1	7/19/01	192	0.00131	50	76.25513	70	4.24	50	25.177	95	3.88456	17.9859
DMPO-3	7/19/01	192	0.00172	50	76.21952	70	3.60	50	27.127	95	4.22208	21.1603
DMPO-4	7/19/01	192	0.00145	50	68.33424	70	4.74	50	25.117	95	3.93285	14.424
DMPO-5	11/1/01	192	0.00146	50	75.37146	70	4.63	50	27.385	95	4.12318	16.2886
DMPO-6	11/1/01	192	0.00138	50	62.530	70	3.28	50	27.399	95	4.264	19.0587
Average					**71.742**		**4.097**		**26.205**		**4.085**	**17.783**
STD					**6.125**		**0.637**		**1.227**		**0.170**	**2.578**
Successful rate:		**50%(5 out of 10)**										

Table C.2: Summary of gas transport data after correction for back permeation.

Coupons	Date tested	Test duration [hr]	Thickness [cm]	CO_2 perm. [Barrer]	CH_4 perm. [Barrer]	O_2 perm. [Barrer]	N_2 perm. [Barrer]	CO_2/CH_4	O_2/N_2
R/53.6/A-1	10/04/2001	264	0.0022	42.263	0.905	8.172	1.160	46.694	7.046
R/53.6/A-3	10/04/2001	264	0.00123	36.832	0.820	8.113	0.865	44.893	9.376
R/53.6/A-6	10/04/2001	264	0.00205	36.412	1.145	7.947	1.265	31.795	6.281
R/53.6/A-4	09/07/2001	264	0.00226	44.580	1.214	9.191	1.320	36.727	6.964
R/53.6/A-5	09/07/2001	264	0.00257	44.763	1.269	9.424	1.329	35.265	7.089
R/53.6/A-6	09/07/2001	264	0.00238	44.944	1.252	9.408	1.280	35.911	7.351
Average		**264**		**41.632**	**1.101**	**8.709**	**1.203**	**38.547**	**7.3513**
Std		**0.000**		**4.004**	**0.191**	**0.701**	**0.176**	**5.887**	**1.0542**

Successful rate: **60%(6 out of 10)**

Coupons	Date tested	Test duration	Thickness	CO_2 perm.	CH_4 perm.	O_2 perm.	N_2 perm.	CO_2/CH_4	O_2/N_2
R/75.6/A-1	05/09/2001	216	0.00218	41.236143	1.18357	9.407747	1.11823	34.84	8.4131
R/75.6/A-3	05/09/2001	216	0.00167	35.614824	1.05754	8.693668	1.12673	33.677	7.7159
R/75.6/A-5	05/09/2001	216	0.00239	33.615655	1.23379	10.96236	1.19494	27.246	9.174
R/75.6/A-6	05/09/2001	216	0.00207	45.336057	1.0518	7.208195	1.17678	43.103	6.1254
R/75.6/A-3	19/09/2001	192	0.00418	39.891162	1.14495	6.243986	1.13816	34.841	5.486
R/75.6/A-4	19/09/2001	192	0.00226	35.580722	1.0365	10.62153	1.01099	34.328	10.506
Average R/75.6/A				**38.54576**	**1.11803**	**8.856248**	**1.12764**	**34.673**	**7.9034**
Std				**4.401004**	**0.08138**	**1.866682**	**0.06442**	**5.0478**	**1.8809**

Successful rate: **67% (6 out of 9)**

Coupons	Date tested	Test duration	Thickness	CO_2 perm.	CH_4 perm.	O_2 perm.	N_2 perm.	CO_2/CH_4	O_2/N_2
R/28/A-1	01/08/2001	216	0.0022	77.204704	1.68825	16.14592	1.98865	45.731	8.119
R/28/A-3	01/08/2001	216	0.00246	58.645215	1.89877	14.49226	2.13506	30.886	6.7878
R/28/A-4	01/08/2001	216	0.00262	55.326262	1.87684	13.82684	2.02855	29.478	6.8161
R/28/A-5	01/08/2001	216	0.00236	66.775681	2.15505	16.89271	2.31166	30.986	7.3076
R/28/A-6	01/08/2001	216	0.00273	52.065508	1.52225	12.13817	2.26269	34.203	5.3645
Average R/28/A				**62.003474**	**1.82823**	**14.69918**	**2.14532**	**34.257**	**6.879**
Std				**10.105414**	**0.23841**	**1.888597**	**0.14118**	**6.6436**	**1.0034**

Successful rate: **83.3 % (5 out of 6)**

Coupons	Date tested	Test duration	Thickness	CO_2 perm.	CH_4 perm.	O_2 perm.	N_2 perm.	CO_2/CH_4	O_2/N_2
DPPO-1	24/05/2001	192	0.00266	39.312	0.861	6.135	1.133	45.655	5.417
DPPO-6	24/05/2001	192	0.00242	38.134	0.777	5.580	0.848	49.054	6.576
DPPO-1	21/06/2001	192	0.0017	41.450	1.148	6.439	0.918	36.104	7.014
DPPO-5	21/06/2001	192	0.00193	43.798324	1.258	6.312	1.046	34.811	6.037
DPPO-6	21/06/2001	192	0.00321	36.174888	0.894	6.128	0.794	40.449	7.720
Average DPPO				**39.774**	**0.988**	**6.119**	**0.948**	**41.214**	**6.553**
STD				**2.952**	**0.205**	**0.328**	**0.140**	**6.101**	**0.885**

Successful rate: **45.50%** **(5 out of 11)**

Coupons	Date tested	Test duration	thickness	CO_2 perm.	CH_4 perm.	O_2 perm.	N_2 perm.	CO_2/CH_4	O_2/N_2
B/75.7/A-1	26/09/2000	288	0.00173	29.762	0.864	5.226	0.917	34.429	5.700
B/75.7/A-2	26/09/2000	288	0.00093	29.199	0.763	5.135	0.874	38.288	5.877
B/75.7/A-3	26/09/2000	288	0.00149	29.546	0.841	5.292	0.849	35.125	6.234
B/75.7/A-6	26/09/2000	288	0.00125	28.670	0.828	5.383	0.783	34.641	6.878
Average B/75.7/A				**29.294**	**0.824**	**5.259**	**0.856**	**35.621**	**6.172**
STD				**0.476**	**0.044**	**0.105**	**0.056**	**1.802**	**0.520**
Successful rate:		**66.70%**		**(4 out of 6)**					

Coupons	Date tested	Test duration	Thickness	CO_2 perm.	CH_4 perm.	O_2 perm.	N_2 perm.	CO_2/CH_4	O_2/N_2
B/16.8/A-1	18/10/2000	312	0.00212	49.278345	1.66527	12.08379	1.9553	29.592	6.180
B/16.8/A-2	18/10/2000	312	0.00212	49.24718	1.36131	13.13609	1.27166	36.176	10.330
B/16.8/A-3	18/10/2000	312	0.00153	50.300591	1.55267	13.53554	1.94651	32.396	6.954
B/16.8/A-4	18/10/2000	312	0.00176			9.034521	1.82288		4.956
B/16.8/A-5	18/10/2000	312	0.00217	49.200578	1.51454	12.06636	1.66565	32.486	7.244
B/16.8/A-6	18/10/2000	312	0.00168			10.48365	1.08665		9.648
Average				**49.507**	**1.523**	**11.723**	**1.625**	**32.662**	**7.552**
STD				**0.530**	**0.126**	**1.691**	**0.365**	**2.700**	**2.058**
Successful rate:		**66.7% (4 out of 6)**							

Coupons	Date tested	Test duration	Thickness	CO_2 perm.	CH_4 perm.	O_2 perm.	N_2 perm.	CO_2/CH_4	O_2/N_2
B/51.4/A-2	22/07/2000	240	0.00162	49.022735	1.59057	11.14548	1.67682	30.821	6.6468
B/51.4/A-3	22/07/2000	240	0.00126	50.44346	1.72199	10.36865	1.56711	29.294	6.6164
B/51.4/A-5	22/07/2000	240	0.00143	53.798173	1.66711	10.50982	1.6724	32.27	6.2843
B/51.4/A-6	22/07/2000	240	0.00124	48.513897	1.91824	10.69757	1.75265	25.291	6.1037
Average				**50.445**	**1.724**	**10.680**	**1.667**	**29.419**	**6.413**
STD				**2.380**	**0.140**	**0.338**	**0.076**	**3.008**	**0.264**
Successful rate:		**66.7% (4 out of 6)**							

Coupons	Date tested	Test duration	Thickness	CO_2 perm.	CH_4 perm.	O_2 perm.	N_2 perm.	CO_2/CH_4	O_2/N_2
DMPO-1	19/07/2001	192	0.00131	76.255129	4.50552	24.71314	3.89153	16.925	6.3505
DMPO-3	19/07/2001	192	0.00172	76.219515	4.19958	26.62672	4.23219	18.149	6.2915
DMPO-4	19/07/2001	192	0.00145	68.334242	4.72476	24.65423	3.93626	14.463	6.2634
DMPO-5	01/11/2001	192	0.00146	75.371462	4.63103	26.88025	4.12718	16.275	6.513
DMPO-6	01/11/2001	192	0.00138	62.530	3.39501	26.8939	4.26726	18.418	6.3024
Average				**71.742**	**4.291**	**25.722**	**4.091**	**16.846**	**6.344**
STD				**6.125**	**0.539**	**1.204**	**0.170**	**1.595**	**0.099**
Successful rate:		**50%(5 out of 10)**							

Appendix D Intrinsic Viscosity of polymers

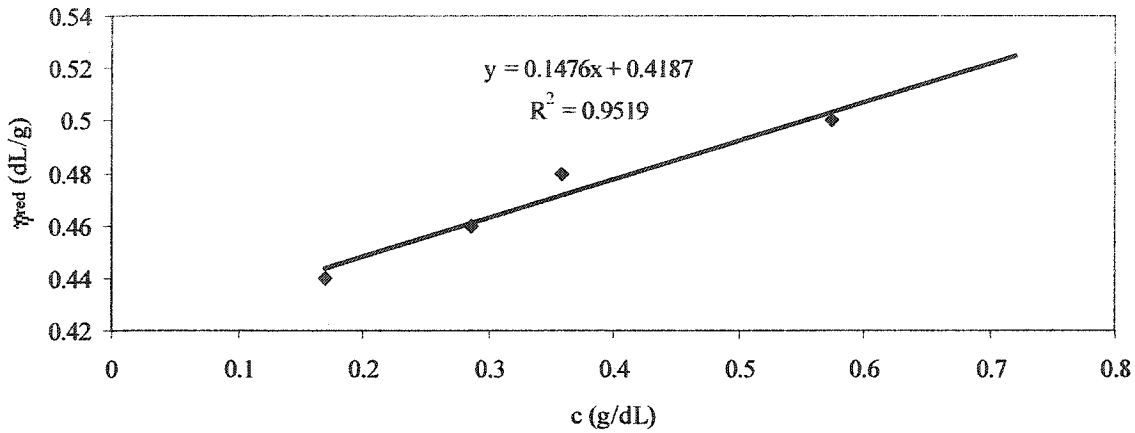

Figure D. 1: Determination of intrinsic viscosity for DMPO

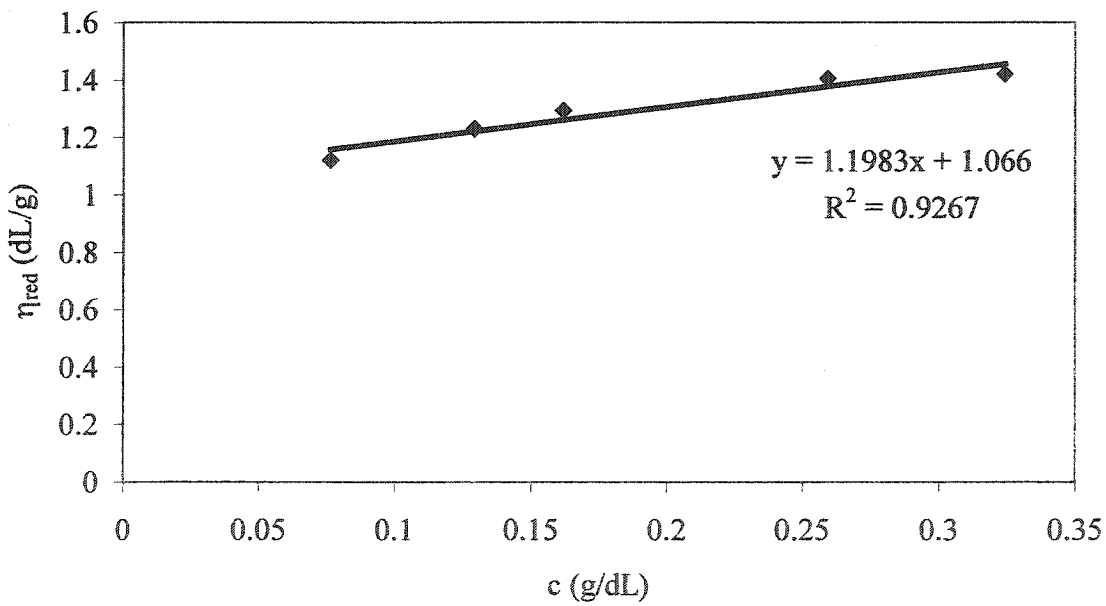

Figure D. 2: Determination of intrinsic viscosity for B/16.8/A

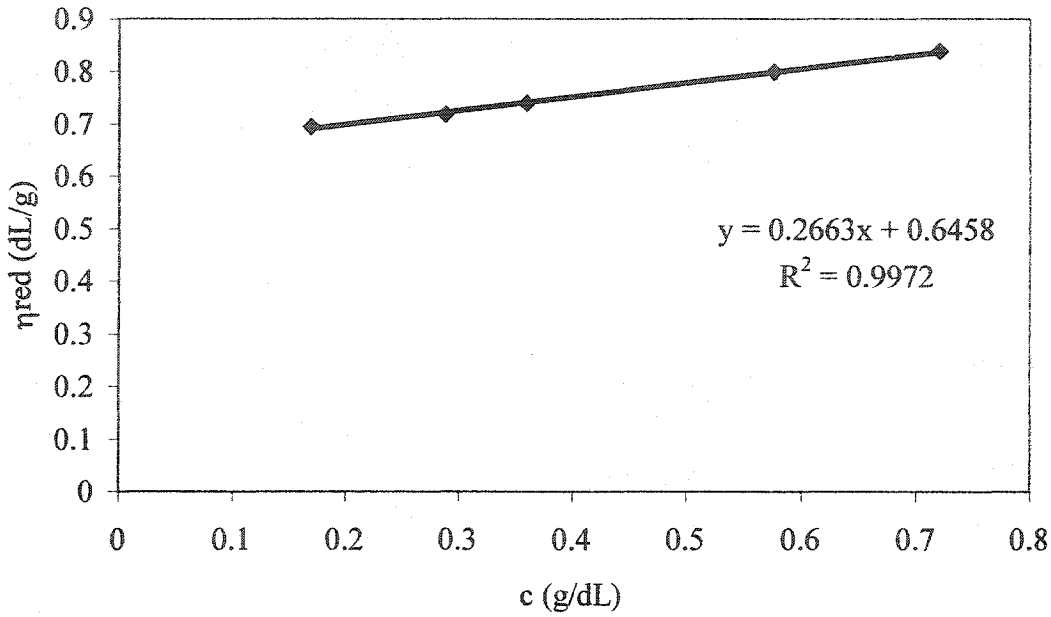

Figure D. 3: Determination of intrinsic viscosity for B/51.4/A

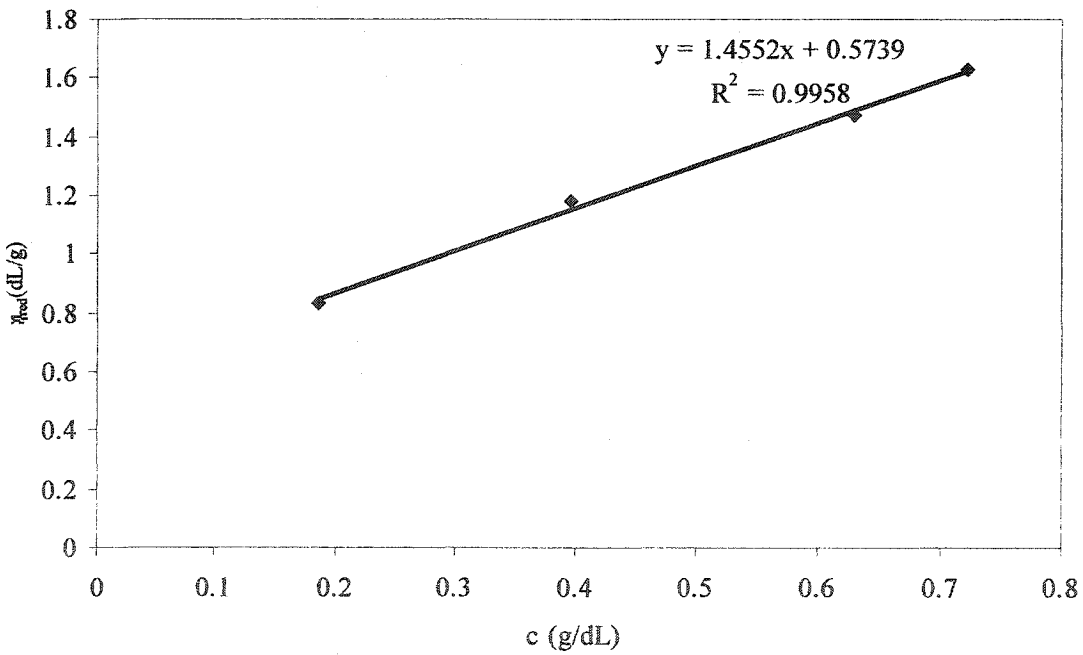

Figure D. 4: Determination of intrinsic viscosity for B/75.7/A

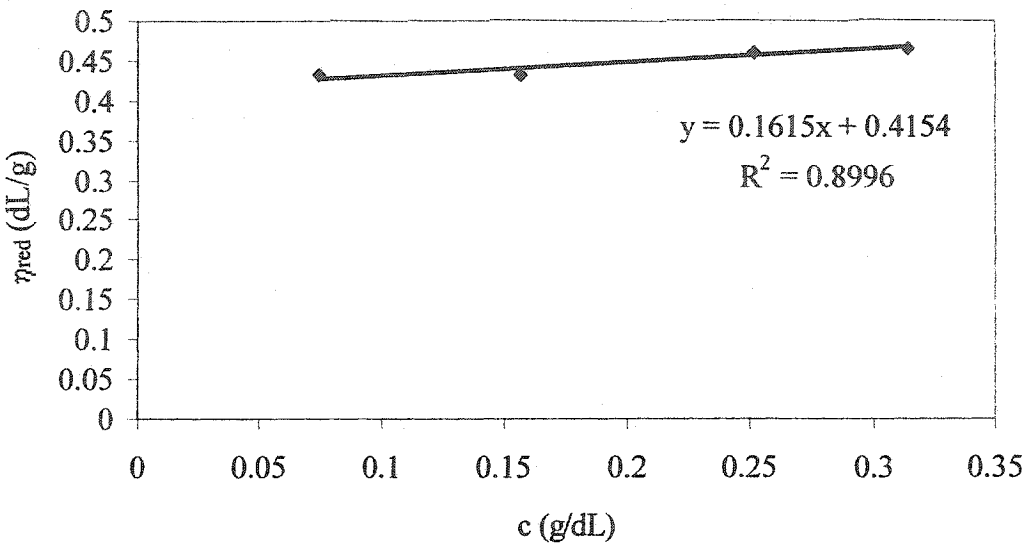

Figure D. 5: Determination of intrinsic viscosity for DPPO

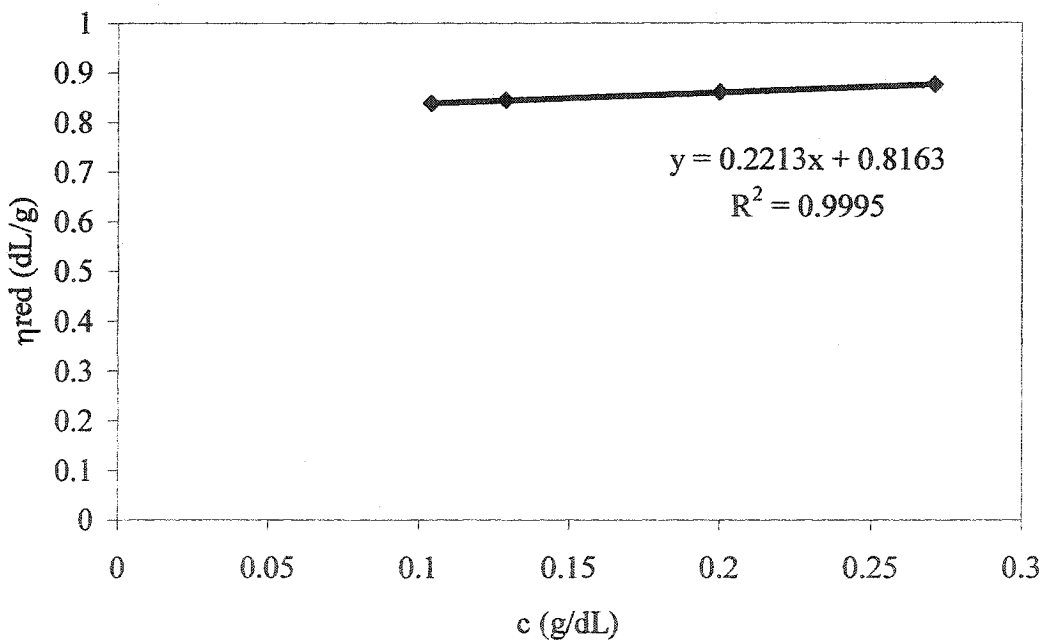

Figure D. 6: Determination of intrinsic viscosity for R/28/A

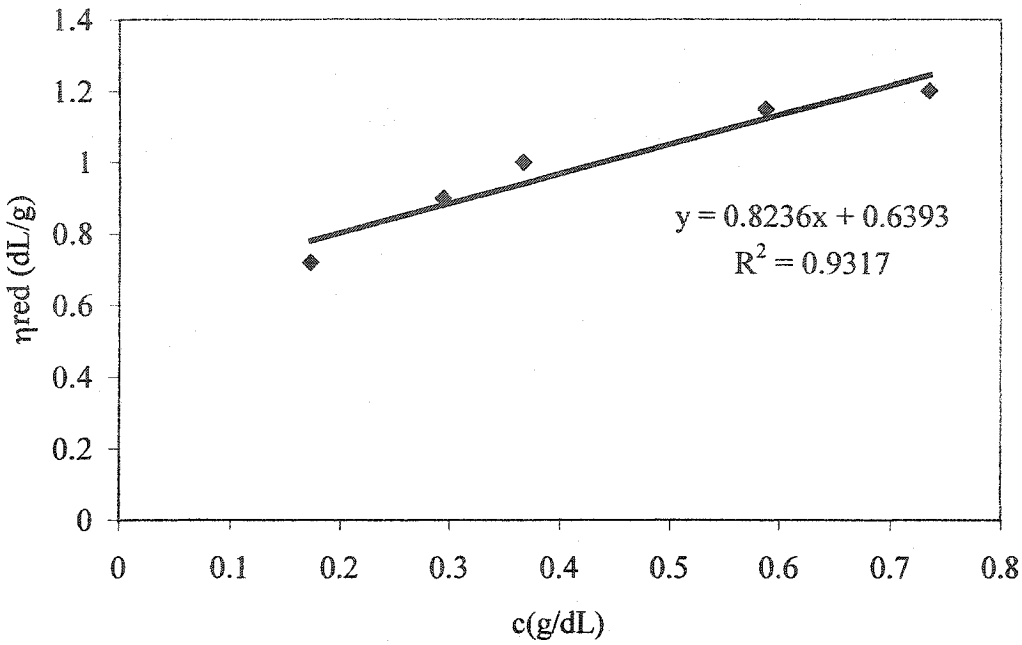

Figure D. 7: Determination of intrinsic viscosity for R/53.6/A

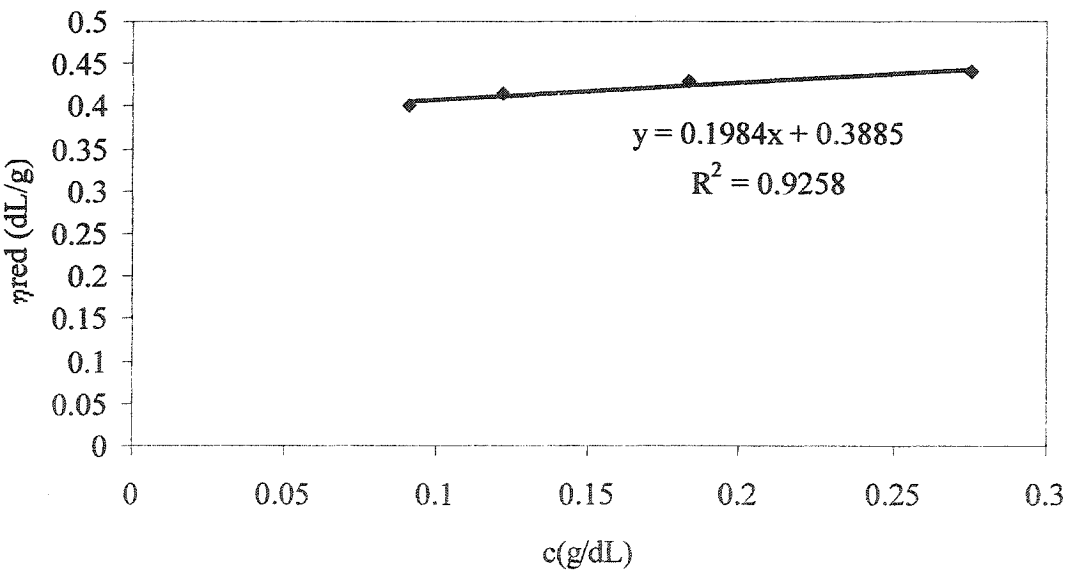

Figure D. 8: Determination of intrinsic viscosity for R/75.6/A